

Lawrence Berkeley National Laboratory

Recent Work

Title

PAE-INFRARED MAGNETIC RESONANCE IN Fe(III) AND Mn(III) PORPHYRINS, MYOGLOBIN, HEMOGLOBIN, FERRICHROME A, AND Fe(III) DITHIOCARBAMATES

Permalink

<https://escholarship.org/uc/item/2s50c1gm>

Author

Brackett, George Conrad.

Publication Date

1970-06-01

FAR-INFRARED MAGNETIC RESONANCE IN
Fe(III) AND Mn(III) PORPHYRINS,
MYOGLOBIN, HEMOGLOBIN, FERRICHROME A,
AND Fe(III) DITHIOCARBAMATES

RECEIVED
LAWRENCE
RADIATION LABORATORY

SEP 17 1970

LIBRARY AND
DOCUMENTS SECTION

George Conrad Brackett
(Ph. D. Thesis)

June 1970

AEC Contract No. W-7405-eng-48

TWO-WEEK LOAN COPY

*This is a Library Circulating Copy
which may be borrowed for two weeks.
For a personal retention copy, call
Tech. Info. Division, Ext. 5545*

LAWRENCE RADIATION LABORATORY
UNIVERSITY of CALIFORNIA BERKELEY

DISCLAIMER

This document was prepared as an account of work sponsored by the United States Government. While this document is believed to contain correct information, neither the United States Government nor any agency thereof, nor the Regents of the University of California, nor any of their employees, makes any warranty, express or implied, or assumes any legal responsibility for the accuracy, completeness, or usefulness of any information, apparatus, product, or process disclosed, or represents that its use would not infringe privately owned rights. Reference herein to any specific commercial product, process, or service by its trade name, trademark, manufacturer, or otherwise, does not necessarily constitute or imply its endorsement, recommendation, or favoring by the United States Government or any agency thereof, or the Regents of the University of California. The views and opinions of authors expressed herein do not necessarily state or reflect those of the United States Government or any agency thereof or the Regents of the University of California.

TABLE OF CONTENTS

ABSTRACT

I. INTRODUCTION----- 1

II. THEORY----- 6

 A. The Spin Hamiltonian----- 6

 B. Eigenvalues and Eigenfunctions----- 6

 C. Polycrystalline Absorption----- 8

III. EXPERIMENTAL TECHNIQUES----- 13

IV. EXPERIMENTAL RESULTS----- 18

 A. Ferrichrome A----- 18

 B. Tris (pyrrolidyl dithiocarbamate) Fe (III)----- 22

 C. Fe (III) Porphyrins----- 24

 D. Mn (III) Porphyrins----- 27

 E. Ferrihemoglobin and Ferrimyoglobin----- 30

 F. Bis Fe (III) Dithiocarbamates----- 34

 G. Additional Spectral Features----- 39

V. CONCLUSIONS----- 42

APPENDIX A - Polycrystalline Magnetic Dipole Absorption----- 43

APPENDIX B - Calculation of the Polycrystalline Absorption
 Coefficient----- 51

APPENDIX C - Polycrystalline Absorption Coefficient for $H' \gg 1$ ----- 56

APPENDIX D - Magnetic Torque for a Paramagnetic Ion in an Axial
 Ligand Field----- 103

APPENDIX E - Stabilization of a 4A_2 State for Fe (III) in bis Fe (III)
 Dithiocarbamates----- 109

APPENDIX F - Exchange-Coupled Paramagnetic Ions with $S=3/2$ in
an Axial Ligand Field----- 114

APPENDIX G - Ferromagnetic Resonance Frequency for Ions in an
Axial Ligand Field with $D < 0$ ----- 118

ACKNOWLEDGEMENTS----- 124

REFERENCES----- 125

TABLES----- 130

FIGURE CAPTIONS----- 135

FIGURES----- 140

Far-Infrared Magnetic Resonance in
Fe(III) and Mn(III) Porphyrins, Myoglobin, Hemoglobin,
Ferrichrome A, and Fe(III) Dithiocarbamates

G. C. Brackett

Department of Physics, University of California
and
Inorganic Materials Research Division,
Lawrence Radiation Laboratory,
Berkeley, California 94720

ABSTRACT

Far infrared spectroscopic techniques are used to study the magnetic resonance of Fe(III) and Mn(III) ions in molecular sites with large axial and rhombic fields. Measurements of transmission spectra over the range $3\text{-}100\text{ cm}^{-1}$ are discussed for a group of polycrystalline compounds, including several biological complexes, at temperatures between 1.3 and 50°K and in applied magnetic fields up to 50 kOe. The spectra show magnetic resonance absorptions which are consistent with a number of cases of the spin Hamiltonian formulation, and the spin Hamiltonian parameters ($D, E \geq 1\text{ cm}^{-1}$) are directly obtained from the spectra. The observation of resonances due to high spin Mn(III) and to the ferromagnetic resonance of $((\text{C}_2\text{H}_5)_2\text{NCS})_2\text{Fe(III)Cl}$ is reported. These measurements show that present far-infrared techniques offer a direct method for the investigation of the effects of large ligand fields on paramagnetic ions in molecules.

I. INTRODUCTION

A number of powerful techniques have been applied to the investigation of the electronic properties of paramagnetic ions in molecules. Considerable information has been obtained from spectroscopic measurements in the microwave, near infrared, visible, and ultraviolet regions of the electromagnetic spectrum, and from Mössbauer resonance at higher frequencies. Although the detailed structure of the electronic spectrum is complex, it has frequently been found that the magnetic properties of the ground term could be adequately described by a simple Hamiltonian first proposed by Abragam and Pryce¹ in 1950. The simplicity of the description results from the interaction of the ion with the surrounding ligands. The ligand field splits the multiply-degenerate free-ion ground state, and the new ground term, which is often an orbital singlet and spin multiplet, is further split by second-order spin-orbit coupling. The ground term may then be described by the spin Hamiltonian

$$\mathcal{H} = \mu_B \vec{H} \cdot \vec{g} \cdot \vec{S} + D[S_z^2 - S(S+1)/3] + E[S_x^2 - S_y^2] \quad (1)$$

where \vec{H} is the applied magnetic field, \vec{g} is the g-tensor, \vec{S} the electronic spin, and D and E are parameters which describe the effects of axial and rhombic ligand fields, respectively.

Conventional electron paramagnetic resonance techniques have been widely used to investigate ions whose ground terms are approximately described by Eq. (1). Such measurements, on compounds for which the values of the ligand field parameters correspond to microwave frequencies, have demonstrated that this description is often adequate, and have obtained accurate values for D and E. However, there is a large class of interesting compounds where the values of the spin Hamiltonian parameters are considerably larger ($D, E > 1 \text{ cm}^{-1}$). This class of compounds contains many extensively-studied biological molecules, the most well-known of which are various derivatives of the hemoproteins, such as myoglobin and hemoglobin. In addition, it also includes a number of metal-organic complexes, such as the transition-metal porphyrins. Microwave measurements on these compounds have been interpreted in terms of Eq. (1), but although the observed resonances can be used to obtain estimates of the spin Hamiltonian parameters, they only depend upon D in second order, and are relatively insensitive to the effects of small modifications of the spin Hamiltonian. However, higher frequency magnetic resonance measurements, using far-infrared spectroscopic techniques, can obtain detailed information on the spin Hamiltonian for substances in this class.

We have measured the far-infrared transmission spectra of a group of such compounds containing Fe(III) and Mn(III). The measurements were made over the frequency interval $3\text{-}100 \text{ cm}^{-1}$. The samples were polycrystalline powders or frozen solutions at temperatures between 1.3 and 50°K, and in magnetic fields up to 52 kOe. The spectra show magnetic field dependent absorptions due to magnetic dipole transitions between states of the

paramagnetic ground multiplet. Our experiments may be thought of as high frequency, high field electron paramagnetic resonance, with the exception that a continuous range of both frequency and field is available. The measurements have enabled us to investigate the validity of the spin Hamiltonian approximation, and to obtain directly values for the parameter D (and occasionally E).

In this paper, we shall present results for ferrichrome A, tris (pyrrolidyl dithiocarbamate) Fe(III), and certain complexes of ferrimyoglobin, ferrihemoglobin, Fe(III) porphyrins, Mn(III) porphyrins, and bis Fe(III) dithiocarbamates. This group of compounds is particularly well suited for such a general study because it contains illustrative examples for a variety of cases of Eq. (1). In terms of the spin Hamiltonian parameters, the cases investigated include: $S=3/2$, 2, and $5/2$; $D > 0$ and $D < 0$; $E/D \ll 1$, and $E/D=0.25$; and $g\mu_B H/D \ll 1$ to $g\mu_B H/D \gg 1$. In addition, one of the compounds, $((C_2H_5)_2NCS_2)_2Fe(III)Cl$, is ferromagnetic, and several show spectra with strong magnetic field-independent absorptions which may be due to low-frequency molecular vibration modes. Our experiments on the manganese porphyrins have obtained the first magnetic resonance data for these complexes which can definitely be attributed to Mn(III). Finally, the results for myoglobin, hemoglobin, and ferrichrome A indicate that detailed information on the effects of the ligand field can be obtained from investigation of intact biological molecules in the far-infrared region.

The organization of this paper is as follows: Section II includes a discussion of the relevant cases of the spin Hamiltonian of Eq. (1)

and brief comments on the calculation methods used to analyze the data;
Section III contains an outline of the experimental techniques employed;
Section IV presents our experimental results for each compound together
with some discussion.

II. THEORY

A. The Spin Hamiltonian

Excellent discussions of crystal or ligand field theory^{2,3} and of more general forms of the spin Hamiltonian^{1,4} are available, and a complete derivation of the spin Hamiltonian for ferrihemoglobin has been given by Weissbluth.⁵ In this section, we shall confine our discussion to the cases of the spin Hamiltonian of Eq. (1) which are applicable to our study. Although the general theory is widely understood, the details of the predictions of Eq. (1) for specific cases may be unfamiliar.

We shall consider a simpler form of Eq. (1) which is sufficient to analyze our polycrystalline spectra:

$$\mathcal{H} = g\mu_B \mathbf{H} \cdot \mathbf{S} + D[S_z^2 - S(S+1)/3] + E[S_x^2 - S_y^2]. \quad (2)$$

In Eq. (2), the \underline{g} tensor has been replaced by an isotropic g -factor with the free spin value $g=2.00$. Our results also do not require the small quartic terms in the spin operators which are occasionally included⁶ in Eq. (1).

B. Eigenvalues and Eigenfunctions

The energy-level spectrum of Eq. (2) is distinguished by two general characteristics:

(i) In zero magnetic field, the eigenvalues of Eq. (2) are separated by "zero-field splittings", which are functions of the parameters D and E .

For $S=3/2$ and $S=5/2$, the states are Kramers doublets. For $S=2$, the states are all singlets except in the case $E=0$ where there are two doublets and a singlet.

(ii) In a magnetic field, the eigenvalues are further split by the Zeeman interaction, and they are strongly dependent on both the magnitude and direction of the applied field.

The behavior of the spin Hamiltonian spectrum for each spin value can be most easily investigated in terms of the dimensionless parameters $\lambda=E/D$ and $H'=g\mu_B H/D$. Departures from axial symmetry are indicated by the value of λ . The range $0 \leq \lambda \leq 1/3$ describes all of the distinct physical possibilities; for $\lambda > 1/3$, a new set of coordinate axes may be chosen⁷ in which the spin Hamiltonian has new parameters D' and E' and a value $\lambda' < 1/3$.

We have calculated the variation of the eigenvalues and eigenfunctions as a function of H' and λ for $S=3/2$, 2 , and $5/2$. Although the detailed behavior is complex, a few simple comments can be made which are very useful in the interpretation of our experimental spectra. In the following discussion, we shall use the eigenstates of S_z as a basis set.

The variation of the zero-field eigenvalues for each S as a function of λ is given in Fig. 1. For $\lambda=0$ ($E=0$), the eigenfunctions of Eq. (2) are eigenstates of S_z with Kramers doublets characterized by the value of $|m_s|$. The zero field splittings are integer multiples of the axial crystal field parameter, D . For $D > 0$, the ground state is given by the minimum value of $|m_s|$; for $D < 0$, the level system is inverted. If λ is non-zero, the term $E[S_x^2 - S_y^2]$ couples states differing by $\Delta m_s = 2$. The eigenfunctions are no longer pure eigenstates of S_z and this

admixture is reflected in a shift of the Kramers doublets for $S = 3/2$ and $S = 5/2$, and a splitting for $S = 2$ (Kramers' theorem does not hold for ions with an even number of electrons.) The zero-field splittings are therefore a function of λ , and this dependence can be used to obtain a value of λ as discussed below.

The eigenvalue spectrum as a function of H' for Eq. (2) with $\lambda=0$ is given for each S in Fig. 2. The eigenvalues depend upon the magnitude and orientation of the external field \underline{H} with respect to the coordinate system in which the spin Hamiltonian is written. For $\lambda=0$, only the polar angle θ_H of the field with respect to the z-axis is required to determine the spectrum, and we have given curves for $\theta_H = 0$ and $\pi/2$. (For $\lambda \neq 0$, the spectrum also depends upon the azimuthal angle ϕ_H , and can differ markedly from the curves shown, although the qualitative characteristics remain the same⁸).

For $\underline{H} \parallel \hat{z}$ ($\theta_H = 0$), the eigenfunctions of Eq. (2) are eigenstates of S_z , and the Zeeman splitting is linear in H' . For $\underline{H} \perp \hat{z}$ ($\theta_H = \pi/2$), the Zeeman term $g\mu_B \underline{H} \cdot \underline{S}$ mixes states differing by $\Delta m_s = \pm 1$. For $H' \ll 1$, this admixture produces a linear splitting of the zero field $m_s = \pm 1/2$ doublet for $S = 3/2$ and $5/2$, with an effective g -value which depends upon S (for $S=3/2$, $g_1=4$; for $S=5/2$, $g_1=6$). The remaining doublets, for each S , split quadratically. For $H' \sim 1$, the eigenfunctions are mixtures of all eigenstates of S_z , and the variation of the eigenvalues with H' is complex. However, for large H' , the eigenfunctions are nearly pure eigenstates of S_H , the projection of \underline{S} onto the magnetic field \underline{H} , and the variation of all eigenvalues with H' then becomes linear.

This behavior is completely analogous to the Zeeman effect in atomic multiplets split by the spin-orbit interaction, and the high field limit corresponds to the Paschen-Back effect. The limiting values of m_s and m_H for $\vec{H} \parallel \hat{z}$ and $\vec{H} \perp \hat{z}$ respectively are indicated on the figures for the case $D > 0$; for $D < 0$, the signs of m_s and m_H should be reversed.

The most important feature of the spectrum for powder spectroscopy is the large variation of the eigenvalues and eigenfunctions with the orientation of the applied magnetic field. In practice, this results in broad, complex absorption lineshapes.

C. Polycrystalline Absorption

The transmission spectra of samples containing paramagnetic ions whose ground multiplet is described by Eq. (2) show absorptions due to magnetic dipole transitions between the states discussed in the previous section. The observed spectrum for a single crystallite can be described by an absorption coefficient $\alpha(\nu)$, which is, in general, a function of D , E , H , θ_H , and ϕ_H , as well as of the direction of propagation and polarization of the incident radiation. For a given transition n between initial state $|i_n\rangle$ and final state $|f_n\rangle$, the absorption coefficient may be written (see Appendix A, Section 1)

$$\alpha_n(\nu) = \frac{4\pi^2 e^2 N_0}{\hbar m^2 c^3} \nu \rho(\nu - \nu_n) |\langle f_n | \hat{k} \times \hat{\pi} \cdot \hat{S} | i_n \rangle|^2 \quad (3)$$

where N_0 is the concentration of paramagnetic ions, ρ is a lineshape function, \hat{k} and $\hat{\pi}$ are unit vectors in the direction of propagation and electric field polarization respectively of the incident radiation, \hat{S} is the spin operator, and ν_n is the frequency corresponding to the

difference of the eigenvalues of the initial and final states. In addition, at a given temperature T , the absorption coefficient must be multiplied by $P_n(T)$, the difference in the thermal population of the two states. The total absorption coefficient for a single crystallite is then

$$\alpha(\nu) = \sum_n \alpha_n(\nu) P_n(T) \quad (4)$$

where the sum is over all transitions within the ground multiplet. The spectrum thus described will show a series of absorption lines, one for each transition.

The transmission spectrum of a polycrystalline specimen in a fixed magnetic field may be obtained by averaging Eq. (4) over all crystallite orientations. In our experiments, the incident radiation was unpolarized and was strongly scattered within the sample, which was placed within a low- Q transmission cavity. Under these conditions, the average over crystallite orientations reduces to three independent averages over the directions of polarization $\hat{\pi}$, propagation \hat{k} , and magnetic field \hat{H} . In general, the first two averages may be carried out analytically, but the last must be performed numerically. (Later, we shall briefly discuss the important case $H' \gg 1$, in which the absorption coefficient may be obtained in closed form.) After the averages over polarization and the direction of propagation have been calculated, the expression for the average of Eq. (4) may be written (see Appendix A, Section 2)

$$\alpha(\nu) = \frac{\pi N_0 e^2 \nu}{h m c^3} \sum_n \int [\rho(\nu - \nu_n) P_n(T) W_n] d\Omega_H \quad (5)$$

where

$$d\Omega_H = \sin\theta_H d\theta_H d\phi_H$$

$$W_n \equiv 1/3 \{ |\langle S_x \rangle_n|^2 + |\langle S_y \rangle_n|^2 + |\langle S_z \rangle_n|^2 \}$$

and

$$|\langle S_x \rangle_n|^2 \equiv |\langle f_n | S_x | i_n \rangle|^2.$$

The integral over the orientation of \underline{H} in Eq. (5) is most easily calculated by numerical methods because W_n and ν_n are in general not simple functions of the parameters of the spin Hamiltonian of Eq. (2).

The results of a calculation of $\bar{\alpha}$ depend upon a few simple properties of the integrand in Eq. (5). The factor of ν , which appears because α is defined as the power absorbed per unit length, enhances high frequency transitions. The term $P_n(T)$ strongly suppresses transitions from states elevated more than $\sim kT$ above the ground state. Furthermore, at high temperatures, when $D/kT \ll 1$, $P_n(T)$ is very small for all transitions. The magnetic dipole transition probability W_n only allows transitions with $\Delta m_s = \pm 1, 0$. Finally, the solid angle $d\Omega_H$ strongly enhances transitions corresponding to $H \perp z$.

As an example of the effects of $P_n(T)$ and W_n , we consider the absorption coefficient for $S=5/2$ in zero applied field. For low temperatures, only transitions from the ground state will contribute appreciably. If $\lambda = 0$, only the transition from the ground state to the first excited state is allowed by the selection rules of W_n , and $\bar{\alpha}$ will show only one peak. However, if $\lambda \neq 0$, the admixture of states described previously will allow a transition to the second excited state.

The strength of this second transition increases rapidly with λ , and for $\lambda > 0.1$, two strong peaks will appear. The frequencies of the two corresponding experimental absorptions are sufficient to measure both D and λ .

If the temperature is sufficiently high to populate the first excited state, a third peak due to the transition between the first and second excited states will appear in $\bar{\alpha}$ for any value of λ ; in particular, for small λ , the positions of the first and third peaks can be used to obtain D and λ . Therefore, the zero-field spectrum is sufficient in principle to determine the parameters of the spin Hamiltonian. We shall later discuss specific examples of these two cases. Similar observations may be made for the zero-field spectrum in the case $S = 2$, with the exception that the splitting of the doublets with λ provides additional information. However, for $S = 3/2$, measurement of the zero-field absorption coefficient is not sufficient to obtain values for D and λ , and it is necessary to measure the absorption spectrum in an applied field.

In order to compare our experimental spectra for $S = 3/2$ with the predictions of the spin Hamiltonian, we have written a program to calculate $\alpha(\nu)$ for a specified D , E , H , T , and linewidth. This calculation is described in Appendix B. A Gaussian lineshape function, due to site inhomogeneities, was assumed, and the linewidth was chosen to fit the zero field spectrum. An example of the results of this calculation for $D < 0$, $|D|/kT = 0.8$, and a small value of λ are shown for several values of $H' = g\mu_B H/D$ in Fig. 3. The upper graph shows the contributions of the various transitions to the total lineshape, and the lower diagram is a composite plot of the variation of $\bar{\alpha}$ with H' . These curves illustrate the complex nature of the powder lineshape. We shall compare these

calculations with experiment in a later section.

For $H' \gg 1$, the bare polycrystalline absorption coefficient (calculated assuming $\rho(\nu - \nu_n) = \delta(\nu - \nu_n)$) can be obtained in closed form, because the quantities ν_n and W_n can be expressed as simple functions of the spin Hamiltonian parameters and the angles specifying the orientation of H . This can be seen by writing Eq. (2) in a coordinate system $\{x'y'z'\}$ where $H \parallel z'$, and choosing the eigenstates of $S_{z'}$ as a basis set. In this system, off-diagonal terms may be neglected, since the eigenfunctions are very nearly eigenstates of $S_H \equiv S_{z'}$. The magnetic dipole transition probability W_n is large only for transitions between adjacent levels, and the transition frequencies cluster about $\nu = g\mu_B H$ with a spread that is a different linear function of D and λ for each transition. The lineshape for each transition can be calculated by expressing the solid angle $d\Omega_H$, which is a function of two angles, in terms of the transition frequency and one angle using a Jacobian determinant. The double integral in Eq. (5) then reduces to a single integral which can be expressed in terms of the complete elliptic integral of the first kind. The resulting individual lineshapes can then be multiplied by the appropriate factors $P_n(T)$ and W_n , and added to give the total bare absorption coefficient. This calculation is described in greater detail in Appendix C. We shall compare the results of this calculation for $S = 5/2$ with our experimental results for ferrichrome A in a later section of the paper.

III. EXPERIMENTAL TECHNIQUES

Our spectra were obtained using the techniques of far-infrared Fourier transform spectroscopy.⁹ The Michelson interferometer, sample dewar, and detection system employed have been recently described elsewhere.¹⁰ Although the results obtained are analogous to those of electron paramagnetic resonance, there are a number of significant differences. Our spectra were measured for samples in fixed magnetic fields over a continuous range of frequencies roughly determined by the spectral bandpass of the sample, and the experimental methods used more nearly resemble those of near infrared spectroscopy than conventional microwave techniques. In addition, the lack of intense broad-band far-infrared sources places severe restrictions upon the application of far-infrared spectroscopy to problems of the type discussed in this paper. Since these restrictions do not generally apply to other magnetic resonance methods, we shall briefly discuss them.

The most widely-used far infrared source is the Rayleigh-Jeans region of the black body spectrum emitted by a high pressure mercury arc lamp. The intensity of the radiation emitted by the lamp varies approximately as ν^2 , and the total power radiated by the lamp used in our experiments into the f:1.5 optics of the Michelson interferometer in the region 0-100 cm^{-1} is $\sim 2 \times 10^{-5}$ W. Our experiments were typically made over the smaller spectral range 0-30 cm^{-1} , where the power falling on the detector, with no sample in place, is of the order of 10^{-8} W. This very small power requires the use of high sensitivity, low temperature detectors; the Ge bolometer¹¹ used in our experiments has a noise

equivalent power of $\sim 10^{-12} \text{W}/\sqrt{\text{Hz}}$, and it is the limiting source of noise in our detection system. The methods of Fourier transform spectroscopy are especially suited⁹ to this situation. However, in practice the small available source intensity means that:

(i) Spectral features in the sample which absorb less than 5 per cent of the incident radiation cannot be accurately measured.

(ii) Spectral regions in which the sample transmission is less than 1% are virtually inaccessible to our present techniques.

These two practical limitations have several implications for the present study. For example, accurate measurements of magnetic dipole lineshapes in the far infrared require samples which contain in excess of $\sim 10^{19}$ spins: for compounds such as myoglobin where the paramagnetic ion concentration is very dilute, a typical sample consists of 1 gram of material. Many large biological molecules are difficult to obtain in such quantities. In addition, the sample temperature must be low enough so that there is an appreciable Boltzmann population difference $P_n(T)$. For values of D on the order of a few cm^{-1} , liquid helium temperatures are necessary. Low temperatures are also required because the thermal population of higher frequency excitations in the sample, such as vibrational modes, may substantially reduce the low frequency transmission, and because magnetic resonance linewidths generally increase rapidly with temperature.

We have also observed strong broad-band absorption at high frequencies in all of the compounds investigated. This absorption, which may be due to low-lying vibrational modes, has an onset which varies roughly inversely with molecular weight, and it essentially creates a low

frequency spectral window which limits the frequency range in which our measurements may be performed. For example, the available frequency range for our measurements of myoglobin and hemoglobin was approximately $3.5\text{-}16\text{ cm}^{-1}$. The low frequency limit is approximately the same for all samples, and is due to the small source intensity at low frequencies.

Within the restrictions outlined above, however, far infrared magnetic resonance has several advantages over other techniques. The major advantage is that both frequency and field information can be obtained over relatively wide ranges; in particular, large zero field splittings for polycrystalline samples may be directly measured. The observed spectra clearly show the variation of the transition frequencies with field, and the individual transitions are easily identified. Paramagnetic resonances which are too broad to be accurately measured by microwave techniques can be observed more easily at higher magnetic fields in the far infrared, and the high frequency information which can be obtained is particularly sensitive to the approximations of the spin Hamiltonian. Finally, far infrared results can be used to determine the parameters of the spin Hamiltonian even when the zero field splittings lie in the microwave region (we shall illustrate this point in the discussion of our results for ferrichrome A).

Our far infrared transmission spectra show effects due to both magnetic resonance transitions and the background transmission spectrum of the sample. In order to remove the background, spectra were customarily obtained at several values of applied magnetic field, and ratios of spectra for different fields were computed. An example of this method is illustrated in Fig. 4. The upper graph shows an observed

spectrum for zero applied field compared with the spectrum obtained with no sample in place. The shape of the latter curve is due to the ν^2 rise of the source intensity, the frequency variation of the efficiency of the dielectric film beam splitter, and the attenuation of low-pass filters which are used to eliminate unwanted high frequencies. The sample spectrum shows a weak magnetic resonance absorption at $\nu \cong 33 \text{ cm}^{-1}$, and a strong broad band attenuation at frequencies above $\sim 20 \text{ cm}^{-1}$. The broad band attenuation is due both to the absorption in large molecules previously mentioned and to the onset of large scattering within the polycrystalline sample at wavelengths approximately equal to crystallite dimensions.¹² The lower graph is a plot of the ratio of a spectrum for high applied field to the spectrum for zero field. The ratio shows clearly the zero field absorption and the resonance due to the Zeeman splitting of the ground state, as well as noise on either end of the frequency range which is enhanced by computing the ratio of small numbers. This technique works well whenever the shift of the magnetic resonance spectrum with field is large compared to the linewidths, but for spectra such as those described in Fig. 3, the analysis is difficult.

Several of our spectra show effects due to alignment of the sample crystallites in a magnetic field. The alignment is due to the torque produced by the interaction of the low temperature ionic moment with the applied field, and is discussed in Appendix D. This torque is widely used¹³ to measure the low temperature magnetic susceptibility of paramagnetic ions whose ground term is described by Eq. (2). The torque acts to align one of the coordinate axes of the spin Hamiltonian with the applied field, and therefore strongly affects the observed magnetic

resonance spectrum. In addition, the crystallite alignment can significantly increase or decrease the high frequency background attenuation due to scattering if the crystallites are plate-like. We have attempted to avoid these effects in our measurements by dispersing the crystallites in transparent glasses, such as mineral oil, and fine magnesium oxide powders, or by packing samples which are too valuable to disperse.

The samples were typically placed within the far-infrared light pipe in cylindrical polyethylene containers with a sheet of thin Mylar covering the top. The container diameter was ~1.1 cm, and the sample length varied from 0.1 to 2.5 cm. Metal cones were placed above and below the sample container to form a low-Q transmission cavity. For temperatures $T \leq 4.2^\circ\text{K}$, the sample mount was immersed in liquid helium. For higher temperatures, the sample mount was placed in an evacuated tube and heated by means of a heating coil. The temperature was monitored by measuring the resistance of a GaAs diode in thermal contact with the sample mount.

IV. EXPERIMENTAL RESULTS

A. Ferrichrome A

Ferrichrome A¹⁴ is a metabolic product of the smut fungus Ustilago sphaerogena; its precise biological function is unknown. The crystal and molecular structure of ferrichrome A tetrahydrate have been recently obtained by X-ray crystallography.¹⁵ The molecule contains one Fe(III) ion in the configuration shown in Fig. 5. Although the iron coordination is roughly octahedral, the local symmetry is that of a lefthanded propeller, which suggests that there should be a large rhombic component in the ligand field at the iron site.

Electron paramagnetic resonance measurements⁷ at 9 GHz for polycrystalline ferrichrome A have been reported by Wickman, Klein, and Shirley. These measurements showed a broad asymmetric resonance at 1550 Oe for temperatures between 1.0 and 300°K and additional smaller structure was observed at both higher and lower fields in the spectra for temperatures less than 4.2°K. The spin Hamiltonian of Eq. (2) was used to analyze the spectra, under the assumption that the Zeeman term was small compared to the ligand field terms, and reasonable agreement was obtained for $S=5/2$, $D > 0$, and $\lambda=0.25 \pm 0.04$. The assignment $D > 0$ was based upon a fit of the low field effective g-values for the two possible ground doublets to the additional low temperature structure, and the range of λ was obtained from an approximate fit to all of the observed resonances. The temperature variation of the spectra was used to give a rough estimate of 3.5 cm^{-1} for the zero field splitting between the two lowest Kramers' doublets, and the temperature dependence of subsequent

Mössbauer effect measurements¹⁶ was used to obtain an improved estimate of $2.4 - 3.5 \text{ cm}^{-1}$ for this splitting.

Our far infrared spectra for approximately 70 mg of polycrystalline ferrichrome A, kindly supplied by Dr. M. P. Klein, showed no absorptions in zero field above our experimental lower frequency limit of 3.0 cm^{-1} ; spectra were obtained at $T = 1.3$ and $4.2 \text{ }^\circ\text{K}$. In high applied field, a broad asymmetric absorption which peaked at a frequency slightly less than $\nu = 2\mu_B H$ was observed. The average of three experimental absorption coefficient measurements for $H=52.2 \text{ kOe}$ and $T=4.2^\circ\text{K}$ is plotted in Fig. 6. The positions of the absorption maximum and the shoulders on either side were quite reproducible. No evidence of crystallite orientation due to magnetic torques was observed.

The absence of zero field absorptions above 3.0 cm^{-1} suggests that the observed high field lineshape corresponds to the limit $H' \gg 1$. The bare polycrystalline absorption coefficient in this limit was calculated according to the method outlined in Section II-C for various values of D and λ , and the results for two sets of values are also plotted in Fig. 6. The theoretical absorption coefficient at $T = 4.2^\circ\text{K}$ is largely given by the sum of the lineshapes for the two transitions from the ground and first excited states. The small delta-function at $\nu=2\mu_B H$ on the curve for $D < 0$ is due to the transition from the second excited state, and the contribution of the remaining transitions is negligible. The major features of the calculated $\bar{\alpha}$ are the absorption edges and the position of the maxima; the frequencies at which they occur can be easily expressed in terms of the spin Hamiltonian parameters. The absorption

edges occur at frequencies ν_i given by

$$\nu_{1a} = g\mu_B H + 2D(1+3|\lambda|)$$

$$\nu_{1b} = g\mu_B H - 4D$$

$$\nu_{2a} = g\mu_B H + D(1+3|\lambda|)$$

$$\nu_{2b} = g\mu_B H - 2D$$

where $i = 1, 2$ indicate the transitions from the ground and first excited states respectively, and the maxima occur at frequencies ν'_i given by

$$\nu'_1 = g\mu_B H + 2D(1-3|\lambda|)$$

$$\nu'_2 = g\mu_B H + D(1-3|\lambda|).$$

These frequencies are indicated in Fig. 6 for the solid curve. Although D and λ have the same sign,^{7,8} the calculated absorption coefficient for a given field depends only upon the sign and magnitude of D and the magnitude $|\lambda|$. Therefore, apart from the effects of the Boltzmann term $P_n(T)$, the lineshape for $D < 0$ may be obtained from the lineshape for $D > 0$ by reflecting through the line $\nu = g\mu_B H$. For $|\lambda| = 1/3$, the absorption coefficient depends only upon the magnitude $|D|$, and the sign of D can be regarded as arbitrary. This result is due to the symmetry properties of the spin Hamiltonian.^{7,8} As $|\lambda|$ approaches $1/3$, the distinction between positive and negative D becomes smaller, and consequently the sign of D becomes more difficult to obtain from paramagnetic resonance spectra.

The theoretical absorption coefficient for $g = 2.00$, $D = -0.27 \text{ cm}^{-1}$, and $|\lambda| = 0.25$, which is plotted in Fig. 6, represents our best fit to the observed lineshape; reasonable agreement places limits of $\pm 0.01 \text{ cm}^{-1}$ on D and ± 0.02 on $|\lambda|$. Considerably poorer fits are obtained for positive values of D , since the calculated maxima lie at frequencies higher than $\nu = 2\mu_B H$ for $|\lambda| < 1/3$. The best fit to all of the observed features for $D > 0$ requires $|\lambda| = 1/3$ and $D = +0.27 \text{ cm}^{-1}$; however, as indicated above, the same curve would be obtained for a negative D . The curve for these values is also plotted in Fig. 6. Both sets of values derived from our data yield zero field splittings between adjacent Kramers' doublets in the range 0.8 to 1.0 cm^{-1} . These values are considerably smaller than the estimates previously obtained.

The analysis of the paramagnetic resonance spectra of ferrichrome A, given by Wickman, Klein, and Shirley, rests upon the assumption that the Zeeman terms of Eq. (2) are much smaller than the ligand field terms, which is approximately equivalent to the statement that the energy of the microwave quantum is much less than the zero-field splittings. Our measurements indicate that this assumption is not justified at the experimental microwave frequency of 0.3 cm^{-1} . It has recently been pointed out⁸ that the effective g -factors in finite fields (such that $g_{\text{eff}} \mu_B H \sim D, E$) may vary considerably from those calculated in the limit of infinitesimal fields, and that resonances due to transitions between states originating in adjacent zero field doublets may also be observed. Under these conditions, the analysis of the low temperature paramagnetic resonances for ferrichrome A in the small field approximation is inconclusive with respect to the sign of D . Our data are fit more accurately

by negative values of D , as indicated in Fig. 6. Preliminary calculations of the X-band electron paramagnetic resonance spectrum,¹⁷ using the methods outlined in Ref. 8, indicate that the values $D = -0.27 \text{ cm}^{-1}$ and $|\lambda| = 0.25$ obtained from our data can account for the published resonances. More accurate values of D and λ could possibly be obtained by further analysis of X-band spectra, or by directly obtaining the zero field splittings at K-band.

B. Tris (pyrrolidyl dithiocarbamate) Fe(III)

A series of interesting tris Fe(III) dithiocarbamates, Fe(III) $(S_2CNRR')_3$ where R,R' are alkyl groups, have recently been synthesized.¹⁸ Although X-ray crystallographic data are unavailable, the molecular structure of these compounds is presumed on steric grounds¹⁹ to be that shown in Fig. 7. A comparison of Fig. 5 and Fig. 7 illustrates the similarity of the iron environment in these complexes to that in ferrichrome A.

Most of these substances show room temperature magnetic moments which lie between those of the limiting "low spin" ($S=1/2$) and "high spin" ($S=5/2$) states of the Fe(III) ion. Visible and infrared spectra and the temperature and pressure dependence of the magnetic susceptibility for several compounds have been reported,¹⁹ as well as Mössbauer effect²⁰ and nuclear magnetic resonance²¹ studies. Good agreement with the qualitative effects observed in these measurements has been obtained by assuming that the octahedral 2T_2 and 6A_1 terms of Fe(III) are separated by only a few hundred cm^{-1} in these complexes. However, quantitative agreement with the experimental results has been frequently hampered

by the lack of detailed information on the effects of the ligand field at the iron site. For example, the similarity of the iron site in the tris Fe(III) dithiocarbamates to that in ferrichrome A suggests that the ligand field should have a strong rhombic component in these complexes. Such information can in principle be obtained by electron paramagnetic resonance techniques, and a study at microwave frequencies is now in progress.¹⁷

One of the compounds, tris (pyrrolidyl dithiocarbamate) Fe(III), shows only high spin behavior. We have measured the far infrared spectra of a polycrystalline sample of this substance at $T=4.2^\circ\text{K}$. The sample was supplied by Dr. A. M. Trozzolo. Data obtained from our spectra are plotted in Fig. 8. The zero field spectrum shows a strong absorption at 8.4 cm^{-1} and a weaker one at 13.2 cm^{-1} . The first absorption corresponds to a transition between the ground and first excited Kramers doublets, and the second corresponds to a transition between the ground and second excited doublets. As discussed in Section II-C, the presence of the second absorption at low temperature implies that $\lambda \neq 0$. Our zero field data are fit by the values $D = -2.14 \pm 0.05\text{ cm}^{-1}$ and $\lambda = -0.10 \pm 0.01$. The sign of D was established by observing that the first absorption occurs at a frequency more than half of the total zero field splitting, 13.2 cm^{-1} ; if $D > 0$, the reverse is true. In addition, no absorption due to the Zeeman splitting of the ground doublet was observed, which is further evidence for a negative value of D .

Our measurements indicate that the ligand field in this compound does in fact have an appreciable rhombic component, as expected. It is

interesting to note that low temperature microwave magnetic resonance measurements¹⁷ for frozen solutions of this compound in N,N dimethyl formamid indicate that $|\lambda| \sim 1/3$ and that $|D|$ is somewhat smaller. Previous experiments¹⁸ have also shown differences between the room temperature magnetic moments of solid and dissolved compounds of this series.

C. Fe(III) Porphyrins

Metalloporphyrins²² have been investigated by a variety of techniques because of their occurrence as the prosthetic group of paramagnetic ions in many biological molecules. In particular, studies on iron porphyrins (hemes)²³ have been stimulated by interest in related work in hemoproteins.²⁴ The approximate structure of such heme compounds and the local coordination of the iron ion in the porphyrin molecule are indicated in Fig. 9. The iron is coordinated to the four pyrrole nitrogens of the porphyrin, and two other coordination positions, labeled 5 and 6, are available in positions approximately perpendicular to the plane defined by the four nitrogen atoms. In the compounds we shall discuss, one of these positions is unoccupied, and the other is occupied by one of a number of ligands. Under these conditions, X-ray crystallographic measurements²⁵ have indicated that the iron lies slightly above the nitrogen plane in the direction of the fifth ligand. Hemes are also identified by the presence of various groups attached to the periphery of the porphyrin skeleton. Protoheme (iron protoporphyrin), the prosthetic group of hemoglobins, myoglobins, and several other hemoproteins, is the best-known.

The far-infrared spectra of several halogeno deuterio- and proto-porphyrin Fe(III) complexes have recently been reported.²⁶ The spectra

for these compounds were successfully analyzed in terms of the spin Hamiltonian in Eq. (2) for $S = 5/2$, $D > 0$, and $\lambda \cong 0$. The observed zero field splittings for the compounds investigated were quite large, ranging from 11.1 cm^{-1} to $\sim 33 \text{ cm}^{-1}$. Preliminary results for several other complexes were also reported.

We have measured the far-infrared spectra of four polycrystalline Fe(III) porphyrins. The sample preparation and characterization techniques were similar to methods recently described elsewhere.²⁷ These measurements have yielded more accurate values of the ligand field parameters for two compounds included in the previous work, iodo- and azido deuteroporphyrin IX dimethyl ester Fe(III). In addition, we have also obtained data for two additional compounds, fluoro- and azido protoporphyrin IX dimethyl ester Fe(III). The last two substances are of particular interest because of the existence of the corresponding myoglobin and hemoglobin complexes.

The spectra for all of the compounds investigated showed absorptions characteristic of high spin Fe(III) and positive values of D . A typical transmission spectrum has been previously shown in Fig. 4. The frequencies of the experimental absorption peaks at $T = 4.2^\circ\text{K}$ are plotted as a function of field for fluoro protoporphyrin IX dimethyl ester Fe(III) in Fig. 10. The observation of absorptions corresponding to the Zeeman splitting of the ground doublet establishes the sign of D as positive. The frequency of the zero-field absorption corresponds to the zero-field splitting Δ_1 between the ground and first excited Kramers doublets. If $\lambda = 0$, as we would expect for this complex,²⁸ $\Delta_1 = 2D$. The calculated frequencies of strong transitions for the spin Hamiltonian in Eq. (2)

for $D = +5.0 \text{ cm}^{-1}$, $\lambda = 0$, $T = 4.2^\circ\text{K}$, and $H \parallel \hat{z}$ are also plotted in Fig. 10 for comparison. The values of the zero field splittings and derived values of D obtained from our data for the two halogeno complexes investigated and previously reported values for related complexes are listed in Table I.

The azide complex of ferrihemoglobin has a static magnetic susceptibility²⁹ characteristic of the low spin $S = 1/2$ state of Fe(III). Electron paramagnetic resonance measurements³⁰ show a strongly asymmetric g -tensor which has been successfully analyzed^{31,32} in terms of a rhombic ligand field. Similar results have been obtained for the azide complex of ferrimyoglobin. The origin of the rhombic field in these complexes is in dispute. It has been ascribed to the attachment of the distal histidine³⁰ (which is coordinated to the iron in the fifth position in these compounds), to the displacement of the iron atom out of the nitrogen plane,³² and to a non-axial attachment of the azide ion.³¹ An X-ray crystallographic study of ferrimyoglobin azide,³³ which showed that the azide ion is inclined at 21° to the porphyrin plane, has given support to the latter explanation.

Our measurements for the corresponding heme compound, azido protoporphyrin IX dimethyl ester Fe(III) and the similar deuteroheme complex show spectra characteristic of high spin Fe(III). However, an orientation of the azide ligand in these substances similar to that observed in ferrimyoglobin should produce a substantial rhombic component in the ligand field. In order to determine the value of λ for these complexes, zero-field spectra were obtained at $T = 4.2$ and 50°K . At the higher temperature, an additional absorption was observed in the spectra

at a frequency corresponding to the second zero-field splitting Δ_2 between the first and second excited Kramers doublets. As discussed in Section II-C, the values of Δ_1 and Δ_2 obtained in this fashion can be used to obtain values for D and λ . The observed splittings and the derived values of D and λ for the two compounds are also listed in Table I. Both complexes show non-zero values of λ , indicating that the ligand field does in fact have a rhombic component. The value of λ for the protoheme complex is particularly large compared to the limiting value $\lambda = 1/3$ for a completely rhombic field. (A typical value of λ for an axial complex, obtained from high-temperature data for chloro protoporphyrin IX Fe(III),²⁶ is $\lambda = 0.01 \pm 0.01$.) Although the iron atom in these compounds may be displaced out of the nitrogen plane, an axial displacement cannot account for a rhombic component to the ligand field.⁵ The most likely source of such a field is an inclination of the azide ion to the porphyrin plane such as that observed in ferrimyoglobin azide. If this is the case, our measurements on these complexes indicate that the orientation of the azide ligand can significantly contribute to the rhombic character of the ligand field in ferrimyoglobin and ferrihemoglobin.

D. Mn(III) Porphyrins

Studies of manganese porphyrins, like those of iron porphyrins, have been stimulated by interest in their properties in relation to biological systems. For example, several studies have investigated the possible role of these compounds in the oxidation-reduction systems of photosynthesis.^{34,35} In addition, synthetic enzymes made by replacing

heme prosthetic groups with Mn porphyrins have been shown to have partial activity.³⁶ Elemental analysis and magnetic susceptibility measurements on manganese hematoporphyrins³⁴ have shown that the stable oxidation state of the manganese in these complexes is Mn(III), with a spin $S=2$. However, no electron paramagnetic resonances that can be directly attributed to Mn(III) have been observed.

We have measured the far infrared spectra of four polycrystalline Mn(III) deuteroporphyrins. The spectra for three of the compounds investigated show magnetic resonance absorptions which are consistent with the predictions of the spin Hamiltonian in Eq. (2) for $S=2$, $D < 0$, and $\lambda \cong 0$. Data for a sample of azido deuteroporphyrin IX dimethyl ester Mn(III) at $T=4.2^\circ\text{K}$ are shown in Fig. 11. The zero-field spectrum for this complex showed only one absorption, indicating that $\lambda \sim 0$. For small λ , the zero-field spectrum should show two absorptions separated by $6E$, as indicated in Fig. 1. The width of the observed zero-field lineshape was used to obtain the upper limit $E \leq 0.1 \text{ cm}^{-1}$. Since transitions corresponding to the Zeeman splitting of the pair of zero field states with $m_s \cong \pm 2$ are forbidden to first order, the absence of such absorptions in the observed spectra does not imply that D is positive. In order to establish the sign of D , we have obtained spectra for this complex in zero field at temperatures up to 40°K . No additional absorptions appeared above 3.5 cm^{-1} , which shows that D is negative and that therefore the observed zero-field splitting is $\Delta_1 = 3|D|$. These observations yield $D = -3.08 \pm 0.10 \text{ cm}^{-1}$ and $\lambda \leq 0.04$. The calculated transition frequencies for Eq. (2) with $D = -3.08 \text{ cm}^{-1}$, $\lambda = 0$, and $\underline{H} \parallel \hat{z}$ are also plotted in

Fig. 11 for comparison. Similar observations were used to derive values of D and λ for chloro deuteroporphyrin IX dimethyl ester Mn(III). However, no absorption in zero field was observed for the third complex, bromo deuteroporphyrin IX dimethyl ester Mn(III). The spectra in an applied field showed substantial changes in the background attenuation at high frequencies due to crystallite orientation. In addition, a broad magnetic resonance absorption with a peak at $\nu = 2\mu_B H + 3.4 \text{ cm}^{-1}$ was observed at high field. These observations are only consistent with a small negative value of D , and analysis of the observed high field lineshape in the manner described for ferrichrome A yields the value $D = -1.1 \pm 0.1 \text{ cm}^{-1}$. The derived values of the spin Hamiltonian parameters for these three complexes are listed in Table II. The fourth compound studied, iodo deuteroporphyrin IX dimethyl ester Mn(III), showed spectra similar to those observed for the bromo derivative, indicating a small absolute value of D . However, the extremely broad absorptions observed prevented an accurate measurement of either the sign or magnitude of D for this complex.

Our measurements have therefore shown magnetic resonance absorption which is definitely due to high-spin ($S=2$) Mn(III). The observed large values of D , coupled with the small transition probabilities for transitions between Zeeman-split "doublets" for $S=2$, may account for the lack of microwave paramagnetic resonance signals for these complexes. In addition, we can make some interesting comparisons of the spin Hamiltonian parameters obtained for corresponding Mn(III) and Fe(III) porphyrins. For example, the values of D obtained for halogeno proto- and deuteroheme

complexes increase in the order $F < Cl < Br < I$, as indicated in Table I. The relation of this effect to various chemical series (nephelauxetic, electronegativity, and metal-halide bond strength) and to π -bonding in the porphyrin system has been recently discussed.³⁷ The algebraic values of D obtained for halogeno manganese porphyrins also show this behavior. It is interesting to note that the small negative value of D for the bromo derivative implies that D for the iodo complex may be positive. In addition, the algebraic value of D for the azido derivatives of both Fe(III) and Mn(III) deuteroporphyrins is less than that for the chloro derivatives. Finally, the limits of λ for azido deuteroporphyrin IX dimethyl ester Mn(III) include the measured value for the corresponding deuteroheme compound, indicating that the effects of the azide ligand are similar in the two complexes.

E. Ferrihemoglobin and Ferrimyoglobin

Hemoglobins and myoglobins are found in all vertebrates: hemoglobin in the red blood cells and myoglobin in the tissues. A large number of chemical, biological, and physical techniques have been applied to the study of these compounds because of their central importance to the process of respiration.

Both hemoglobin and myoglobin contain iron atoms coordinated to a protoporphyrin prosthetic group and to a nitrogen atom of a histidine residue of the globin. Hemoglobin contains four such iron atoms, and myoglobin contains one. In the respiratory process, the iron atom is in the Fe(II) state, and the sixth coordination position is available for the reversible bonding of molecular oxygen. Studies of hemoglobin and myoglobin where the iron is in this state are therefore of

greater value to the understanding of the biological function of these compounds. However, a large amount of useful information has been obtained from measurements on complexes containing Fe(III). Perhaps the most striking examples of such measurements are the determination of the orientation of the heme planes in hemoglobin³⁸ and myoglobin³⁹ by electron paramagnetic resonance measurements on Fe(III), in the high spin ($S=5/2$) state. In particular, such paramagnetic resonance measurements have been restricted to complexes containing Fe(III) since the low spin ($S=0$) Fe(II) derivatives have no paramagnetism and since no electron paramagnetic resonance has been observed for high spin ($S=2$) Fe(II) compounds.

Hemoglobin and myoglobin derivatives in which the sixth coordination position is occupied by a water molecule (we shall refer to these as met-hemoglobin and met-myoglobin) or a fluoride ion have been shown to contain Fe(III) in the high spin state. Static magnetic susceptibility measurements for these complexes⁴⁰ have found room-temperature magnetic moments slightly less than the value of 5.92 Bohr magnetons expected for $S=5/2$. Microwave electron paramagnetic measurements⁴¹ for these complexes have found $g_{\parallel} = 2.0$ and an isotropic $g_{\perp} = 6.0$, which is characteristic of the Zeeman splitting of the ground doublet for the spin Hamiltonian in Eq. (2) for $S=5/2$, $D > 0$, and a magnitude of D much larger than the microwave quantum. A number of indirect methods have been used to obtain values of D for these compounds: for example, microwave paramagnetic resonance,⁴² temperature dependence of the magnetic susceptibility,⁴³ torque magnetometer measurements of magnetic anisotropy,¹³ and Mössbauer resonance.⁴⁴ As the results discussed for heme compounds indicate, far-

infrared spectroscopy can, in principle, directly measure the zero-field splitting and thus the value of D for such compounds.

We have measured the far-infrared spectra of bovine hemoglobin and sperm whale myoglobin with both water and fluoride ligands. The spectra for each compound show absorptions corresponding to the Zeeman splitting of the ground doublet in applied fields up to 52.2 kOe, and to the zero-field splitting for the fluoro derivatives. The polycrystalline sample of met-myoglobin was supplied by Dr. G. Feher. The remaining samples were pastes made by mixing approximately 1 gm. of lyophilized material (obtained from Mann Research Laboratories and Sigma Chemical Company) into 1 ml of distilled water buffered to pH 7.0 with a drop of 1 M mixed phosphate buffer. The fluoro derivatives were obtained by using an aqueous solution containing approximately four molar equivalents of fluoride. The composition of the paste samples was verified by measuring the optical spectra of suitably diluted aliquots.

Data obtained from the far-infrared spectra of the two fluoro complexes at 4.2°K are shown in Fig. 12. Since $\lambda \sim 0$ for these complexes, the observed absorption in zero field corresponds to $\Delta_1 = 2D$. Curves for the transitions calculated from Eq. (2), using values of D derived from the zero field splitting, are also plotted for $\lambda = 0$ and $H \perp \hat{z}$. The frequency region in which accurate data can be obtained from the far infrared spectra for these compounds is indicated by the plotted range. For comparison, the typical transmission range for a heme compound sample with approximately the same number of Fe(III) ions is indicated in Fig. 4. In addition, the high-frequency attenuation in hemoglobin and myoglobin increases very rapidly with frequency. For example, a reduction of the

sample path length by a factor of two only increases the available frequency range by $\sim 1 \text{ cm}^{-1}$.

Absorption corresponding to the Zeeman splitting of the ground doublet was observed in the spectra for met-hemoglobin and met-myoglobin. However, no absorptions were observed in zero field below the maximum frequency limit for these compounds of $\sim 16 \text{ cm}^{-1}$. This observation implies $D \geq 8 \text{ cm}^{-1}$ for these complexes. A more accurate estimate of D for met-myoglobin can be obtained from our data for the Zeeman splitting of the ground doublet, shown in Fig. 13. The points plotted are the average values of the measured frequencies of peak absorption obtained from eight experimental runs at 4.2°K . The curves are the transition frequencies calculated from Eq. (2) with $\lambda = 0$, $H \parallel \hat{z}$, and the indicated values of D . A comparison of this figure with the data obtained for the fluoro derivative in Fig. 12 indicates that $D \cong 9 \text{ cm}^{-1}$, and a conservative estimate places D in the range $D = 9.5 \pm 1.5 \text{ cm}^{-1}$. Preliminary observations for met-hemoglobin indicate that D is slightly larger ($\sim 10.5 \text{ cm}^{-1}$) in this compound.

The values of D derived from the far-infrared data are listed in Table III. We have also included several values of D obtained from indirect measurements, and have reproduced the value for fluoro protoporphyrin IX dimethyl ester Fe(III), for comparison. It is interesting to note that the value of D for the fluoro derivatives of myoglobin, hemoglobin, and protoheme are very similar, indicating that the influence of the protein on the ligand field at the iron site is relatively small. In addition, no evidence for inequivalent sites due to the two different protein chains in hemoglobin was found in the far-infrared spectra for

the fluoro derivative. If two inequivalent sites are assumed, the observed zero-field lineshape places an upper limit of $\sim 0.4 \text{ cm}^{-1}$ on the difference of the value of D between the two sites.

F. Bis Fe(III) Dithiocarbamates

Further studies of the tris Fe(III) dithiocarbamates, discussed in Section IV-B, have resulted in the synthesis of a series of novel bis Fe(III) dithiocarbamate compounds, the bis (N,N dialkyl dithiocarbamate) Fe(III) halides: $(R_2NCS_2)_2 FeX$ where R is an alkyl group and X is a halogeno ligand. X-ray crystallographic measurements⁴⁶ on one of the complexes in this series have obtained the molecular structure shown in Fig. 14. The iron atom in these compounds is pentacoordinate, and lies approximately at the centroid of a rectangular pyramid formed by the four sulfur atoms of the two dithiocarbamate ligands and the halide atom. The local symmetry of the iron site is thus nearly square pyramidal, but the total symmetry is much lower (C_{2v}).

Measurements of the static magnetic susceptibility,^{46,47} electron paramagnetic resonance,⁴⁸ and Mössbauer resonance⁴⁹ have shown that the Fe(III) ground multiplet is described by the spin Hamiltonian in Eq. (2) with the unusual "intermediate spin" value $S=3/2$, $\lambda=0$, and large values of D. Although the energy of the ${}^4T_{1g}$ octahedral state never lies lowest,⁵⁰ the low C_{2v} symmetry of the iron site in these complexes completely removes the degeneracy of the d^1 levels. A simple argument, given in Appendix E, shows that under these conditions it is possible to stabilize a 4A_2 ground state derived from the $(t_{2g}^4 e_g)$ ${}^4T_{1g}$ octahedral state.

In order to investigate the validity of the spin Hamiltonian

parameters, we have measured the far-infrared spectra of seven polycrystalline compounds in this series. A brief account of this work has been recently published elsewhere.⁵¹ Data obtained from the far-infrared spectra of $((i-C_3H_7)_2NCS_2) Fe(III) Cl$ at $4.2^\circ K$ are shown in Fig. 15. As discussed in Section II-C, the zero field spectrum for $S=3/2$ shows only one absorption, and is therefore not sufficient to determine D and λ . However, electron paramagnetic resonance measurements on this compound⁴⁷ have obtained the value $\lambda=0.036\pm 0.003$. Using this value, the measured zero-field splitting $\Delta = |D|[1+3\lambda^2]^{1/2}$ gives $|D|=2.35 \pm .03 \text{ cm}^{-1}$. A comparison of the polycrystalline absorption coefficient, calculated using the program discussed in Section II-C, with the observed spectra showed that $D < 0$. The frequencies of the calculated absorption maxima for $D = -2.35 \text{ cm}^{-1}$, $\lambda = 0.036$, and $T=4.2^\circ K$ are also plotted in Fig. 15. The calculated polycrystalline absorption coefficients for these parameters have been shown in Fig. 3. The fit between the observed absorptions and the calculated maxima is excellent. The zero field splittings and derived values of the spin Hamiltonian parameters obtained in this manner from the far-infrared spectra for the compounds investigated are listed in Table IV. Since the polycrystalline spectra are relatively insensitive to values of $\lambda < 0.1$, we have only listed the values of λ obtained for two compounds. The listed values of D for the remaining compounds were obtained from the zero field splitting, assuming $\lambda = 0$. In addition, the calculated polycrystalline absorption coefficient is relatively insensitive to small changes in the spin Hamiltonian, such as the assumption of a slightly

anisotropic g-factor.

One of the compounds investigated, $((C_2H_5)_2NCS_2)_2 Fe(III) Br$, can be obtained in relatively large crystals ($0.5 \times 3 \times 3$ mm). The far-infrared spectra of a polycrystalline sample of this compound at $4.2^\circ K$ showed sharp absorptions that were approximately consistent with the predictions of the spin Hamiltonian in Eq. (2) for $D > 0$ and θ_H near $\pi/2$, indicating a substantial alignment of the crystallites by the low-temperature magnetic torque discussed in Section III. (A calculation of the torque (given in Appendix D) for this compound at $T = 4.2^\circ K$ and $H = 52.2$ kOe yields a maximum torque per unit volume of 8.65×10^5 dyne/cm² which tends to rotate the crystallites toward $H \perp \hat{z}$.) In order to obtain a more accurate comparison of the predictions of the spin Hamiltonian with the observed spectra, an ordered sample of this complex was constructed with the crystallites approximately oriented with $H \perp \hat{z}$. The data obtained from the far-infrared spectra of this sample is plotted in Fig. 16. A "best fit" to the observed spectra was calculated from Eq. (2) by varying θ_H and using values of D and λ chosen to fit the zero-field splitting and the Zeeman splitting of the ground doublet ($g_1 \sim 4$). The calculated transition frequencies for the values obtained, $\theta_H \sim 3\pi/8$, $D = + 7.50$ cm⁻¹, and $\lambda = 0.067$, are also plotted in Fig. 16. The value of θ_H obtained was consistent with both the construction of the sample and the effects of the magnetic torque. Although the fit to the observed absorptions is quite good, the deviation of the high-frequency experimental absorption maxima from the calculated curves is more than the experimental error (0.1 cm⁻¹). This small discrepancy cannot be explained by imperfect alignment of the crystallites. It is

more likely due to the assumption of an isotropic g -factor made in Eq. (2).

Another compound in this series, $((C_2H_5)_2NCS_2)_2 Fe(III) Cl$, has been shown⁴⁹ to be a ferromagnet with a low transition temperature $T_c = 2.43^\circ K$. Mössbauer resonance data for this complex in the paramagnetic state have indicated that $D < 0$. Our zero-field spectra for this compound at $4.2^\circ K$ showed only a very weak, broad absorption in the range 2.5 to 5 cm^{-1} , in contrast to the sharp (half width $\sim 0.4\text{ cm}^{-1}$) absorptions observed for other complexes in this series. The large width of the zero-field resonance is probably due to the effects of exchange broadening, since the Heisenberg exchange coupling parameter J is of the same order as D (see Appendix F). For $T = 1.3^\circ K$, the spectra showed a sharp ferromagnetic resonance absorption at 3.85 cm^{-1} in zero field. The zero-field resonance frequency is related to the anisotropy of the iron environment which is reflected in the strong axial ligand field. A simple classical calculation, suggested by Dr. A. M. Portis,⁵² can be used to derive the relationship between the zero field resonance frequency at $T = 0$, ν_0 , and D . This calculation, given in Appendix G, obtains the effective anisotropy field H_A at $T=0$ due to the axial term in the spin Hamiltonian by expanding it in a power series in the polar angle. The result, for $D < 0$, is $\nu_0 = 2|D|S$. This expression, which is exact in the limit of large spin, must be corrected by the factor⁵³ $\eta = (1-1/(2S))$. Thus, for spin $S = 3/2$, $\nu_0 = 2|D|$. In this case, the zero-field resonance should broaden, and the absorption maximum may shift, as T approaches T_c (see the discussion in Appendix G). Our measurements, obtained for temperatures between 1.3 and $2.3^\circ K$, showed

a progressive broadening and a decrease of only $\sim 0.05 \text{ cm}^{-1}$. We have therefore taken $2|D| = 3.85 \text{ cm}^{-1}$. Data obtained from the spectra for a polycrystalline sample of this compound at $T = 1.3^\circ\text{K}$ are shown in Fig. 17. The observed absorption maxima lie close to the line $\nu = 2\mu_{\text{B}}H + 3.85 \text{ cm}^{-1}$, which corresponds to an orientation of $\vec{H} \parallel \hat{z}$ (or $\vec{H} \parallel \vec{H}_{\text{A}}$). These observations are consistent with the simple theory of ferromagnetic resonance⁵⁴ and with the effects of the expected large magnetic torque.

The ferromagnetic coupling in this complex presumably arises from a super-exchange interaction via the sulfur atoms of neighboring molecules, which lie at normal Van der Waals distances.⁴⁵ This observation is interesting in the light of recent measurements on the iron-sulfur protein spinach ferridoxin⁵⁵ which indicate that the two iron atoms in this compound are antiferromagnetically coupled at low temperatures.

The similarity of the chemical and macroscopic properties of the bis dithiocarbamates indicates that they form an isostructural series obtained by substitution of either the halide ligand or the alkyl groups. As an example of the effects of such a substitution, we have listed in Table IV the change in the zero field splitting on substitution of a chloro ligand for a bromo ligand for a fixed alkyl group. This quantity, $\Delta_{\text{Br}} - \Delta_{\text{Cl}}$, is nearly independent of the dithiocarbamate ligand for the first two pairs of complexes, which implies that the effect of alkyl group substitution upon Δ is either small or independent of the halide ligand. However, $\Delta_{\text{Br}} - \Delta_{\text{Cl}}$ for the pyrrolidynyl derivatives is very different, indicating a substantially different bonding in these complexes. This effect may be due to a greater degree of π -bonding for the

pyrrolidynyl derivatives because of the existence of a pseudo-ring structure including the nitrogen atom. A similar effect may explain the temperature-independent high spin magnetic moment of tris (pyrrolidyl dithiocarbamate) Fe(III), discussed in Section IV-B, compared with the temperature-dependent magnetic moments of the other tris dithiocarbamates.

All of the compounds investigated also showed an increase in the algebraic value of D upon substitution of bromo for chloro ligands for a fixed dithiocarbamate ligand. As discussed in Section IV-D, similar effects are observed in the Fe(III) and Mn(III) porphyrins. Furthermore, we may compare the values of D obtained for the bis Fe(III) dithiocarbamates with the quadrupole splitting ΔE_Q , obtained from Mössbauer effect measurements, which is also listed in Table IV. Since ΔE_Q and D both depend upon the strength and asymmetry of the ligand field, we might expect a correlation between them. This comparison has been made for the Fe(III) porphyrins,³⁷ where an approximately linear variation of ΔE_Q with D, passing through the origin, is observed. Our data clearly eliminates such a correlation for the bis dithiocarbamates, but does not discriminate against other possible zero-intercept functions. For example, the data can be fit to a saturating function of D with either even or odd parity. Mössbauer resonance and far-infrared measurements on the fluoride and iodide complexes would help to clarify this point.

G. Additional Spectral Features

A number of the compounds investigated in this study showed additional sharp structure which was not magnetic field-dependent. These absorptions were typically at higher frequencies than the observed paramagnetic resonances, and were stronger by factors ranging from

approximately two to ten. In general, more sharp lines were observed in the spectra of compounds with relatively small molecular weight, such as the bis Fe(III) dithiocarbamates, than in the spectra for the large biological molecules. However, all of the compounds showed the broad high-frequency attenuation discussed in Section III.

In most cases, the samples used for the magnetic resonance measurements did not transmit sufficient far-infrared radiation to observe such absorptions at frequencies above approximately 30 cm^{-1} . In order to investigate these absorptions in $((\text{C}_2\text{H}_5)_2\text{NCS}_2)_2\text{Fe(III) Br}$, we measured the far-infrared spectrum of a thin polycrystalline sample at $T = 4.2^\circ\text{K}$. The spectrum obtained in zero applied field is shown in Fig. 18. Although the linewidths and strengths of the observed absorptions are typical, the number of observed lines is not. For example, similar measurements on another bis Fe(III) dithiocarbamate, $((i\text{-C}_3\text{H}_7)_2\text{NCS}_2)_2\text{Fe(III) Cl}$, showed only one such absorption in the same frequency interval. The frequencies of the absorption maxima for several compounds, obtained from the far-infrared spectra at 4.2°K , are listed in Table V. It is interesting to note that a sharp absorption (width $\sim 0.75 \text{ cm}^{-1}$) was observed at 8.9 cm^{-1} in the spectra for the fluoro derivative of ferri-myoglobin. The strength of this absorption was approximately twice that of the zero-field magnetic resonance. In addition, we have included data from preliminary measurements on phenoxo deuteroporphyrin IX dimethyl ester Mn(III). High-temperature spectra for this compound show an increase in the strength of the field-independent absorptions for temperatures up to 77°K .

Although we have not investigated the source of the additional structure in the far-infrared spectra of these compounds, our observations suggest that they are due to transitions between excited molecular vibration states. The linewidths are much too small for absorptions due to lattice vibrations. The temperature dependence of the structure in the manganese deuteroporphyrin compound indicates that the transitions observed are between excited states. In addition, the structure depends strongly upon changes in ligands within a series of similar compounds. Finally, the observed strengths indicate that the absorptions are due to electric quadrupole transitions, rather than electric dipole transitions.

V. CONCLUSIONS

Our measurements have shown that far-infrared spectroscopic techniques offer a direct method for the investigation of the effects of large axial and rhombic ligand fields upon paramagnetic ions in molecules. The polycrystalline magnetic resonance absorptions observed are consistent with the predictions of a wide variety of cases of the simple spin Hamiltonian of Eq. (2). We have directly obtained values of the axial ligand field parameter D from the spectra for twenty-one compounds, and have measured $\lambda \equiv E/D$ for several substances with a large rhombic ligand field. In addition, our investigation has shown that such detailed information can also be obtained for paramagnetic ions in intact biological molecules.

APPENDICES

A. Polycrystalline Magnetic Dipole Absorption

In this appendix, we shall derive the form of the polycrystalline absorption coefficient $\bar{\alpha}$ for magnetic dipole transitions between states of an orbitally non-degenerate term described by the spin Hamiltonian of Eq. (2). The derivation of α in the first section parallels a derivation of the electric dipole absorption coefficient given by J. S. Griffith in The Theory of Transition Metal Ions (Cambridge University Press, London, 1961), chapter 3.

1. Derivation of the Expression for α

The transition probability per unit time \mathcal{R}_{if} between two states ψ_i and ψ_f due to a perturbation Hamiltonian \mathcal{H}_p is given by Fermi's Golden Rule

$$\mathcal{R}_{if} = \frac{2\pi}{\hbar} \rho(E_f) |M_{if}|^2 \quad (\text{A1})$$

where $\rho(E_f)$ is the density of final states in energy, and M_{if} is a matrix element given by

$$M_{if} \equiv \langle \psi_f | \mathcal{H}_p | \psi_i \rangle. \quad (\text{A2})$$

In the case of the interaction of an electromagnetic wave with an atom or ion with N electrons of momentum \vec{P}_j , the classical perturbation Hamiltonian may be written

$$\mathcal{H}_p = \frac{e}{mc} \sum_{j=1}^N \sum_{\beta} (q_{\beta} \tilde{A}_{j\beta} \cdot \tilde{P}_j + q_{\beta}^* \tilde{A}_{j\beta}^* \cdot \tilde{P}_j) \quad (A3)$$

where we have "quantized" the electromagnetic field into modes with vector potential $\tilde{A}_{j\beta}$ at the position of the j -th electron. The * indicates the complex conjugate. The total vector potential \tilde{A} of the radiation field is given by

$$\tilde{A} = \sum_{\beta} \tilde{A}_{\beta} q_{\beta} + \sum_{\beta} \tilde{A}_{\beta}^* q_{\beta}^*$$

where \tilde{A}_{β} and q_{β} are respectively functions of space and time only:

$$\tilde{A}_{\beta} = \left(\frac{4\pi c^2}{V} \right)^{1/2} \hat{n}_{\beta} \exp(ik_{\beta} \cdot r) \quad (A4)$$

and

$$q_{\beta} = |q_{\beta}| \exp(-i\omega_{\beta} t) \quad (A5)$$

where V is the volume of space over which the (periodic) boundary conditions are applied, \hat{n}_{β} is the direction of polarization of the radiation mode β , ω_{β} is its angular frequency, and k_{β} its wave vector.

The quantum-mechanical perturbation Hamiltonian is obtained by replacing the functions q_{β} , q_{β}^* by the corresponding operators q_{β} and \bar{q}_{β} , where the radiation field alone for one mode is described by

$$\mathcal{H}_{\beta} = 2\omega_{\beta} \bar{q}_{\beta} q_{\beta} \quad (A6)$$

and

$$[\bar{q}_\beta, q_\beta] = -\frac{\hbar}{2\omega_\beta}. \quad (A7)$$

The operators q_β and \bar{q}_β now correspond to photon annihilation and creation operators, respectively. We write

$$|\psi_i\rangle = |n_{i\beta}\rangle |a_i\rangle, \quad \langle\psi_f| = \langle n_{f\beta}| \langle a_f|$$

where $|n_\beta\rangle$ is an eigenstate of the radiation field with n photons of mode β and $|a\rangle$ is an atomic state. The matrix element Eq. (A2) becomes

$$M_{if} = \frac{e}{mc} \sum_{j=1}^N \sum_{\beta} \langle a_f | \langle n_{f\beta} | (q_{\beta} \cdot \hat{p}_j + \bar{q}_{\beta} \cdot \hat{p}_j) | n_{i\beta} \rangle | a_i \rangle. \quad (A8)$$

For the absorption of one photon of mode β , $n_{f\beta} = n_{i\beta} - 1$, and since

$$\langle n_{\beta} - 1 | \bar{q}_{\beta} | n_{\beta} \rangle = 0$$

and

$$\langle n_{\beta} - 1 | q_{\beta} | n_{\beta} \rangle = \left(\frac{n_{\beta} \hbar}{2\omega_{\beta}} \right)^{1/2}$$

the matrix element Eq. (A8) becomes, for a single mode,

$$M_{if}^{\beta} = \frac{e}{mc} \left(\frac{4\pi c^2 n_{\beta} \hbar}{2\omega_{\beta} V} \right)^{1/2} \sum_{j=1}^N \langle a_f | \hat{p}_j \cdot \hat{\pi}_{\beta} \exp(i \mathbf{k}_{\beta} \cdot \mathbf{r}_j) | a_i \rangle. \quad (A9)$$

Since the maximum value of $\mathbf{k}_{\beta} \cdot \mathbf{r}_j$ is

$$|\mathbf{k}_{\beta} \cdot \mathbf{r}_j|_{\max} = \frac{\omega_{\beta} r_j}{c} = 2\pi\nu_{\beta} (\text{cm}^{-1}) r_j$$

$$\approx 2\pi \times 10 \times 10^{-8} \approx 10^{-6}$$

we may expand the exponential in M_{if}^{β} :

$$\exp(i\mathbf{k}_{\beta} \cdot \mathbf{r}_j) \approx 1 + i(\mathbf{k}_{\beta} \cdot \mathbf{r}_j)$$

The first term leads to the well-known electric dipole absorption, which we shall not consider. The second term leads to a matrix element of the operator $(\mathbf{k}_{\beta} \cdot \mathbf{r}_j)(\mathbf{P}_j \cdot \hat{\pi}_{\beta})$ which may be expanded

$$(\mathbf{k}_{\beta} \cdot \mathbf{r}_j)(\mathbf{P}_j \cdot \hat{\pi}_{\beta}) = \frac{1}{2} \mathbf{k}_{\beta} \times \hat{\pi}_{\beta} \cdot \mathbf{l}_j$$

+ electric quadrupole term

where \mathbf{l}_j is the angular momentum of the j -th electron. The inclusion of the electronic spin \mathbf{s}_j leads to a similar term in $\mathbf{k}_{\beta} \times \hat{\pi}_{\beta} \cdot \mathbf{s}_j$, and the matrix element Eq. (A9) with this addition becomes, for a magnetic dipole transition,

$$M_{if}^{\beta} = \frac{i}{2} \left\{ \frac{e}{mc} \left(\frac{4\pi c^2 n_{\beta} \hbar}{2\omega_{\beta} V} \right)^{1/2} \langle a_f | \mathbf{k}_{\beta} \times \hat{\pi}_{\beta} \cdot \sum_j (\mathbf{l}_j + 2\mathbf{s}_j) | a_i \rangle \right\} \quad (\text{A10})$$

For an orbitally non-degenerate ground term,

$$\langle \sum_j \mathbf{l}_j \rangle = 0, \quad \langle \sum_j \mathbf{s}_j \rangle = \mathbf{S}$$

where \mathbf{S} is the total spin, and Eq. (A10) reduces to

$$M_{if}^{\beta} = i \left\{ \frac{e}{mc} \left(\frac{4\pi c^2 n_{\beta} \hbar}{2\omega_{\beta} V} \right)^{1/2} \langle a_f | \mathbf{k}_{\beta} \times \hat{\pi}_{\beta} \cdot \mathbf{S} | a_i \rangle \right\}$$

If we define

$$\mathbf{k}_{\beta} \equiv \frac{\omega_{\beta}}{c} \hat{\mathbf{k}}_{\beta}$$

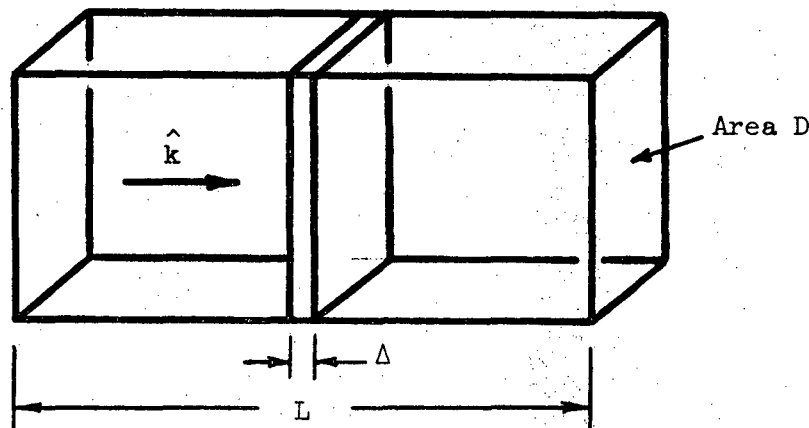
where $\hat{\mathbf{k}}_{\beta}$ is a unit vector in the direction of propagation of the radiation,

we can finally write

$$|M_{if}^{\beta}|^2 = \frac{2\pi e^2 n_{\beta} \hbar \omega_{\beta}}{m^2 c^2 V} |\langle a_f | \hat{\mathbf{k}}_{\beta} \times \hat{\pi}_{\beta} \cdot \mathbf{S} | a_i \rangle|^2 \quad (\text{A11})$$

This is a reasonable form, since $\hat{k} \times \vec{A}_\beta$ is in the direction of the magnetic vector of the perturbing radiation. At this point, we shall drop the mode index β , and continue the calculation under the assumption that only photon absorption processes from particular modes are included.

The absorption coefficient is defined as the power absorbed per unit length from a radiation beam of unit intensity passing through a substance. In order to calculate this quantity, we assume the boundary conditions indicated in the following figure:



A sheet of infinitesimal thickness Δ containing N_0 absorbing atoms per unit volume is positioned normal to the propagation vector of the radiation field, in periodic boundary conditions defined by the box shown of length L and cross-sectional area D . We wish to calculate the power P_1 absorbed in the thin sheet; the absorption coefficient α is then defined by

$$\alpha \equiv \frac{P_1}{P_0 \Delta} \quad (A12)$$

where P_0 is the incident power. We assume that

$$\vec{A} = \left(\frac{4\pi c^2}{LD} \right)^{1/2} \hat{u} \left(q \exp(i\vec{k} \cdot \vec{r}) + \text{C.C.} \right) \quad (A13)$$

and that Δ is so small that the absorbing atoms are bathed in the same radiation. We also write

$$\rho(E_f) = \frac{1}{\hbar} \rho(\omega - \omega_{if})$$

It is easy to show that

$$P_o = \frac{1}{L} n \hbar \omega c$$

and

$$P_l = \hbar \omega \mathcal{R}_{if} N_o$$

Using the expression for \mathcal{R}_{if} , Eq. (A1), and the equation for $|M_{if}|^2$, Eq. (A11), the expression for α_{if} , the absorption coefficient for one transition, is

$$\alpha_{if} = \frac{4\pi^2 \rho(\omega - \omega_{if}) \omega N_o e^2}{\hbar m^2 c^3} |\langle a_f | \hat{k} \times \hat{n} \cdot \tilde{S} | a_i \rangle|^2 \quad (A14)$$

This expression can be written in the form of Eq. (3) by labeling each possible transition by an index n and observing that

$$\omega \rho(\omega - \omega_{if}) \equiv \omega \rho(\omega - \omega_n) = \nu \rho(\nu - \nu_n)$$

where ν is the frequency in any appropriate units. Then

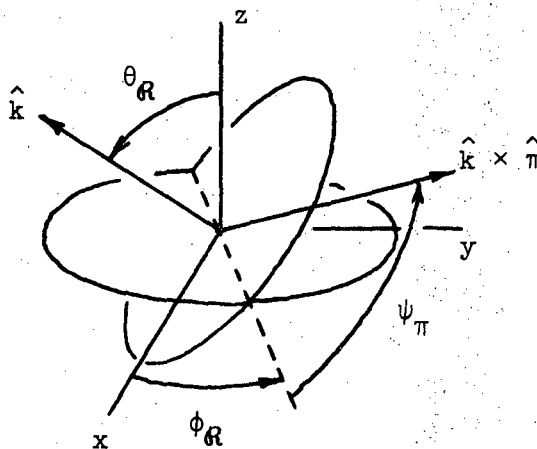
$$\alpha_n = \frac{4\pi^2 e^2 N_o}{\hbar m^2 c^3} \nu \rho(\nu - \nu_n) |\langle f_n | \hat{k} \times \hat{n} \cdot \tilde{S} | i_n \rangle|^2 \quad (A15)$$

2. Derivation of the Expression for $\bar{\alpha}$

In order to obtain the polycrystalline average absorption coefficient $\bar{\alpha}_n$ we must average α_n over the direction of \hat{k} and \hat{n} , which are expressly indicated in Eq. (A15), and over the direction of the external magnetic field H in the spin Hamiltonian of Eq. (2), which enters into Eq. (A15) through the states $|i_n\rangle$ and $|f_n\rangle$. In general, these averages are not independent. For example, if $\hat{k} \parallel H$, the averages are related through this constraint. However, if the incident radiation is not parallel

and is strongly scattered by a sample placed in a transmission cavity, we may assume that \hat{k} is randomly oriented with respect to both \hat{H} and the coordinate system in which the spin Hamiltonian is written. If, in addition, the radiation is unpolarized, the three averages can be taken independently. Both of these conditions hold to a good approximation in the experiments described in this paper.

The first two averages may be performed analytically because of the explicit dependence of the operator $\hat{k} \times \hat{\pi} \cdot \hat{S}$ on the directions of \hat{k} and $\hat{\pi}$. The orientation of these two vectors with respect to the axes of the spin Hamiltonian is specified in the following figure:



We have chosen the angles θ_R , ϕ_R , and ψ_π to be Euler angles, as defined by Herbert Goldstein, Classical Mechanics (Addison Wesley Publishing Company, Inc., Reading, Massachusetts, 1950).

Using these angles and the transformation matrix (Goldstein, p. 109), we may write the matrix element in Eq. (A15) as

$$\begin{aligned}
 \langle f_n | \hat{k} \times \hat{n} \cdot \mathbf{S} | i_n \rangle &= [\cos \psi_\pi \cos \phi_\alpha - \cos \theta_\alpha \sin \phi_\alpha \sin \psi_\pi] \langle S_x \rangle_n \\
 &+ [\cos \psi_\pi \sin \phi_\alpha + \cos \theta_\alpha \cos \phi_\alpha \sin \psi_\pi] \langle S_y \rangle_n \\
 &+ [\sin \theta_\alpha \sin \psi_\pi] \langle S_z \rangle_n
 \end{aligned} \tag{A16}$$

where we have defined

$$\langle S_x \rangle_n \equiv \langle f_n | S_x | i_n \rangle$$

The square of Eq. (A16) contains a number of cross terms as well as terms like $|\langle S_x \rangle_n|^2$. However, upon integrating, all of the cross terms vanish, and the result for the average over \hat{k} and \hat{n} is

$$\begin{aligned}
 \langle f_n | \hat{k} \times \hat{n} \cdot \mathbf{S} | i_n \rangle_{\text{ave}}^2 &= \frac{1}{3} \{ |\langle S_x \rangle_n|^2 + |\langle S_y \rangle_n|^2 + |\langle S_z \rangle_n|^2 \} \\
 &\equiv W_n
 \end{aligned} \tag{A17}$$

which is a very reasonable form.

The transition probability between two states $|i_n\rangle$ and $|f_n\rangle$ is also proportional to the difference in thermal populations of the two states,

$$P_n(T) = \frac{\exp(-E_{i_n}/kT) - \exp(-E_{f_n}/kT)}{\sum_i \exp(-E_i/kT)} \tag{A18}$$

where E_i is the eigenvalue of the spin Hamiltonian for state $|i\rangle$. Since $P_n(T)$ depends upon the eigenvalues and therefore upon the orientation of \mathbf{H} , it must be included in the remaining average. We may then write the following expression for the polycrystalline average of Eq. (A15), including all transitions

$$\bar{\alpha}(\nu) = \frac{\pi N e^2 \nu}{\hbar m^2 c^3} \sum_n \int [\rho(\nu - \nu_n) P_n(T) W_n] d\Omega_H \tag{A19}$$

where

$$d\Omega_H = \sin \theta_H d\theta_H d\phi_H$$

and θ_H and ϕ_H are respectively the polar and azimuthal angles of \mathbf{H} with respect to the spin Hamiltonian axes.

B. Calculation of the Polycrystalline Absorption Coefficient

In this appendix, we shall briefly describe the calculation techniques used to evaluate the polycrystalline average absorption coefficient $\bar{\alpha}$, derived in Appendix A, for the case $S = 3/2$. We shall also include a discussion of the program SHAZAM, written for the CDC 6600 computer, which performs the calculation.

1. Calculation Techniques

We have evaluated the modified form of $\bar{\alpha}$

$$\bar{\alpha}(\nu) = \frac{1}{4\pi} \sum_n \int [v_n \rho(\nu - \nu_n, \Delta) P_n(T) W_n] d\Omega_H \quad (B1)$$

where the numerical factors have been eliminated. The transition frequency ν_n has been substituted for ν since the absorption coefficient for each n is large only at frequencies $\nu \approx \nu_n$. Finally, the assumed Gaussian lineshape function ρ now explicitly depends upon a linewidth parameter Δ , defined as the half width at half maximum. The definitions of the ladder operators

$$S_+ \equiv S_x + iS_y$$

$$S_- \equiv S_x - iS_y$$

can be used to rewrite W_n in terms of matrix elements of S_+ , S_- , and S_z , and symmetry considerations imply that the integral in Eq. (B1) need only be evaluated over the first octant in θ_H and ϕ_H . Finally, for $S = 3/2$ there are in general four separate energy eigenfunctions and therefore six distinct transitions of index n . With these observations, Eq. (B1) becomes

$$\bar{\alpha}(\nu) = \frac{2}{3\pi} \sum_{n=1}^6 \int_0^{\frac{\pi}{2}} d\phi_H \int_0^{\frac{\pi}{2}} d\theta_H \left\{ \nu_n \rho(\nu - \nu_n, \Delta) P_n(T) \sin \theta_H \cdot \left[\frac{1}{2} |\langle S_+ \rangle_n|^2 + \frac{1}{2} |\langle S_- \rangle_n|^2 + |\langle S_z \rangle_n|^2 \right] \right\} \quad (B2)$$

The integrand in Eq. (B2) is an exceedingly complex function of the parameters ν , H , D , E , T , Δ , θ_H and ϕ_H . Furthermore, since the evaluation of the integrand for a particular pair of values (θ_H, ϕ_H) involves diagonalization of the 4×4 spin Hamiltonian matrix, straightforward integration of $\bar{\alpha}$ is a very time-consuming process, even on the highest speed computers presently available. We have therefore used several specialized calculational techniques which can greatly reduce the required computation time.

The calculation of $\bar{\alpha}$ can easily be divided into six separate calculations, one for each transition. This division reduces the complexity of the calculation, and has the added advantage that the contribution of each transition to the total lineshape is explicitly obtained. We shall describe one of these calculations of $\bar{\alpha}_n$ in detail to illustrate the methods employed in the program SHAZAM.

We use as input parameters the values of H , D , E , T , and Δ . For specified values of H , D , and E , we may construct a surface, defined by the value of ν_n as a function of θ_H and ϕ_H , by obtaining the eigenvalues of the spin Hamiltonian for a net of values of θ_H and ϕ_H and computing the energy difference which corresponds to the transition n . The absorption coefficient $\bar{\alpha}_n(\nu)$ will only have appreciable values for frequencies ν which lie between the minimum and maximum values of ν_n

over this surface. (In fact, since a lineshape is included, the appropriate limits are approximately $v_n^{\min} - 2\Delta$ to $v_n^{\max} + 2\Delta$.) For a given v in this range, the integrand of Eq. (B2) will be a sharply peaked function of θ_H for a given ϕ_H . Conventional integration techniques converge slowly for such functions, since the general approach is to subdivide the entire integration interval into an increasing number of equal divisions. With such methods, a large amount of time is spent evaluating the integrand at points where it is nearly zero. This disadvantage has been avoided in our calculations by determining the region of (θ_H, ϕ_H) where the integrand is appreciable, and using the limits of this region to define the integration interval. This corresponds to determining the (θ_H, ϕ_H) region between the intersection of planes at $v_n = v \pm \gamma \cdot \Delta$ with the v_n surface, where γ is a parameter that may be adjusted until the desired accuracy is obtained. Since a scan of this kind need not be made over ϕ_H for small E , we have used a single calculation for $\phi_H = 0$ to determine the limits of integration; for large E , provision has been made to integrate over the entire θ_H range. In addition, we have included a calculation of $P_n(T)$ over the (θ_H, ϕ_H) net for all n corresponding to transitions from excited states. Whenever the maximum value of $P_n(T)$ is less than a specified minimum value, no calculation of $\bar{\alpha}_n$ is made. Finally, in order to concentrate on frequency regions where $\bar{\alpha}_n$ is rapidly varying, the calculation has been arranged so that input data may specify a range of frequency and number of frequencies to be calculated within that range for any transition.

These techniques have reduced the time required for an accurate

calculation of $\bar{\alpha}_n$ with high resolution by about a factor of fifty. The results of the calculation for each transition and frequency for the specified set of input parameters H, D, E, T, and Δ are then used as input data to a short program, POST, which interpolates and adds them to give the total absorption coefficient, $\bar{\alpha}(\nu)$.

2. Program SHAZAM

The program SHAZAM (Spin Hamiltonian Averaged Zeeman Absorption: Magnetic-dipole) was written to perform the calculation of $\bar{\alpha}_n$ for $S=3/2$ according to the methods described in the preceding section. An extensively annotated listing of the program SHAZAM and a listing of the program POST are included at the end of this section. Also, a flow chart of the main subroutine of SHAZAM, ABSRBNC, is given in Fig. B1. The compiled field length of the listed version of SHAZAM on the Lawrence Radiation Laboratory CDC 6600 computer is 54300_8 , and the execution length is approximately 30000_8 . Approximately 20 decimal seconds are required to compile the program and to generate all of the transition tables, and the calculation of $\bar{\alpha}_n(\nu)$ for a single frequency requires approximately 1.5-3. decimal seconds. To avoid duplicate calculation of the transition tables, they are transferred to a tape and subsequently punched or stored on a disk. Further calculations for the same input parameters (H,E,D,T, Δ) can then make use of the stored tables. This option is exercised by placing a card with READ TABLES in the first 11 columns anywhere in the parameter input string, which contains a card each for H,E,D,T,DELTA, and PMIN in any order according to the format specified in the program. The tables supplied by an earlier run are then appended as the last cards in the deck. Otherwise,

a card with TABLES in the first six columns causes transition tables for the specified parameters to be generated. Finally, if integration over the entire range of θ_H is desired for a large input value of E, a card with $\theta_T \theta_{PI}/2$ in the first seven columns should be inserted in the input parameter card string.

If a card with zero in the first column immediately follows the parameter input cards, a standard integration of five frequencies for each transition, equally spaced over the entire frequency range for that transition. If any other character appears in this column, SHAZAM reads cards containing a transition index, frequency range, and number of points to be calculated within that range. The format is specified in the program. For each transition (the transition index is defined in a note in the program), the value of PMUMAX, the maximum value of $P_n(T)$ for the transition, is compared with the input value PMIN. If PMUMAX is less than PMIN, no calculation for that transition is performed. Finally, when a zero is encountered in column one, the calculation ends. Some examples of the results of the calculation with SHAZAM are shown in Fig. 3.

C		SHAZAM.
C		SHAZAM.
	PROGRAM SHAZAM(INPUT=401,OUTPUT,TAPE4=401,TAPE5)	SHAZAM.
C		SHAZAM.
C		SHAZAM.
*	PROGRAM SHAZAM CALCULATES THE POWDER AVERAGE MAGNETIC DIPOLE	SHAZAM.
*	ABSORPTION OF A SYSTEM DESCRIBED BY THE APPROXIMATE SPIN	SHAZAM.
*	HAMILTONIAN	SHAZAM.
*		SHAZAM.
*	(H) = GB H*S + D(S(Z)**2 - 1/3(S(S+1))) + E(S(X)**2 - S(Y)**2)	SHAZAM.
*		SHAZAM.
*	WHERE S = 3/2 AND THE INPUT PARAMETERS ARE	SHAZAM.
*		SHAZAM.
*	H = EXTERNAL MAGNETIC FIELD IN UNITS OF AMPERES THROUGH A	SHAZAM.
*	SUPERCONDUCTING SOLENOID WITH H(KOE) = 3.48 * I(AMP)	SHAZAM.
*	D = TETRAGONAL CRYSTAL FIELD PARAMETER IN UNITS OF CM**-1	SHAZAM.
C	E = RHOMBIC CRYSTAL FIELD PARAMETER IN UNITS OF CM**-1	MODS.1
*		SHAZAM.
*	FURTHER INPUT PARAMETERS ARE	SHAZAM.
*		SHAZAM.
*	T = TEMPERATURE OF SYSTEM IN DEGREES KELVIN	SHAZAM.
*	DELTA = HALF WIDTH AT HALF MAXIMUM OF H = 0 TRANSITION	SHAZAM.
*		SHAZAM.
*	THE FOLLOWING ASSUMPTIONS ARE MADE IN THE CALCULATION	SHAZAM.
*		SHAZAM.
*	(1) THE HAMILTONIAN IS WRITTEN IN A COORDINATE SYSTEM FIXED IN	SHAZAM.
*	THE CRYSTALLITE, AND THE CALCULATED ABSORPTION IS FOR A SAMPLE	SHAZAM.
*	OF CRYSTALLITES WITH RANDOM ORIENTATION TO THE EXTERNAL MAGNETIC	SHAZAM.
*	FIELD, H.	SHAZAM.
*	(2) LARGE SCATTERING OF THE INCIDENT RADIATION WITHIN THE	SHAZAM.
*	SAMPLE IS ASSUMED-- THAT IS, THE DIRECTION OF PROPAGATION OF THE	SHAZAM.
*	PERTURBING LIGHT IS ASSUMED TO BE RANDOMLY ORIENTED WITH RESPECT	SHAZAM.
*	TO THE EXTERNAL MAGNETIC FIELD, H.	SHAZAM.
*	(3) INDIVIDUAL TRANSITIONS ARE UNIFORMLY ASSUMED TO HAVE A	SHAZAM.
*	GAUSSIAN LINE SHAPE DUE TO SITE INHOMOGENEITY. THE HALF WIDTH	SHAZAM.
*	AT HALF MAXIMUM IS ASSUMED TO BE DELTA FOR ALL TRANSITIONS. THE	SHAZAM.
*	LINE SHAPE FUNCTION HAS BEEN NORMALIZED SO THAT THE TOTAL ABSORPTION	SHAZAM.
*	FOR A TRANSITION IS INDEPENDENT OF DELTA.	SHAZAM.
*	(4) THE G-FACTOR IS ASSUMED TO BE ISOTROPIC WITH A VALUE G = 2.00	SHAZAM.
C	(5) THE THERMAL ENERGY KT IS ASSUMED TO BE OF THE	SHAZAM.
C	ORDER OF D, SO THAT THE THERMAL POPULATION OF THE INITIAL	SHAZAM.
C	STATE OF A TRANSITION MU, P(MU, T), MUST BE INCLUDED	SHAZAM.
C	IN THE CALCULATION VIA THE DENSITY OF INITIAL STATES.	SHAZAM.
C		SHAZAM.
C		SHAZAM.
	CALL ABSRBNC	SHAZAM.
98	FORMAT(15F8.3)	SHAZAM.
	CALL EXIT	SHAZAM.
	END	SHAZAM.
	SUBROUTINE ABSRBNC	SHAZAM.
C		SHAZAM.
C		SHAZAM.
C		SHAZAM.
C	SUBROUTINE ABSRBNC (ABSORBANCE) IS THE MAIN CONTROL	SHAZAM.
C	ROUTINE FOR SHAZAM. IT CALLS ALL OF THE NECESSARY	SHAZAM.


```
C      MU = 6                      W(4) TO W(3)                      SHAZAM.
C                                                                              SHAZAM.
C                                                                              SHAZAM.
C      IF(MU .NE. 6) GO TO 155                      SHAZAM.
C      PRINT 901                      SHAZAM.
901    FORMAT( / * ITH,JPHI *                      SHAZAM.
* *E-NDX*                      SHAZAM.
* * MU * 4X 6THETA ,6X,4HPHI ,10X10EIGENVALUE ,    SHAZAM.
* 10X 5H 3/2 ,5X 5H 1/2 , 5X 5H-1/2 ,5X 5H-3/2 )    SHAZAM.
155    CONTINUE                      SHAZAM.
C                                                                              SHAZAM.
C      THE MINIMUM AND MAXIMUM OF EIG(MU) ARE PRINTED OUT    SHAZAM.
C      LATER, AS EIGMIN AND EIGMAX.  HERE THEY ARE INITIALIZED.  SHAZAM.
C                                                                              SHAZAM.
C      EIGMAX(MU)=0                      SHAZAM.
C      EIGMIN(MU)=1.E5                      SHAZAM.
C                                                                              SHAZAM.
C                                                                              SHAZAM.
C                                                                              SHAZAM.
C      IMU AND JMU ARE THE INDICES OF THE INITIAL AND FINAL    SHAZAM.
C      STATES FOR TRANSITION MU.  THEY ARE DEFINED IN A DATA    SHAZAM.
C      STATEMENT IN FUNCTION FNCTN, AS IN THE TABLE ABOVE, AND    SHAZAM.
C      STORED IN A COMMON BLOCK, IMUJMU.                      SHAZAM.
C                                                                              SHAZAM.
C      IMU = IMUT(MU)                      SHAZAM.
C      JMU = JMUT(MU)                      SHAZAM.
C                                                                              SHAZAM.
C      GENERATE EIG, PHITAB, THTAB.  PHITAB AND THTAB ARE    SHAZAM.
C      TABLES OF THE PHI(H), THETA(H) VALUES FOR WHICH THE    SHAZAM.
C      TRANSITION FREQUENCIES ARE EVALUATED.                      SHAZAM.
C                                                                              SHAZAM.
C      DO 140  JPHI= 1,5                      SHAZAM.
C      PHI = 0 + (JPHI-1)* DELPHI                      SHAZAM.
C      PHITAB(JPHI) = PHI                      SHAZAM.
C      COSPHI = COS(PHI)                      SHAZAM.
C      SINPHI = SIN(PHI)                      SHAZAM.
C      DO 180  ITH = 1,29                      SHAZAM.
C      ITAB(ITH,JPHI,MU)=ITH                      SHAZAM.
C      TH = 0 +(ITH-1)* DELTH                      SHAZAM.
C      THTAB(ITH) = TH                      SHAZAM.
C      COSTH = COS(TH)                      SHAZAM.
C      SINTH = SIN(TH)                      SHAZAM.
C                                                                              SHAZAM.
C                                                                              SHAZAM.
C      SUBROUTINE HERMIT SETS UP THE HAMILTONIAN MATRIX AND CALLS THE    SHAZAM.
C      ROUTINES THAT GENERATE THE EIGENVALUES AND EIGENVECTORS.    SHAZAM.
C      SUBROUTINE EIGVCTR PRINTS THE INDEX NUMBERS OF THETA(H)    SHAZAM.
C      AND PHI(H), THE ANGLES, THE EIGENVALUE INDEX AND    SHAZAM.
C      EIGENVALUE, AND THEIR RESPECTIVE EIGENVECTORS.  EIGVCTR    SHAZAM.
C      ONLY PRINTS OUT FOR TRANSITION INDEX MU = 6.                      SHAZAM.
C                                                                              SHAZAM.
C                                                                              SHAZAM.
C      EIG IS THE TRANSITION TABLE, USED TO DETERMINE THE LIMITS    SHAZAM.
C      OF INTEGRATION IN THETA(H) FOR A GIVEN TRANSITION INDEX    SHAZAM.
C      MU AND FREQUENCY OMEGA.  THE LIMITS ARE FOUND BY    SHAZAM.
C      DETERMINING THE INTERVAL OF THETA(H) WHERE EIG(MU) LIES    SHAZAM.
C      BETWEEN OMEGA PLUS OR MINUS 2.*DELTA.                      SHAZAM.
C      THIS IS THE REGION OF THETA(H) WHERE THE INTEGRAND (OR    SHAZAM.
C      TRANSITION PROBABILITY) FOR THE SPECIFIED MU CAN BE    SHAZAM.
C      EXPECTED TO BE NON-ZERO.                      SHAZAM.
```



```
C INITIALIZE SHAZAM.
C SHAZAM.
INDEX(MU)=1 SHAZAM.
LOW(1,MU)=1 SHAZAM.
C SHAZAM.
C SCAN SHAZAM.
C SHAZAM.
DO 510 I=3,29 SHAZAM.
SB=SIGN(1.,EIG(I,1,MU)-EIG(I-1,1,MU)) SHAZAM.
IF(SB .EQ. S ) GO TO 505 SHAZAM.
NDX=INDEX(MU) SHAZAM.
LHI(NDX,MU)=I-1 SHAZAM.
LOW(NDX+1,MU) = I-1 SHAZAM.
INDEX(MU)=NDX+1 SHAZAM.
500 S=SB SHAZAM.
GO TO 510 SHAZAM.
505 CONTINUE SHAZAM.
NDX=INDEX(MU) SHAZAM.
LHI(NDX,MU)=29 SHAZAM.
510 CONTINUE SHAZAM.
C SHAZAM.
C PRINT SHAZAM.
C SHAZAM.
PRINT 8010,INDEX(MU),(LOW(KNDX,MU),LHI(KNDX,MU),KNDX=1,NDX) SHAZAM.
8010 FORMAT(* NUMBER OF INTERVAL PARTITIONS = * I5, / SHAZAM.
* * LOW , HI* , / SHAZAM.
* (2I5) ) SHAZAM.
PRINT 8021, EIGMIN(MU), EIGMAX(MU) SHAZAM.
8021 FORMAT(20X,*EIGMIN =*E18.4, * EIGMAX =* E18.4) SHAZAM.
100 CONTINUE SHAZAM.
C SHAZAM.
C SHAZAM.
C SHAZAM.
C SHAZAM.
C THE FOLLOWING PLACES THE TABLES EIG, THTAB, PMUTAB, INDEX, SHAZAM.
C LOW, AND LHI ON TAPE 5, FROM WHICH THEY CAN BE PUNCHED OUT SHAZAM.
C OR STORED ON A DISK FOR SUBSEQUENT DATA-DIRECTED RUNS. SHAZAM.
C SHAZAM.
C SHAZAM.
C SHAZAM.
WRITE(5,801) EIG,THTAB,PMUTAB SHAZAM.
WRITE(5,802) INDEX,LOW,LHI SHAZAM.
801 FORMAT(5E16.6) SHAZAM.
802 FORMAT(8I10) SHAZAM.
ENDFILE 5 SHAZAM.
REWIND 5 SHAZAM.
C SHAZAM.
C SHAZAM.
C SHAZAM.
C WE NOW HAVE THE NECESSARY INFORMATION TO PERFORM THE SHAZAM.
C AVERAGING INTEGRAL FOR EACH TRANSITION IN THE MOST SHAZAM.
C EFFICIENT MANNER, I. E., BY CHOOSING REGIONS OF THETA SHAZAM.
C FOR FREQUENCY OMEGA WHERE TRANSITION MU LIES WITHIN SHAZAM.
C (STDEV) HALF-WIDTHS OF OMEGA. SHAZAM.
C SHAZAM.
C SHAZAM.
125 CONTINUE SHAZAM.
IF(NCNTRL .EQ. 0 ) GO TO 153 SHAZAM.
C SHAZAM.
C SHAZAM.
C SHAZAM.
C SHAZAM.
C IF NCNTRL = 0 THE PROGRAM USES EIG AND THE OTHER TABLES SHAZAM.
```



```
C      ASCENTF (MACHINE LANGUAGE) SUBROUTINE ITBLKP                SHAZAM.
C (TABLE LOOK-UP) IS A BINARY SEARCH ROUTINE.  IN THE FIRST      SHAZAM.
C CALL, IT FINDS THE INDEX, ITBLKP, OF EIGENS BETWEEN NDLOW      SHAZAM.
C AND NDLOW + (ITSIZE-1) WHERE                                    SHAZAM.
C                                                                    SHAZAM.
C EIGENS(ITBLKP) .LE. OMDLA .LT. EIGENS(ITBLKP + 1)             SHAZAM.
C                                                                    SHAZAM.
C THAT IS, IT FINDS THE THETA INDICES OF THE EIG INTERVAL ND    SHAZAM.
C BETWEEN WHICH EIG CROSSES OMDLA = OMEGA - 2.*DELTA.           SHAZAM.
C THEN I1 IS THE LOWER LIMIT THETA INDEX OF THE INTEGRATION     SHAZAM.
C INTERVAL.  I2 SIMILARLY BECOMES THE UPPER LIMIT INDEX.        SHAZAM.
C                                                                    SHAZAM.
C                                                                    SHAZAM.
C      I1=ITBLKP(OMDLA,ITSIZE,EIGENS) + NDLOW -1                 SHAZAM.
C      I2=ITBLKP(OMDELB,ITSIZE,EIGENS) + NDLOW -1                 SHAZAM.
C                                                                    SHAZAM.
C THE FOLLOWING SECTION CHECKS THE INDICES I1 AND I2             SHAZAM.
C AND SETS THE THETA INDICES NTHMIN AND NTHMAX TO THE PROPER    SHAZAM.
C VALUES AS THE SCAN OVER PHI IS MADE.                          SHAZAM.
C                                                                    SHAZAM.
C      IF( I1 .LT. NDLOW) GO TO 516                                SHAZAM.
C      IF( I2 .GE. NDHI ) GO TO 515                                SHAZAM.
C      I2=I2+1                                                    SHAZAM.
512  NTHMIN=MINO(NTHMIN,I1)                                       SHAZAM.
C      NTHMAX=MAX0(NTHMAX,I2)                                       SHAZAM.
C      GO TO 520                                                    SHAZAM.
515  CONTINUE                                                       SHAZAM.
C      IF( I1 .GE. NDHI) GO TO 520                                SHAZAM.
C      I1=MAX0(MINO(I1,NDHI-1),NDLOW)                               SHAZAM.
C      I2=NDHI                                                       SHAZAM.
C      GO TO 512                                                    SHAZAM.
516  CONTINUE                                                       SHAZAM.
C      IF( I2.LT.NDLOW) GO TO 520                                SHAZAM.
C      I1=NDLOW                                                       SHAZAM.
C      I2=MINO(I2+1,NDHI)                                           SHAZAM.
C      GO TO 512                                                    SHAZAM.
520  CONTINUE                                                       SHAZAM.
C                                                                    SHAZAM.
C      END OF PHI SCAN LOOP.                                       SHAZAM.
C                                                                    SHAZAM.
C NOW CHECK TO SEE WHETHER NTHMIN AND NTHMAX LIE                 SHAZAM.
C OUTSIDE THE WHOLE INTERVAL.  IF THEY DO, THE GO TO 540        SHAZAM.
C STATEMENT SETS THE INTEGRAL EQUAL TO THE INITIAL VALUE       SHAZAM.
C OF SUMINT, ZERO.                                               SHAZAM.
C                                                                    SHAZAM.
C OTHERWISE, THE THETA LIMITS, THMIN, THMAX ARE SET             SHAZAM.
C EQUAL TO THE APPROPRIATE VALUES.  THESE ARE EQUIVALENCED    SHAZAM.
C TO A(2), B(2) RESPECTIVELY, AND PLACED IN THE COMMON          SHAZAM.
C BLOCK, INT.                                                    SHAZAM.
C                                                                    SHAZAM.
C      IF( (NTHMAX .EQ. 0) .OR. (NTHMIN .EQ. (29 +1)) ) GO TO 540 SHAZAM.
C      THMIN=THTAB(NTHMIN)                                           SHAZAM.
C      THMAX=THTAB(NTHMAX)                                           SHAZAM.
C                                                                    SHAZAM.
C                                                                    SHAZAM.
610  CONTINUE                                                       SHAZAM.
C                                                                    SHAZAM.
C SMALL AND EPS CONTROL THE ACCURACY OF THE INTEGRATION         SHAZAM.
C ROUTINES ASMP5N AND ASMP5N2.  IF A IS THE VALUE OF THE       SHAZAM.
C INTEGRAL AFTER SOME NUMBER OF ITERATIONS, DA IS THE           SHAZAM.
```



```
C DIFFERENCE OF THE LAST TWO SUCCESSIVE ITERATIONS, THEN          SHAZAM.
C THE CONVERGENCE TEST IS                                         SHAZAM.
C   ABS(DA) / ABS(A + SMALL) LESS THAN EPS                         SHAZAM.
C   EPS IS A TWO-COMPONENT VECTOR. EPS(1) IS USED FOR             SHAZAM.
C THE OUTER (PHI) INTEGRAL, AND EPS(2), STORED IN THE             SHAZAM.
C COMMON BLOCK INT, FOR THE INNER (THETA) INTEGRAL.              SHAZAM.
C   TR=SMALL                                                        SHAZAM.
C   HERE THE INNER (THETA) INTEGRAL ITERATION INDICES             SHAZAM.
C ARE INITIALIZED.                                                SHAZAM.
C   MNA=20                                                          SHAZAM.
C   MXA=-20                                                        SHAZAM.
C INTEGRATE. SUBROUTINES ASMPNS AND ASMPNS2 ARE VIRTUALLY         SHAZAM.
C IDENTICAL ADAPTIVE SIMPSON INTEGRATION ROUTINES. TR IS          SHAZAM.
C A TEMPORARY RESULT. IF MORE THAN ONE INTERVAL IN THETA         SHAZAM.
C OCCURS, THE TR VALUES ARE ADDED IN SUMINT TO GIVE THE         SHAZAM.
C TOTAL INTEGRAL.                                                 SHAZAM.
C   EXTERNAL FUNCTION FINT CALCULATES THE INNER (THETA)          SHAZAM.
C INTEGRAL AND SETS THE INNER ITERATION INDICES, MNA AND         SHAZAM.
C MXA.                                                            SHAZAM.
C   AFLAG=ASMPNS(FINT,A,B,EPS,TR)                                  SHAZAM.
C   REMOVE SMALL FROM TR AND APPLY FACTOR OF (2/(3*PI)).          SHAZAM.
C   TR=(TR-SMALL)*.3333333/1.57079                                  SHAZAM.
C   PRINT 8000,OMEGA,TR,A(1),B(1),A(2),B(2)                       SHAZAM.
C   PRINT INNER (THETA) INTEGRAL ITERATION INDICES               SHAZAM.
C   PRINT 8020,MNA,MXA                                             SHAZAM.
C 8020 FORMAT( 5X,*MIN = *I5,* MAX =*I5)                          SHAZAM.
C   UPDATE OUTER (PHI) INTEGRAL ITERATION INDICES TO             SHAZAM.
C MAXIMUM AND MINIMUM OVER ALL PRECEDING INTEGRALS.             SHAZAM.
C   MNAFLG=MIN0(IFIX(AFLAG),MNAFLG)                               SHAZAM.
C   MXAFLG=MAX0(IFIX(AFLAG),MXAFLG)                               SHAZAM.
C   ADD TR TO PRECEDING RESULTS FOR OTHER THETA INTERVALS.       SHAZAM.
C   SUMINT=SUMINT+TR                                              SHAZAM.
540   CONTINUE                                                    SHAZAM.
C   RE-INITIALIZE NTHMIN, NTHMAX FOR NEXT PASS                   SHAZAM.
C   NTHMIN=29+1                                                  SHAZAM.
C   NTHMAX=0                                                      SHAZAM.
C   END OF THETA INTERVAL (ND) LOOP                               SHAZAM.
550   RESULT=SUMINT                                              SHAZAM.
```

C	STORE RESULTS ON TAPE 4.	SHAZAM.
C	WRITE (4,8014) HIN1,E,D,T,DELTA,MU,OMEGA,RESULT	SHAZAM.
C	8014 FORMAT(5F6.2,I5,2E20.4)	SHAZAM.
	PRINT 8011,RESULT	SHAZAM.
	8011 FORMAT(10X , *INTEGRAL(OMEGA) = * E16.4)	SHAZAM.
	8000 FORMAT(5X *OMEGA =*F9.3,* INTEGRAL = *E16.4,* PHI =(* F6.2,	SHAZAM.
	* *,*F6.2,*) , THETA =(* F6.2, *,* F6.2, *)*)	SHAZAM.
C	END OF OMEGA (NO) LOOP	SHAZAM.
C	220 CONTINUE	SHAZAM.
C	END OF TRANSITION (MU) LOOP	SHAZAM.
C	200 CONTINUE	SHAZAM.
	PRINT 8020,MNAFLG,MXAFLG	SHAZAM.
C	WRITE(4,8014) HIN1,E,D,T,DELTA	SHAZAM.
	ENDFILE 4	SHAZAM.
	REWIND 4	SHAZAM.
	STOP	SHAZAM.
C	END	SHAZAM.
	FUNCTION XMINMZ(AMIN,B,J,JMIN)	SHAZAM.
	XMINMZ=AMIN	SHAZAM.
	IF(AMIN .LE. B) RETURN	SHAZAM.
	XMINMZ=B	SHAZAM.
	JMIN=J	SHAZAM.
	RETURN	SHAZAM.
	END	SHAZAM.
	SUBROUTINE MOVE(N,A,B)	SHAZAM.
	DIMENSION A(1),B(1)	SHAZAM.
	DO 10 K=1,N	SHAZAM.
	B(K)=A(K)	SHAZAM.
10	CONTINUE	SHAZAM.
	RETURN	SHAZAM.
	END	SHAZAM.
	FUNCTION FINT(X)	SHAZAM.
	COMMON/ARGS/PHI	SHAZAM.
	COMMON/ANGLES/TH,COSPHI,SINPHI,COSTH,SINTH	SHAZAM.
	COMMON/INT/A(2),B(2),EPS(2)	SHAZAM.
	COMMON/FINTER/MNA,MXA	SHAZAM.
	EXTERNAL FNCTN	SHAZAM.
	DATA SMALL/1.E-2/	SHAZAM.
	DATA SMALL /1.E-1/	SHAZAM.
	PHI=X	SHAZAM.
	COSPHI=COS(PHI)	SHAZAM.
	SINPHI=SIN(PHI)	SHAZAM.
	RESULT=SMALL	SHAZAM.
	ASMP=ASMPN2(FNCTN,A(2),B(2),EPS(2),RESULT)	SHAZAM.
	MNA=MINO(IFIX(ASMP),MNA)	SHAZAM.
	MXA=MAXO(IFIX(ASMP),MXA)	SHAZAM.
	RESULT=RESULT-SMALL	SHAZAM.


```
C          SHAZAM.  
          SHAZAM.  
          SHAZAM.  
          SHAZAM.  
100 CONTINUE          SHAZAM.  
C          SHAZAM.  
C          SHAZAM.  
C          SHAZAM.  
          MUT=MU          SHAZAM.  
          IMUT=IMU(MUT)  SHAZAM.  
          JMUT=JMU(MUT)  SHAZAM.  
C          SHAZAM.  
          SPLUS(JMUT,IMUT) = STRANS(JMUT,IMUT,SRPLUS)  SHAZAM.  
          SMINUS(JMUT,IMUT) = STRANS(JMUT,IMUT,SRMINUS)  SHAZAM.  
          SZEE(JMUT,IMUT) = STRANS(JMUT,IMUT,SRZEE)  SHAZAM.  
C          SHAZAM.  
C          SHAZAM.  
C          SHAZAM.  
          RETURN          SHAZAM.  
          END          SHAZAM.
```

```
          COMPLEX FUNCTION STRANS(JM,IM,S)          SHAZAM.  
C          SHAZAM.  
C          SHAZAM.  
          COMPLEX SUM          SHAZAM.  
          COMPLEX ALPHA          SHAZAM.  
          COMMON/EIGEN/ALPHA(4,4),W(4)          SHAZAM.  
          DIMENSION S(4,4)          SHAZAM.  
C          SHAZAM.  
          SUM=0          SHAZAM.  
C          SHAZAM.  
          DO 10 K=1,4          SHAZAM.  
C          SHAZAM.  
          DO 10 L=1,4          SHAZAM.  
C          SHAZAM.  
C          SHAZAM.  
C          JMU = FINAL STATE          SHAZAM.  
C          IMU = INITIAL STATE          SHAZAM.  
C          SHAZAM.  
          SUM=SUM+ALPHA(L,IM)*CONJG(ALPHA(K,JM)) *S(K,L)  SHAZAM.  
C          SHAZAM.  
10 CONTINUE          SHAZAM.  
C          SHAZAM.  
          STRANS = SUM          SHAZAM.  
C          SHAZAM.  
          RETURN          SHAZAM.  
          END          SHAZAM.
```

```
          FUNCTION GPW(MU)          SHAZAM.  
C          SHAZAM.  
* GPW = G((W-WMU),DELTA) * P(MU,T) * WMU          SHAZAM.
```

```
C      COMMON/PARAMS/H(1),E,D,T,DELTA,OMEGA      SHAZAM.
COMMON/PARAMS/WT,WH      SHAZAM.
COMPLEX ALPHA      SHAZAM.
COMMON/EIGEN/ALPHA(4,4),W(4)      SHAZAM.
COMMON/IMUJMU/IMU(6),JMU(6)      SHAZAM.
COMMON/PROB/P      SHAZAM.
C      SHAZAM.
C      I=IMU(MU)      SHAZAM.
      J=JMU(MU)      SHAZAM.
      WMU=W(J)-W(I)      SHAZAM.
      SUM=0      SHAZAM.
C      DO 10 L=1,4      SHAZAM.
10     SUM=SUM+EXP(-W(L) / WT )      SHAZAM.
C      P = (EXP(-W(I)/WT) - EXP(-W(J)/WT))/ SUM      SHAZAM.
      CDELT = DELTA/ 1.1773      SHAZAM.
C      THIS MAKES GAUSSIAN HWHM = MEASURED HWHM      SHAZAM.
*      G = (EXP(-.5*( (OMEGA - WMU) / CDELT)**2 ) ) / CDELT      SHAZAM.
C      MODS.4
*      FACTOR OF (1./CDELT) NORMALIZES G      SHAZAM.
C      MODS.5
      GPW=G * P * WMU      SHAZAM.
C      MODS.6
      RETURN      SHAZAM.
      END      SHAZAM.

SUBROUTINE READATA      SHAZAM.
COMMON/PARAMS/H(6)      SHAZAM.
COMMON/INPUT/HIN1(6)      SHAZAM.
DIMENSION KEYTAB(6)      SHAZAM.
DATA KEYTAB/1HH,1HE,1HD,1HT,5HDELTA/      SHAZAM.
DATA KEYTAB(6) / 4HPMIN/      SHAZAM.
COMMON/THLIMIT/LIMITS      SHAZAM.
DATA LIMITS/0/      SHAZAM.
DATA NRANGE/7HOTOPI/2/      SHAZAM.
C      SHAZAM.
      DO 100 K=1,6      SHAZAM.
5      CONTINUE      SHAZAM.
      READ 900,KEY,VALUE      SHAZAM.
900     FORMAT(A10,F10.2)      SHAZAM.
C      SHAZAM.
C CHECK TO SEE IF FULL THETA INTERVAL FOR INTEGRATION      SHAZAM.
C (0 TO PI/2) IS TO BE USED.      SHAZAM.
C      SHAZAM.
      IF(KEY.NE.NRANGE) GO TO 25      SHAZAM.
      LIMITS = 1      SHAZAM.
      GO TO 5      SHAZAM.
25     CONTINUE      SHAZAM.
C      SHAZAM.
      DO 20 J=1,6      SHAZAM.
C      SHAZAM.
      SHAZAM.
```



```
LSAVE=1. SHAZAM.
AI=0 SHAZAM.
IF(EPS .LT. 0 ) AI=AREA SHAZAM.
X(5)=XA $ X(7)=XB SHAZAM.
FX(5)=F(XA) $ FX(7)=F(XB) SHAZAM.
X(6)=(X(5)+X(7))/2 SHAZAM.
FX(6)=4*F(X(6)) SHAZAM.
DX=(X(7)-X(5))/2 SHAZAM.
AEST(3)=DX*(FX(5)+FX(6)+FX(7))/3 SHAZAM.
EST=AEST(3) +AI SHAZAM.
C SHAZAM.
50 ERRSUM=0 SHAZAM.
TOTSUM=EST SHAZAM.
L=1 SHAZAM.
J=3 SHAZAM.
C SHAZAM.
C BEGIN ADAPTIVE PROCEDURE SHAZAM.
C INCREASE LEVEL SHAZAM.
C SHAZAM.
100 L1=L SHAZAM.
L=L+1 SHAZAM.
LSAVE=MAX0(LSAVE,L) SHAZAM.
TOL(L)=TOL(L1)/THREE SHAZAM.
J1=J(L1) SHAZAM.
DX(L)=DX(L1)/3 SHAZAM.
C SHAZAM.
C PUSH DOWN OLD COORDINATES SHAZAM.
C SHAZAM.
150 KJ=2*J1-2 SHAZAM.
DO 110 KK=1,3 SHAZAM.
KA=KJ+KK SHAZAM.
K=3*KK-2 SHAZAM.
KL1=7*L1 SHAZAM.
KL=KL1+K SHAZAM.
C (K,L) = KL SHAZAM.
KLA=KL1-7+KA SHAZAM.
C (KA,L1)=KLA SHAZAM.
X(KL)=X(KLA) SHAZAM.
110 FX(KL)=FX(KLA) SHAZAM.
C SHAZAM.
C CALCULATE NEW COORDINATES SHAZAM.
DXL=DX(L) SHAZAM.
H=DXL/3 SHAZAM.
J(L)=1 SHAZAM.
C SHAZAM.
DO 120 KA=2,3 SHAZAM.
DO 120 K=KA,6,3 SHAZAM.
KL=7*L1+K SHAZAM.
C (K,L) = KL SHAZAM.
X(KL)=X(KL-1)+DXL SHAZAM.
120 FX(KL)=F(X(KL))*(4-3*MOD(K,2)) SHAZAM.
C SHAZAM.
SUMK=0 SHAZAM.
DO 130 K=1,3 SHAZAM.
KA=2*K-1 SHAZAM.
KB=KA+2 SHAZAM.
KL=3*L1+K SHAZAM.
C (K,L) = KL SHAZAM.
AEST(KL)=0 SHAZAM.
DO 135 KJ=KA,KB SHAZAM.
SHAZAM.
```

```
135  AEST(KL)=AEST(KL)+FX(KJ,L)          SHAZAM.  
    AEST(KL)=H*AEST(KL)                SHAZAM.  
130  SUMK=SUMK+AEST(KL)                 SHAZAM.  
C                                         SHAZAM.  
    DSUMK=SUMK-AEST(J1,L1)              SHAZAM.  
    SUMK=SUMK+DSUMK/80                  SHAZAM.  
    ABD=ABS(DSUMK)                      SHAZAM.  
C                                         SHAZAM.  
    TOTSUM=TOTSUM+DSUMK + AI            SHAZAM.  
    IF(ABS((SUMK+AI) * EPS) .GE. ABD .OR.TOL(L)*TOTSUM .GE. ABD) SHAZAM.  
    * GO TO 200                          SHAZAM.  
    IF(L .LT. LMAX) GO TO 100           SHAZAM.  
C                                         SHAZAM.  
    HIT BOTTOM OF TREE                  SHAZAM.  
C                                         SHAZAM.  
C                                         SHAZAM.  
C                                         SHAZAM.  
200  ERRSUM=ERRSUM+ABD                  SHAZAM.  
C                                         SHAZAM.  
205  AEST(J1,L1)=SUMK                   SHAZAM.  
    IF(J1 .GE. 3 ) GO TO 210            SHAZAM.  
    J1=J1+1                              SHAZAM.  
    J(L1)=J1                              SHAZAM.  
    GO TO 150                             SHAZAM.  
C                                         SHAZAM.  
210  IF(L .LE. 2) GO TO 220             SHAZAM.  
    L=L1                                   SHAZAM.  
    L1=L-1                                 SHAZAM.  
    J1=J(L1)                              SHAZAM.  
    L13=3*L1+1                            SHAZAM.  
    (1,L)=L13                             SHAZAM.  
    SUMK=AEST(L13)+AEST(L13+1)+AEST(L13+2) SHAZAM.  
    GO TO 205                             SHAZAM.  
C                                         SHAZAM.  
220  AREA=AEST(3)+AI                    SHAZAM.  
    ASMPNS2=MIN0(LSMPS,LSAVE)              SHAZAM.  
    IF (ABS(EPS*AREA) .GE. ERRSUM/80.) RETURN SHAZAM.  
    IF(FIRST .NE. 0. ) GO TO 300          SHAZAM.  
    LSMPS=0                                SHAZAM.  
    FIRST=1.                               SHAZAM.  
    THREE=3.                               SHAZAM.  
    GO TO 50                               SHAZAM.  
C                                         SHAZAM.  
300  ASMPNS=-LMAX                        SHAZAM.  
    ASMPNS2=-LMAX                          SHAZAM.  
    RETURN                                  SHAZAM.  
    END                                    SHAZAM.  
  
    FUNCTION ASMPNS(F,XA,XB,EPS,AREA)     SHAZAM.  
C    ADAPTIVE SIMPSONS RULE                SHAZAM.  
C    NOV. 3, 1966                          SHAZAM.  
C                                         SHAZAM.  
    DIMENSION X(7,15),FX(7,15),AEST(3,15),DX(15),TOL(15),J(15) SHAZAM.  
    DATA LMAX/15/                          SHAZAM.  
C                                         SHAZAM.  
    THREE=1. $ FIRST=0                     SHAZAM.
```



```
DIMENSION A(2,6,6),E(6),Z1(6,6),Z2(6,6) SHAZAM.
DIMENSION ALPHA(6),BETA(6) SHAZAM.
DIMENSION BB(7) SHAZAM.
DIMENSION TAU(2,6) SHAZAM.
C ETA = RELATIVE MACHINE PRECISION SHAZAM.
ETA = 2.**(-48) SHAZAM.
GAMMA=ETA**2 SHAZAM.
CALL HHERM (A,N,GAMMA,TOL,BETA,ALPHA,TAU) SHAZAM.
BB(1)=0.0 SHAZAM.
DO 2 I=1,N SHAZAM.
E(I)=ALPHA(I) SHAZAM.
2 BB(I+1)=BETA(I)**2 SHAZAM.
C INFINITY NORM OF TRIDIAGONAL MATRIX SHAZAM.
RNORM=0.0 SHAZAM.
DO 5 I=1,N SHAZAM.
5 RNORM=MAX1F(RNORM,SQRT(BB(I))+ABS(E(I))+SQRT(BB(I+1))) SHAZAM.
DELTA=ETA*RNORM SHAZAM.
EPS=DELTA**2 SHAZAM.
C SHAZAM.
C W.KAHAN AND J.VARAH, TWO WORKING ALGORITHMS FOR THE EIGENVALUES OF A SHAZAM.
C SYMMETRIC TRIDIAGONAL MATRIX. TECHNICAL REPORT NO. CS43, AUGUST 11, SHAZAM.
C 1966. COMP.SC.DEPT. STANFORD UNIVERSITY. SHAZAM.
C SHAZAM.
K=N SHAZAM.
6 M=K SHAZAM.
IF(M.LE.0)GO TO 56 SHAZAM.
8 K=K-1 SHAZAM.
IF(BB(K+1).GE.EPS)GO TO 8 SHAZAM.
C NEXT SHAZAM.
IF(K.NE.M-1)GO TO 13 SHAZAM.
BB(K+1)=0.0 SHAZAM.
GO TO 6 SHAZAM.
C TWOBY2 SHAZAM.
13 T=E(M)-E(M-1) SHAZAM.
R=BB(M) SHAZAM.
IF(K.GE.M-2)GO TO 22 SHAZAM.
W=BB(M-1) SHAZAM.
C=T**2 SHAZAM.
S=R/(C+W) SHAZAM.
IF(S*(W+S*C).GE.EPS)GO TO 22 SHAZAM.
M=M-1 SHAZAM.
BB(M+1)=0.0 SHAZAM.
GO TO 13 SHAZAM.
C END NEGLIGIBLE BB SHAZAM.
22 IF(ABS(T).GE.DELTA)GO TO 25 SHAZAM.
S=SQRT(R) SHAZAM.
GO TO 28 SHAZAM.
25 W=2.0/T SHAZAM.
S=W*R/(SQRT(W**2*R+1.0)+1.0) SHAZAM.
28 IF(K.NE.M-2)GO TO 33 SHAZAM.
E(M)=E(M)+S SHAZAM.
E(M-1)=E(M-1)-S SHAZAM.
BB(K+1)=0.0 SHAZAM.
GO TO 6 SHAZAM.
C DO A QR STEP ON ROWS AND COLUMNS K+I THROUGH M SHAZAM.
33 SHIFT=E(M)+S SHAZAM.
IF(ABS(T).GE.DELTA)GO TO 37 SHAZAM.
W=E(M-1)-S SHAZAM.
IF(ABS(W).LT.ABS(SHIFT))SHIFT=W SHAZAM.
37 S=0.0 SHAZAM.
```


C	INTEGER N,M1	SHAZAM.
	REAL NORM,MACHEPS	SHAZAM.
	DIMENSION C(6),B(6),W(6),Z(6,6)	SHAZAM.
	REAL M(6),P(6),Q(6),R(6),INT(6)	SHAZAM.
	REAL X(8)	SHAZAM.
C	INTEGER I,J	SHAZAM.
C	REAL BI,BI1,Z1,LAMBDA,U,S,V,H,EPS,ETA	SHAZAM.
	LAMBDA=NORM	SHAZAM.
	EPS=MACHEPS*NORM	SHAZAM.
	DO 90 J=1,M1	SHAZAM.
	LAMBDA=LAMBDA-EPS	SHAZAM.
	IF(W(J).LT.LAMBDA)LAMBDA=W(J)	SHAZAM.
	U=C(1)-LAMBDA	SHAZAM.
	V=B(1)	SHAZAM.
	IF(V.EQ.0)V=EPS	SHAZAM.
	NMINUS1=N-1	SHAZAM.
	DO 60 I=1,NMINUS1	SHAZAM.
	BI=B(I)	SHAZAM.
	IF(BI.EQ.0)BI=EPS	SHAZAM.
	BI1=R(I+1)	SHAZAM.
	IF(BI1.EQ.0)BI1=EPS	SHAZAM.
	IF(ABS(BI).LT.ABS(U))GO TO 50	SHAZAM.
	M(I+1)=U/BI	SHAZAM.
	IF((M(I+1).EQ.0).AND.(BI.LE.EPS))M(I+1)=1	SHAZAM.
	P(I)=BI	SHAZAM.
	Q(I)=C(I+1)-LAMBDA	SHAZAM.
	R(I)=BI1	SHAZAM.
	U=V-M(I+1)*Q(I)	SHAZAM.
	V=-M(I+1)*R(I)	SHAZAM.
	INT(I+1)=+1	SHAZAM.
	GO TO 60	SHAZAM.
50	M(I+1)=BI/U	SHAZAM.
	P(I)=U	SHAZAM.
	Q(I)=V	SHAZAM.
	R(I)=0	SHAZAM.
	U=C(I+1)-LAMBDA-M(I+1)*V	SHAZAM.
	V=BI1	SHAZAM.
	INT(I+1)=-1	SHAZAM.
60	CONTINUE	SHAZAM.
	P(N)=U	SHAZAM.
	Q(N)=0	SHAZAM.
	R(N)=0	SHAZAM.
	X(N+1)=0	SHAZAM.
	X(N+2)=0	SHAZAM.
	H=0	SHAZAM.
	ETA=1.0/N	SHAZAM.
	DO 67 II=1,N	SHAZAM.
	I=N-II+1	SHAZAM.
	U=ETA-Q(I)*X(I+1)-R(I)*X(I+2)	SHAZAM.
	IF(P(I).NE.0)GO TO 65	SHAZAM.
	X(I)=U/EPS	SHAZAM.
	GO TO 66	SHAZAM.
65	X(I)=U/P(I)	SHAZAM.
66	H=H+ABS(X(I))	SHAZAM.
67	CONTINUE	SHAZAM.
	DO 68 I=1,N	SHAZAM.
68	X(I)=X(I)/H	SHAZAM.


```
RATIO=VR/ROOT
TAU(1,1)=-RATIO*A(1,R,RM1)
TAU(2,1)=RATIO*A(2,R,RM1)
A(1,R,RM1)=(RATIO+1)*A(1,R,RM1)
A(2,R,RM1)=(RATIO+1)*A(2,R,RM1)
70 DO 90 J=R,N
TAU(1,J)=A(1,J,RM1)/DELTA
TAU(2,J)=A(2,J,RM1)/DELTA
C(J)=B(J)=0.
DO 80 L=R,J
C(J)=C(J)+A(1,J,L)*A(1,L,RM1)-A(2,J,L)*A(2,L,RM1)
B(J)=B(J)+A(1,J,L)*A(2,L,RM1)+A(2,J,L)*A(1,L,RM1)
80 CONTINUE
JPLUS1=J+1
DO 90 L=JPLUS1,N
IF(L.GT.N) GO TO 90
C(J)=C(J)+A(1,L,J)*A(1,L,RM1)+A(2,L,J)*A(2,L,RM1)
B(J)=B(J)+A(1,L,J)*A(2,L,RM1)-A(2,L,J)*A(1,L,RM1)
90 CONTINUE
RHO=0.
DO 100 L=R,N
RHO=RHO+C(L)*TAU(1,L)+B(L)*TAU(2,L)
100 CONTINUE
DO 110 I=R,N
DO 110 J=R,I
X1=TAU(1,I)*C(J)+TAU(2,I)*B(J)
X2=TAU(2,I)*C(J)-TAU(1,I)*B(J)
Q1=C(I)-RHO*A(1,I,RM1)
Q2=B(I)-RHO*A(2,I,RM1)
T1=Q1*TAU(1,J)+Q2*TAU(2,J)
T2=Q2*TAU(1,J)-Q1*TAU(2,J)
A(1,I,J)=A(1,I,J)-X1-T1
A(2,I,J)=A(2,I,J)-X2-T2
110 CONTINUE
TAU(1,R)=TAU(1,1)
TAU(2,R)=TAU(2,1)
120 CONTINUE
DO 130 I=1,N
C(I)=A(1,I,I)
130 CONTINUE
IF (NM1) 150,150,140
140 TAU(1,N)=A(1,N,NM1)
TAU(2,N)=-A(2,N,NM1)
150 TAU(1,1)=1.
TAU(2,1)=B(N)=0.
DO 180 I=2,N
IM1=I-1
BB=B(IM1)=SQRT(TAU(1,I)*TAU(1,I)+TAU(2,I)*TAU(2,I))
IF (BB)170,160,170
160 TAU(1,I)=BB=1.
170 TT1=TAU(1,I)*TAU(1,IM1)-TAU(2,I)*TAU(2,IM1)
TT2=TAU(1,I)*TAU(2,IM1)+TAU(2,I)*TAU(1,IM1)
TAU(1,I)=TT1/BB
TAU(2,I)=TT2/BB
180 CONTINUE
RETURN
END
```

C
C

```
SUBROUTINE REVERSE(B,A,TAU,N,M1,GAMMA,TOL,Z1,Z2)          SHAZAM.
DIMENSION B(6),A(2,6,6),TAU(2,6),Z1(6,6),Z2(6,6)        SHAZAM.
DIMENSION ALPHA(2,6)                                     SHAZAM.
INTEGER R,RM1                                             SHAZAM.
DO 10 J=2,N                                              SHAZAM.
DO 10 K=1,M1                                             SHAZAM.
P1=Z1(J,K)*TAU(1,J)+Z2(J,K)*TAU(2,J)                   SHAZAM.
P2=Z2(J,K)*TAU(1,J)-Z1(J,K)*TAU(2,J)                   SHAZAM.
Z1(J,K)=P1                                               SHAZAM.
Z2(J,K)=P2                                               SHAZAM.
10 CONTINUE                                              SHAZAM.
NMINUS2=N-2                                              SHAZAM.
DO 60 MR=1,NMINUS2                                       SHAZAM.
R=N-MR                                                    SHAZAM.
RM1=R-1                                                  SHAZAM.
IF (B(RM1)-GAMMA*TOL**2) 60,60,20                       SHAZAM.
20 DELTA=B(RM1)*SQRT(A(1,R,RM1)**2+A(2,R,RM1)**2)       SHAZAM.
DO 40 J=1,M1                                             SHAZAM.
ALPHA(1,J)=ALPHA(2,J)=0.                                SHAZAM.
DO 30 K=R,N                                             SHAZAM.
ALPHA(1,J)=ALPHA(1,J)+A(1,K,RM1)*Z1(K,J)+A(2,K,RM1)*Z2(K,J) SHAZAM.
ALPHA(2,J)=ALPHA(2,J)-A(2,K,RM1)*Z1(K,J)+A(1,K,RM1)*Z2(K,J) SHAZAM.
30 CONTINUE                                              SHAZAM.
ALPHA(1,J)=ALPHA(1,J)/DELTA                             SHAZAM.
ALPHA(2,J)=ALPHA(2,J)/DELTA                             SHAZAM.
40 CONTINUE                                              SHAZAM.
DO 50 J=1,M1                                             SHAZAM.
DO 50 K=R,N                                             SHAZAM.
Z1(K,J)=Z1(K,J)-A(1,K,RM1)*ALPHA(1,J)+A(2,K,RM1)*ALPHA(2,J) SHAZAM.
Z2(K,J)=Z2(K,J)-A(1,K,RM1)*ALPHA(2,J)-A(2,K,RM1)*ALPHA(1,J) SHAZAM.
50 CONTINUE                                              SHAZAM.
60 CONTINUE                                              SHAZAM.
RETURN                                                  SHAZAM.
END                                                       SHAZAM.
```

XBL 706-1257

```
PROGRAM POST(INPUT,OUTPUT,TAPE2=INPUT,TAPE3=OUTPUT)
*
*
DIMENSION OMEGAT(200),VALUE(200)
DIMENSION ICNT(6),OMEGA(27,6),VALUE(27,6)
DIMENSION PARAMS(5)
COMMON/PRAMDTA/H(1),E,D,T,DELTA,MUIN,OMEGAIN,VALUEIN
DIMENSION HEADING(3)
DATA HEADING/30H      H      E      D      T      DELTA /
DATA ICNT/6*1/
DATA OMEGA/0/,VALUE/0/
DIMENSION FOM(3)

C READ IN NO. OF PTS TO BE USED IN INTERPOLATION
*
READ (2,913) NPTS
913 FORMAT(I10)
*
READ (2,900) PARAMS
900 FORMAT(5F6.2,I5,2E20.4)
C ABOVE TO READ IN PARAMETERS
C
C NOW READ IN ALL CARDS AND JUST KEEP THOSE THAT MATCH
C THE INPUT PARAMETER DATA
C
1 CONTINUE
READ(2,900) (H(I),I=1,8)
IF(H.EQ. 0) GO TO 101
10 CONTINUE
IF(EQVCTR(H,PARAMS,5) .NE. 0) GO TO 100
IO=ICNT(MUIN) +1
ICNT(MUIN)=IO
OMEGA (IO,MUIN) = OMEGAIN
VALUE(IO,MUIN) = VALUEIN
100 CONTINUE
IF(EOF,2) 101,1
C
C 101 CONTINUE
C
*****
*****
* NOW SORT ALL VECTORS FOR EACH MU
C
DO 200 MU=1,6
IO=ICNT(MU)
IF(IO .EQ. 1) GO TO 200

CALL SORTV(IO-1,OMEGA(2,MU),VALUE(2,MU))
OMEGA(1,MU)=OMEGA(2,MU) - 2.*DELTA
OMEGA(IO+1,MU)=OMEGA(IO,MU) + 2.*DELTA
VALUE(IO+1,MU)=0
VALUE(1,MU)=0
200 CONTINUE
C
C
```


C FORM SUMS OF ALL INTERPOLATED VALUES

JOM=0
DO 300 MUA=1,6

NA=ICNT(MUA) +1
IF(NA .LE. 2) GO TO 300

DO 400 N=1,NA
SUM=0
JOM=JOM+1

DO 500 MUB=1,6

IT=ITBLKP(OMEGA(N,MUA),ICNT(MUB)+1,OMEGA(1,MUB))
IF((IT .EQ. 0) .OR. ((IT-1) .GE. ICNT(MUB))) GO TO 500
IT=MAX(1,IT-(NPTS-1)/2)
NDX=MIN(ICNT(MUB)+1-(NPTS-1),IT)

* INTERPOLATE

CALL NTPO(OMEGA(N,MUA),FOM,NPTS,OMEGA(NDX,MUB),VALUE(NDX,MUB))

SUM=SUM+FOM
500 CONTINUE

VALUET(JOM)=SUM
OMEGAT(JOM)=OMEGA(N,MUA)
400 CONTINUE

300 CONTINUE

* EDIT

PRINT 901
901 FORMAT (1H1)

PRINT 912,HEADING
912 FORMAT(3A10)
PRINT 900,PARAMS

DO 600 MU=1,6
IO=ICNT(MU)+1
PRINT 910,MU
910 FORMAT(// , 10X * MU =*I2 , /)

IF(IO .LE. 2) GO TO 600
PRINT 911,(I,OMEGA(I,MU),VALUE(I,MU),I=1,IO)
600 CONTINUE

911 FORMAT(10X,I10,2E20.4)
PRINT 901

CALL SORTV(JOM,OMEGAT,VALUET)

PRINT 911,(I,OMEGAT(I),VALUET(I),I=1,JOM)

STOP

END

FUNCTION EQVCTR(A,B,N)
DIMENSION A(1),B(1)

EQ=0

```

DO 10 K=1,N
IF(A(K) .NE. B(K) ) GO TO 20
10 CONTINUE
15 EQVCTR = EQ
RETURN

20 EQ=1.
GO TO 15
END

```

ASCENTF SUBROUTINE ITBLKP (T,L,V)

```

*
*   BINARY SEARCH .. ITBLKP S.T. V(ITBLKP) .LE. T .LT. V(ITBLKP +1)
*   V IS OF DIMENSION L
*

```

```

ENT  BSSZ 5
      BSSZ 1
      SA2 B2           .X2=L
      SB4 1           .B4=1=KL
      SA1 B1           .X1=T
      SB5 X2           .B5=L=KH
      SA3 B3           .X3=V(1)
      IX4 X1-X3       .X4 = T-V(1)
      NG X4,GOD       .GOD FOR T .LT. V(1)
      SB3 B3-1        .B3=LOC(V)-1
      SA5 X2+B3       .X5=V(L)
      IX4 X5-X1       .X4=V(L)-T
      NG X4,GOE       .GOE FOR T .GT. V(L)
GOA  SB7 B5-B4       .B7=KH-KL
      SB7 B7-1       .B7=KH-KL-1
      NE B0,B7,GOB
      SX6= B4
      EQ B0,B0,ENT   .KH=KL+1 ... DONE
GOB  SX4 B4+B5
      AX4 1           .X4=(KH+KL)/2 = J

```

```
SA5 X4+B3      .X5 = V(J)
IX5 X1-X5      .X5=T-V(J)
PL  X5,GOC     .GOC FOR T.GE. V(J)
SB5 X4         .KH = J
EQ  B0,B0,GOA
GOC SB4 X4     .V(J) .LE. T
EQ  B0,B0,GOA .KL=J
GOD MX6 0      .T .LT. V(1)
EQ  B0,B0,ENT .ITBLKP=0
GOE SX6 X2     .T .GT. V(L)
EQ  B0,B0,ENT .ITBLKP = L
END
```

ASCENTF SUBROUTINE SORTV(N,X,Y)

```
XIT BSSZ 5
    RSSZ 1
    SA5 B1
    SB5 =1
    SB1 X5
BGN SB6 B0
    SA1 B2
    SB4 B5
STRT SA2 B2+B4      .C(X2)=X(K) FOR K=2,...,N
    IX5 X2-X1      .X(K)-X(K-1)
    PL  X5,CONT    .GT ... OK
    BX7 X1
    BX6 X2         .PERMUTE X AND YPAIRS
    SA7 A2
    BX2 X1
    SA6 A2-B5
    SA3 B3+B4
    SA4 A3-B5
    BX7 X3
    BX6 X4
    SA7 A4
    SB6 B5
    SA6 A3
CONT BX1 X2
    SB4 B4+B5
    NE  B1,B4,STRT
    NE  B6,B0,BGN
    EQ  B0,B0,XIT
END
```

ASCENTF SUBROUTINE NTPO(XX,FF,N,X,F)

```
ENT BSSZ 7      .LAGRANGIAN INTERPOLATION FOR FF AT XX
    BSSZ 1      .USING N POINTS FROM ARRAYS X AND F
```

```
SA1 B3
MX6 0      .INITIALIZE FF
SB3 X1     .B3 HAS N
SA2 B1     .X2 HAS XX
GE B0,B3,ERR
SX3 3641B
SB6 B0
LX3 47     .X3 HAS FLOATING POINT 1.
SA0 1
LP1 SA4 B5+B6 .FETCH F(I)
    SA5 B4+B6 .FETCH X(I)
    BX7 X3    .INITIALIZE DENOMINATOR TO 1.
    SB7 B0
LP2 SA1 B4+B7 .FETCH X(J)
    FX0 X5-X1 .X(I) - X(J)
    EQ B6,B7,END2
    NX0 X0
    FX1 X2-X1 .XX - X(J)
    FX7 X7*X0 .DENOMINATOR MULTIPLIED BY X(I) - X(J)
    NX0 X1
    FX4 X4*X0 .NUMERATOR MULTIPLIED BY XX - X(J)
END2 SB7 A0+B7 .INCREMENT COUNTER
    LT B7,B3,LP2
    FX1 X4/X7
    SB6 A0+B6
    FX0 X6+X1 .ACCUMULATE FF
    NX6 X0
    LT B6,B3,LP1
    SA6 B2    .STORE FF
    EQ B0,B0,ENT
ERR  FX6 X6/X6 .ERROR RETURN IF N .LE. 0
    SA6 B2
    EQ B0,B0,ENT
END
```

XBL 706-1262

C. Polycrystalline Absorption Coefficient for $H' \gg 1$

In this appendix, we shall outline the general approach to the calculation of the magnetic-dipole absorption coefficient of a paramagnetic ion, described by the spin Hamiltonian of Eq. (2) in the text, in the case $H' \equiv (g\mu_B H)/D \gg 1$. We shall also explicitly calculate the absorption coefficient for $S = 5/2$.

1. Method

The spin Hamiltonian in Eq. (2) contains two types of terms, Zeeman and ligand-field. It is written in a coordinate system which diagonalizes the axial ligand-field term, and which gives a value of $\lambda \equiv E/D \leq 1/3$. However, when $H' \gg 1$, the Zeeman term is the largest in magnitude. If the spin Hamiltonian is written in a coordinate system which diagonalizes the Zeeman term (i.e., where $\underline{H} \parallel \hat{z}$) the off-diagonal contributions to the eigenvalues and eigenstates, due to the ligand-field terms, will be second order in $(1/H')$, and may be neglected. The eigenstates are then simply eigenstates of S_H , the projection of \underline{S} on \underline{H} , and simple expressions for the eigenvalues can be obtained from the diagonal terms of the new spin Hamiltonian. Under these conditions, the expression for $\bar{\alpha}$ can be analytically evaluated, since the magnetic dipole transition probability will be a constant for each transition, independent of the orientation of \underline{H} with respect to the ligand-field coordinate system. The lineshape can be obtained by converting the integrand in Eq. (5), $\alpha_n d\Omega_H$, to $\bar{\alpha}_n d\nu$ by mathematical manipulations involving a single integration and a Jacobian determinant. We shall first calculate the diagonal part of the spin Hamiltonian in the new coordinate system for a general value of the spin, S , and then outline the calculation of $\bar{\alpha}$ for $S = 5/2$.

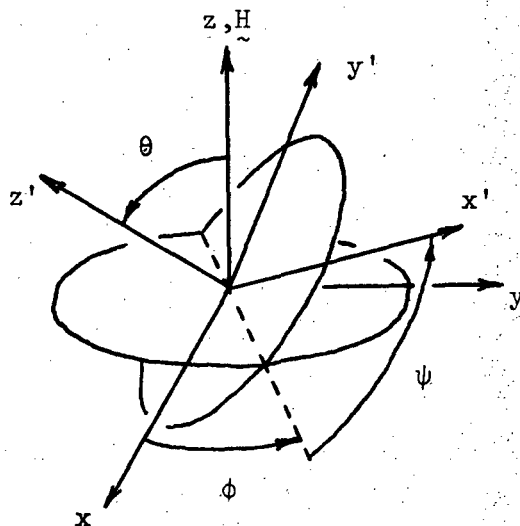
Finally, we shall include a computer program for calculating $\bar{\alpha}$ for $S = 5/2$, $H = 52.2$ kOe, and specified values of D , λ and T .

2. Derivation of the Diagonal Terms of \mathcal{H}

We first write the spin Hamiltonian as

$$\mathcal{H} = g\mu_B \vec{H} \cdot \vec{S} + D[S_z^2 - S(S+1)/3] + E[S_{x'}^2 - S_{y'}^2] \quad (C1)$$

where the coordinates $\{x', y', z'\}$ refer to the proper axes of the ligand field, such that $\lambda \equiv E/D \leq 1/3$. We now define a new coordinate system $\{x, y, z\}$, such that $\vec{H} \parallel \hat{z}$, with the orientation shown in the following figure:



With these definitions,

$$\begin{aligned}
 S_{x'} &= [\cos\psi\cos\phi - \cos\theta\sin\phi\sin\psi]S_x \\
 &\quad + [\cos\psi\sin\phi + \cos\theta\cos\phi\sin\psi]S_y \\
 &\quad + [\sin\theta\sin\psi]S_z \\
 S_{y'} &= [-\sin\psi\cos\phi - \cos\theta\sin\phi\cos\psi]S_x \\
 &\quad + [-\sin\psi\sin\phi + \cos\theta\cos\phi\cos\psi]S_y \\
 &\quad + [\sin\theta\cos\psi]S_z \\
 S_{z'} &= [\sin\theta\sin\phi]S_x + [-\sin\theta\cos\phi]S_y \\
 &\quad + [\cos\theta]S_z
 \end{aligned}
 \tag{C2}$$

When these expressions are substituted into Eq. (C1), a number of terms will result. There will be terms in the operators S_z , S_z^2 , S_x^2 , and S_y^2 , as well as in the cross terms $[S_x S_y + S_y S_x]$, $[S_x S_z + S_z S_x]$, and $[S_y S_z + S_z S_y]$. It is easy to show that the substitution of the ladder operators

$$\begin{aligned}
 S_+ &\equiv (S_x + iS_y) \\
 S_- &\equiv (S_x - iS_y)
 \end{aligned}
 \tag{C3}$$

leads to the relations

$$\begin{aligned}
 S_x^2 &= \frac{1}{4} (S_+^2 + S_+ S_- + S_- S_+ + S_-^2) \\
 S_y^2 &= -\frac{1}{4} (S_+^2 - S_+ S_- - S_- S_+ + S_-^2) \\
 [S_x S_y + S_y S_x] &= \frac{i}{2} (S_-^2 - S_+^2) \\
 [S_x S_z + S_z S_x] &= \frac{1}{2} (S_+ S_z + S_- S_z + S_z S_+ + S_z S_-) \\
 [S_y S_z + S_z S_y] &= \frac{i}{2} (S_- S_z - S_+ S_z + S_z S_- - S_z S_+)
 \end{aligned}
 \tag{C4}$$

It is clear from the properties of the ladder operators that only S_z , S_z^2 , S_+S_- and S_-S_+ terms are diagonal in the new system. These terms only arise from the first set of operators mentioned. This observation considerably simplified the algebra, and substitution of the appropriate terms of Eqs. (C2) into Eq. (C1) yields the diagonal terms of the spin Hamiltonian, $\mathcal{H}_{\text{diag}}$:

$$\begin{aligned} \mathcal{H}_{\text{diag}} = & g\mu_B H S_z + D[1 - \sin^2\theta(1 - \lambda\cos 2\psi)] S_z^2 \\ & + \frac{1}{4} D \sin^2\theta [1 - \lambda\cos 2\psi] [S_+S_- + S_-S_+] \end{aligned} \quad (\text{C5})$$

We note that there is no dependence on the angle ϕ in Eq. (C5). This is true for the complete Hamiltonian as well, and is due to the fact that only two angles are required to specify the orientation of the vector \underline{H} . Thus, only two angles can have physical significance in any system, as long as the relative orientation of the two systems has been properly defined in terms of Euler angles.

3. Derivation of the Form of $\bar{\alpha}$ for $S = 5/2$

For a given value of S , we can easily calculate the eigenvalues of $\mathcal{H}_{\text{diag}}$ using the general formula

$$S_{\pm} |m_s\rangle = [S(S+1) - m_s(m_s \pm 1)]^{1/2} |m_s \pm 1\rangle \quad (\text{C6})$$

where we have set $\hbar=1$. Since the states of $\mathcal{H}_{\text{diag}}$ are eigenstates of $S_H \equiv S_z$, the magnetic dipole transition probability derived in Appendix B

$$W_n \equiv \frac{1}{3} \left\{ \frac{1}{2} |\langle S_+ \rangle_n|^2 + \frac{1}{2} |\langle S_- \rangle_n|^2 + |\langle S_z \rangle_n|^2 \right\} \quad (\text{C7})$$

only allows transitions between adjacent energy levels. For $S = 5/2$, the transitions giving rise to absorption ($\Delta m_s = +1$) occur at energies given by

n	$ i_n\rangle$	$ f_n\rangle$	E_n	
1	$ -\frac{5}{2}\rangle$	$ -\frac{3}{2}\rangle$	$E_1 = g\mu_B H - 4D + 6D\Delta(\theta, \psi)$	
2	$ -\frac{3}{2}\rangle$	$ -\frac{1}{2}\rangle$	$E_2 = g\mu_B H - 2D + 3D\Delta(\theta, \psi)$	
3	$ -\frac{1}{2}\rangle$	$ +\frac{1}{2}\rangle$	$E_3 = g\mu_B H$	(C8)
4	$ +\frac{1}{2}\rangle$	$ +\frac{3}{2}\rangle$	$E_4 = g\mu_B H + 2D - 3D\Delta(\theta, \psi)$	
5	$ +\frac{3}{2}\rangle$	$ +\frac{5}{2}\rangle$	$E_5 = g\mu_B H + 4D - 6D\Delta(\theta, \psi)$	

where the angular dependence is specified by

$$\Delta(\theta, \psi) \equiv \sin^2\theta(1 - \lambda \cos 2\psi) \quad (C9)$$

and the transition probability is proportional to $|\langle S_+ \rangle_n|^2$. Similar relations may be obtained for any value of S. At low temperatures, the factor $P_n(T)$ will be largest for the transition $n=1$, and will rapidly decrease with n.

We shall now concentrate on a single transition, n. Assuming that the lineshape function is given by

$$\rho(\nu - \nu_n) = \delta(\nu - \nu_n) \quad (C10)$$

the expression for the powder average absorption coefficient for a single transition, neglecting numerical factors, becomes

$$\overline{\alpha}_n(\nu_n) = \frac{1}{4\pi} \int \nu_n |\langle S_+ \rangle_n|^2 P_n(T) \sin\theta \, d\theta d\psi \quad (C11)$$

The integrand can be written,

$$\alpha_n(\nu_n) d\Omega_H \equiv \frac{1}{4\pi} |\langle S_+ \rangle_n|^2 [\nu_n(\theta, \psi) P_n(\theta, \psi, T) \sin\theta] \, d\theta d\psi \quad (C12)$$

where we have explicitly indicated the functional dependence of each

term. Note that $|\langle S_+ \rangle_n|^2$ does not depend on (θ, ψ) . We now choose the pair (Δ, ψ) as independent variables, rather than (θ, ψ) . We may then rewrite Eq. (C12) as

$$\alpha_n(\Delta, \psi) d\Delta d\psi = \frac{1}{4\pi} |\langle S_+ \rangle_n|^2 [v_n(\Delta) P_n(\Delta, T) \sin\theta(\Delta, \psi)] \cdot \frac{\partial(\theta, \psi)}{\partial(\Delta, \psi)} d\Delta d\psi \quad (C13)$$

where

$$\frac{\partial(\theta, \psi)}{\partial(\Delta, \psi)} \equiv \begin{vmatrix} \frac{\partial\theta}{\partial\Delta} & \frac{\partial\psi}{\partial\Delta} \\ \frac{\partial\theta}{\partial\psi} & \frac{\partial\psi}{\partial\psi} \end{vmatrix} \quad (C14)$$

is a Jacobian determinant. Note, from Eqs. (C8), that v_n and P_n depend upon Δ alone. The polycrystalline absorption coefficient $\bar{\alpha}_n(\Delta)$ can then be obtained from Eq. (C13) by integrating over ψ :

$$\bar{\alpha}_n(\Delta) d\Delta = \int [\alpha_n(\Delta, \psi) d\Delta] d\psi \quad (C15)$$

and the relation between $\bar{\alpha}_n(\Delta)$ and $\bar{\alpha}_n(v_n)$ is easily made through the relation of v_n and Δ given by Eqs. (C8). It is easy to show that the two "distribution functions" $\bar{\alpha}_n(\Delta)$ and $\bar{\alpha}_n(v_n)$ are equal at the corresponding values of Δ and v_n .

We can write the ψ -dependent part of Eq. (C13) as the distribution function $f(\Delta, \psi)$:

$$f(\Delta, \psi) \equiv \sin\theta(\Delta, \psi) \frac{\partial(\theta, \psi)}{\partial(\Delta, \psi)} \quad (C15)$$

We then use the definition of Δ , Eq. (C9) to obtain equations for $\theta(\Delta, \psi)$, $\psi(\Delta, \theta)$ and $\sin\theta(\Delta, \psi)$, and calculate the Jacobian. After considerable algebraic manipulation, Eq. (C15) can be rewritten

$$f(\Delta, \psi) = \left\{ (1 - \lambda \cos 2\psi) [(1 - \lambda \cos 2\psi) - \Delta] \right\}^{-1/2} \quad (C16)$$

We note, as usual, that only the first octant in (θ, ψ) is required to obtain the full lineshape. In the present terms, then, the integral to be calculated over ψ is

$$\bar{f}(\Delta) = \frac{2}{\pi} \int_0^{\pi/2} [f(\Delta, \psi)] d\psi \quad (C17)$$

and the absorption coefficient will be given by

$$\bar{\alpha}_n(\Delta) = v_n(\Delta) P_n(\Delta, T) \bar{f}(\Delta) |\langle S_+ \rangle_n|^2 \quad (C18)$$

Although the nominal integration limits on ψ are now $(0, \pi/2)$, the change of variable used has introduced a constraint which limits the actual range of ψ for a given Δ . This can be seen by rewriting Eq. (C9) as

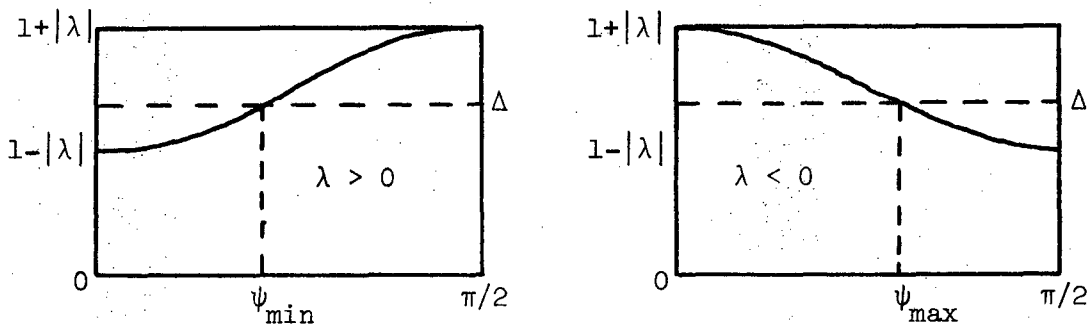
$$\sin^2 \theta = \frac{\Delta}{(1 - \lambda \cos 2\psi)} \quad (C19)$$

Since $0 \leq \sin^2 \theta \leq 1$, this relation places limits on ψ . Since $|\lambda| \leq 1/3$, $(1 - \lambda \cos 2\psi) \geq 2/3$ for all values of ψ , so the lower limit on $\sin^2 \theta$ merely requires $\Delta \geq 0$. The upper limit, however, fixes the possible range of ψ .

There are two cases, $D > 0$ and $D < 0$. If $D > 0, \lambda > 0$; if $D < 0, \lambda < 0$. In either case, the full range of Δ can be seen to be

$$0 \leq \Delta \leq 1 + |\lambda|$$

The appropriate range of ψ for any Δ in this range can be seen by plotting $(1 - \lambda \cos 2\psi)$ as a function of ψ for the two possible signs of λ :



Using Eq. (C19), the condition $\sin^2\theta \leq 1$ can be rewritten

$$(1 - \lambda \cos 2\psi) \geq \Delta \quad (C20)$$

Therefore, for a given Δ , as indicated on the graphs, the condition (C20) establishes a lower limit ψ_{\min} on ψ for $\lambda > 0$, and an upper limit ψ_{\max} for $\lambda < 0$. These limits are both given by

$$\psi_{\min, \max} = \frac{1}{2} \arccos \left[\frac{1 - \Delta}{\lambda} \right] \quad (C21)$$

and only hold for $1 - |\lambda| \leq \Delta \leq 1 + |\lambda|$. For $\Delta \leq 1 - |\lambda|$, the integration range is the whole interval.

With these conditions in mind, the evaluation of the integral in Eq. (C17) is straightforward and exceedingly tedious. The integrand, given by Eq. (C16) can be transformed to a standard form for elliptic integrals by the variable substitution

$$x = \tan \psi$$

With this substitution, the integral can be reduced to the forms

$$\int_0^{\infty} \frac{dx}{[(x^2 + a^2)(x^2 + b^2)]^{1/2}} \quad \text{for } \begin{array}{l} \lambda > 0 \quad 0 \leq \Delta \leq 1 - \lambda \\ \lambda < 0 \quad 0 \leq \Delta \leq 1 - |\lambda| \end{array}$$

$$\int_b^{\infty} \frac{dx}{[(x^2 + a^2)(x^2 - b^2)]^{1/2}} \quad \text{for } \lambda > 0 \quad 1 - \lambda \leq \Delta \leq 1 + \lambda$$

and

$$\int_0^b \frac{dx}{[(x^2 + a^2)(b^2 - x^2)]^{1/2}} \quad \text{for } \lambda < 0 \quad 1 - |\lambda| \leq \Delta \leq 1 + |\lambda|$$

where a and b are functions of λ and Δ . These integrals are related to the complete elliptic integrals of the first kind (see P. F. Byrd and M. D. Friedman, Handbook of Elliptic Integrals for Engineers and Physicists, (Springer Verlag, Berlin, 1954)).

Although the limits and integral forms depend upon the sign of λ , the results do not. The general result, for any sign of λ , and therefore of D , can be written

$$0 \leq \Delta \leq 1 - |\lambda| \quad \bar{f}(\Delta) = \frac{K(k)}{\pi[(1-|\lambda|)(1+|\lambda|-\Delta)]^{1/2}}$$

$$\text{where } k^2 = \frac{2|\lambda|\Delta}{(1-|\lambda|)(1+|\lambda|-\Delta)}$$

and

$$1 - |\lambda| \leq \Delta \leq 1 + |\lambda| \quad \bar{f}(\Delta) = \frac{K(k)}{\pi[2|\lambda|\Delta]^{1/2}}$$

$$\text{where } k^2 = \frac{(1-|\lambda|)(1+|\lambda|-\Delta)}{2|\lambda|\Delta}$$

(C22)

where $K(k)$ is the complete elliptic integral of the first kind.

The function $\bar{f}(\Delta)$ varies between an awning and a circus tent in shape as $|\lambda|$ varies from 0 to 1/3. At the two Δ -limits, 0 and $1+|\lambda|$, it is non-zero, and rises to a sharp peak at $\Delta = 1-|\lambda|$. Examples of $\bar{f}(\Delta)$ for several values of $|\lambda|$ are plotted in Fig. C1.

Eq. (C18) can now be explicitly evaluated for each Δ , and we can write

$$\bar{\alpha}_n(v_n) = v_n P_n v_n(\Delta), T \quad \bar{f}(\Delta(v_n)) \quad | \langle S_+ \rangle_n |^2 \quad (C23)$$

The absorption coefficients for each n , calculated from this equation, can be graphically added to obtain the total $\bar{\alpha}(v)$.

4. Calculation of $\bar{\alpha}$ for $S=5/2$, $H=52.2$ kOe

We have written a computer program for the IBM 1620₂ computer to calculate $\bar{\alpha}_n(v_n)$ for each transition. The program, called LINESHAPES, is listed immediately following this section. The input parameters are D , $|\lambda|$, and T . The results for each transition are printed, and can be graphically added. An example of the results for two values of D and $|\lambda|$ has been plotted in Fig. 6.

```
C PROGRAM LINESHAPES.
C
C PROGRAM LINESHAPES CALCULATES THE BARE POWDER AVERAGE LINESHAPE
C IN THE HIGH FIELD LIMIT FOR S = 5/2 FOR A SPECIFIED ABS(LAMBDA),
C D, AND T. THE APPLIED FIELD IS ASSUMED TO BE 52.2 KOE.
C
C
C DIMENSION AK(101)
C
C READ IN A TABLE OF THE COMPLETE ELLIPTIC INTEGRAL OF THE FIRST
C KIND, AK(K**2).
C
C READ 50, (AK(I), I=1,101)
50 FORMAT(10F7.2)
C
C READ PARAMETERS
C
C READ 51, ALAM
51 FORMAT(1F5.3)
C READ 52, D
52 FORMAT(1F6.3)
C READ 51, T
PRINT 5
5 FORMAT(1H1)
PRINT 53
53 FORMAT(5X,45HABSORPTION LINESHAPES FI(EI) FOR H = 52.2 KOE)
PRINT 54, D, ALAM, T
54 FORMAT(/5X,4HD = F7.3//5X,9HLAMBDA = F5.3//(5X,4HT = F6.3))
C
C CALCULATE DELTA INTERVAL
C
C DMAX = ALAM + 1.
C DMID = 1. - ALAM
C DI1 = DMID / 20.
C ALAMT = 2. * ALAM
C DI2 = ALAMT / 20.
C
C CALCULATE KT IN CM**-1
C
C AKT = 0.695 * T
PRINT 55
55 FORMAT(///8X,2HE1,8X,6HF1(E1),8X,2HE2,8X,6HF2(E2),8X,2HF3,10X
1,2HE4,8X,6HF4(E4),8X,2HE5,8X,6HF5(E5),/)
C
C THIS LOOP CALCULATES THE ABSORPTION COEFFICIENT FOR ALL
C TRANSITIONS FOR DELTA IN THE RANGE 0 TO 1 - ABS(LAMBDA)
C
C
C DO 1 N = 1,20
C AN = N - 1
C DELTA = AN * DI1
C
C CALCULATE TRANSITION FREQUENCIES
C
C EA1 = 4.874 - 4.*D + 6.*D*DELTA
C EA2 = 4.874 - 2.*D + 3.*D*DELTA
C EA3 = 4.874
C EA4 = 4.874 + 2.*D - 3.*D*DELTA
```

```
EA5 = 4.874 + 4.*D - 6.*D*DELTA
C
C CALCULATE EIGENVALUES
C
WA2 = EA1
WA3 = WA2 + EA2
WA4 = WA3 + EA3
WA5 = WA4 + EA4
WA6 = WA5 + EA5
C
C CALCULATE DENOMINATOR OF P(N,T)
C
SUMA = 1. + EXPF(-WA2/AKT) + EXPF(-WA3/AKT) + EXPF(-WA4/AKT)
1+ EXPF(-WA5/AKT) + EXPF(-WA6/AKT)
C
C CALCULATE K**2
C
BKS = (ALAMT*DELTA)/(DMID*(DMAX-DELTA))
C
C INTERPOLATE TO FIND AK(K**2)
C
BKS = (100. * BKS) + 1.
LBKS = BKS
MBKS = LBKS + 1
PBKS = LBKS
DIFK = AK(MBKS) - AK(LBKS)
EIK = AK(LBKS) + DIFK * (BKS - PBKS)
C
C EIK IS AK(K**2)
C
EIK = EIK * 0.0001
C
C TARGA IS MULTIPLICATIVE FACTOR FOR THIS REGION OF DELTA
C
TARGA = 1./(3.14159*SQRTF(DMID*(DMAX-DELTA)))
C
C PATN IS P(N,T)
C
PAT1 = (1. - EXPF(-WA2/AKT))/SUMA
PAT2 = (EXPF(-WA2/AKT) - EXPF(-WA3/AKT))/SUMA
PAT3 = (EXPF(-WA3/AKT) - EXPF(-WA4/AKT))/SUMA
PAT4 = (EXPF(-WA4/AKT) - EXPF(-WA5/AKT))/SUMA
PAT5 = (EXPF(-WA5/AKT) - EXPF(-WA6/AKT))/SUMA
C
C FEAN IS ALPHA(N, EAN)
C
FEA1 = 0.555 * EA1 * PAT1 * TARGA * EIK
FEA2 = 0.888 * EA2 * PAT2 * TARGA * EIK
FEA3 = EA3 * PAT3
FEA4 = 0.888 * EA4 * PAT4 * TARGA * EIK
FEA5 = 0.555 * EA5 * PAT5 * TARGA * EIK
C
C PRINT
C
PRINT 100, EA1,FEA1,EA2,FEA2,FEA3,EA4,FEA4,EA5,FEA5
100 FORMAT(/1X,9F12.4)
1 CONTINUE
C
C THIS LOOP CALCULATES THE ABSORPTION COEFFICIENT FOR DELTA IN THE
```

C
C
C

RANGE 1 - ABS(LAMBDA) TO 1 + ABS(LAMBDA).

```

DO 2 M = 1,20
AM = M
GELTA = DMID + AM * DI2
EB1 = 4.874 - 4.*D + 6.*D*GELTA
EB2 = 4.874 - 2.*D + 3.*D*GELTA
EB3 = 4.874
EB4 = 4.874 + 2.*D - 3.*D*GELTA
EB5 = 4.874 + 4.*D - 6.*D*GELTA
WB2 = EB1
WB3 = WB2 + EB2
WB4 = WB3 + EB3
WB5 = WB4 + EB4
WB6 = WB5 + EB5
SUMB = 1. + EXPF(-WB2/AKT) + EXPF(-WB3/AKT) + EXPF(-WB4/AKT)
1+ EXPF(-WB5/AKT) + EXPF(-WB6/AKT)
CKS = (DMID*(DMAX-GELTA))/(ALAMT*GELTA)
CKS = (100. * CKS) .+ 1.
LCKS = CKS
MCKS = LCKS + 1
PCKS = LCKS
DIRK = AK(MCKS) - AK(LCKS)
ORK = AK(LCKS) + DIRK * (CKS - PCKS)
ORK = ORK * 0.0001
TARGB = 1./((3.14159*SQRT(ALAMT*GELTA))
PBT1 = (1. - EXPF(-WB2/AKT))/SUMB
PBT2 = (EXPF(-WB2/AKT) - EXPF(-WB3/AKT))/SUMB
PBT3 = (EXPF(-WB3/AKT) - EXPF(-WB4/AKT))/SUMB
PBT4 = (EXPF(-WB4/AKT) - EXPF(-WB5/AKT))/SUMB
PBT5 = (EXPF(-WB5/AKT) - EXPF(-WB6/AKT))/SUMB
FEB1 = 0.555 * EB1 * PBT1 * TARGB * ORK
FEB2 = 0.888 * EB2 * PBT2 * TARGB * ORK
FEB3 = EB3 * PBT3
FEB4 = 0.888 * EB4 * PBT4 * TARGB * ORK
FEB5 = 0.555 * EB5 * PBT5 * TARGB * ORK
PRINT 100, EB1,FEB1,EB2,FEB2,EB3,FEB3,EB4,FEB4,EB5,FEB5
CONTINUE

```

2
C
C

CALL EXIT
END

15708	15747	15787	15828	15869	15910	15952	15994	16037	16080
16124	16169	16214	16260	16306	16353	16400	16448	16497	16546
16596	16647	16698	16751	16804	16857	16912	16967	17024	17081
17139	17198	17258	17319	17381	17444	17508	17573	17639	17706
17775	17845	17916	17989	18063	18139	18216	18295	18375	18457
18541	18626	18714	18804	18895	18989	19085	19184	19285	19398
19496	19605	19718	19834	19953	20076	20203	20334	20469	20609
20754	20904	21059	21221	21390	21565	21748	21940	22140	22351
22572	22805	23052	23314	23593	23890	24209	24553	24926	25333
25781	26278	26836	27471	28208	29083	30161	31559	33541	36956
99999									

D. Magnetic Torque for a Paramagnetic Ion in an Axial Ligand Field

In this appendix, we shall derive the general equation for the magnetic torque on a paramagnetic ion in an axial ligand field and an external magnetic field. We shall also give a brief calculation of the torque per unit volume for two specific cases where the ion has spin $S = 3/2$.

1. Derivation of the Expression for the Magnetic Torque

We consider an ion described by the modified form of the spin Hamiltonian

$$\mathcal{H} = g\mu_B \vec{H} \cdot \vec{S} + D[S^2 - S(S+1)/3] \quad (D1)$$

where the form and definitions are the same as those given for Eq. (2) with the exception that we have assumed a strictly axial field, and thus $E=0$. The torque per unit volume, $\vec{\tau}$, is given by

$$\vec{\tau} = \vec{M} \times \vec{H} \quad (D2)$$

where \vec{M} is the magnetic moment per unit volume. For N ions per unit volume, \vec{M} is defined as

$$\vec{M} \equiv N \langle \vec{\mu} \rangle \quad (D3)$$

where $\langle \vec{\mu} \rangle$ is the magnetic moment per ion. We may also define

$$\vec{M} \equiv \underline{\underline{\chi}} \vec{H} \quad (D4)$$

where $\underline{\underline{\chi}}$ is the susceptibility tensor. We may relate $\vec{\tau}$ to the principal values of $\underline{\underline{\chi}}$ by observing that, in the system in which the spin Hamiltonian is written, $\underline{\underline{\chi}}$ is diagonal, so $\chi_{xx} = \chi_{yy} \equiv \chi_{\perp}$, and $\chi_{zz} \equiv \chi_{\parallel}$. If we choose \vec{H} to lie in the x-y plane at an angle θ to the z-axis,

$$\vec{M} = \vec{\chi} \vec{H} = \chi_{\perp} H \sin\theta \hat{e}_x + \chi_{\parallel} H \cos\theta \hat{e}_z \quad (D5)$$

where \hat{e}_x and \hat{e}_z are unit vectors in the x- and z- directions respectively. If we now substitute the expression for \vec{M} , Eq. (D5), into Eq. (D2), the result is

$$\vec{\tau} = \vec{M} \times \vec{H} = [\chi_{\parallel} H^2 \sin\theta \cos\theta - \chi_{\perp} H^2 \sin\theta \cos\theta] \hat{e}_y$$

or

$$\vec{\tau} = \frac{1}{2} (\chi_{\parallel} - \chi_{\perp}) H^2 \sin 2\theta \hat{e}_y. \quad (D6)$$

We may observe the following:

- (i) If $D=0$, $\chi_{\parallel} = \chi_{\perp}$, and $|\vec{\tau}| = 0$.
- (ii) If $\theta=0$ or $\pi/2$, $|\vec{\tau}| = 0$.
- (iii) The maximum torque occurs for $\theta = \pi/4$.

Now, in order to calculate $\vec{\tau}$, we need only calculate χ_{\parallel} and χ_{\perp} . Since $\vec{\chi}$ is diagonal, Eq. (D3) and Eq. (D4) imply that

$$N\langle\mu_{\perp}\rangle = \chi_{\perp} H_{\perp} \quad \text{and} \quad N\langle\mu_{\parallel}\rangle = \chi_{\parallel} H_{\parallel} \quad (D7)$$

Therefore, we need only calculate the quantities $\langle\mu_x\rangle$ for $\vec{H} = H\hat{e}_x$ and $\langle\mu_z\rangle$ for $\vec{H} = H\hat{e}_z$ in order to obtain χ_{\parallel} and χ_{\perp} .

At a temperature T , the thermal average value of $\langle\mu\rangle$ for ions in thermal equilibrium with the lattice is given by

$$\langle\mu\rangle = \frac{\sum_s \mu_s \exp(-E_s/kT)}{\sum_s \exp(-E_s/kT)} \quad (D8)$$

where the sum is over all electronic states s of energy E_s . The

corresponding equations for $\langle \mu_{\perp} \rangle$ and $\langle \mu_{\parallel} \rangle$ follow directly. For ions described by Eq. (D1) at low temperatures, the sum need only include the states in the ground multiplet.

The calculation of $\langle \mu_{\parallel} \rangle$ is simple, since the states are eigenstates of S_z with magnetic moments μ given by

$$\mu_s = -g\mu_B m_s \hat{e}_z \quad (D9)$$

where μ_B is the Bohr magneton, and m_s is the eigenvalue of S_z for the state s . The energies E_s are similarly given by

$$E_s = g\mu_B H m_s + D[m_s^2 - S(S+1)/3] \quad (D10)$$

However, for a perpendicular field $H = H\hat{e}_x$, the situation is slightly more complicated, due to the admixture of states discussed in Section II. We need to calculate the quantity

$$\mu_{s_x} \equiv - \langle \psi_s | g\mu_B S_x | \psi_s \rangle \quad (D11)$$

where $\langle \psi_s |$ is the eigenfunction of the spin Hamiltonian for state s .

However, we note that

$$\begin{aligned} E_s &= \langle \psi_s | \mathcal{H} | \psi_s \rangle \\ &= \langle \psi_s | g\mu_B H S_x | \psi_s \rangle + \langle \psi_s | D[S_z^2 - S(S+1)/3] | \psi_s \rangle \end{aligned} \quad (D12)$$

$$= -H\mu_{s_x} - \frac{DS(S+1)}{3} + D\langle \psi_s | S_z^2 | \psi_s \rangle$$

Therefore

$$\mu_{s_x} = - \frac{1}{H} \left\{ E_s + \frac{DS(S+1)}{3} - D\langle \psi_s | S_z^2 | \psi_s \rangle \right\} \quad (D13)$$

If we have the expansion of $\langle \psi_s |$ in terms of eigenstates of S_z , obtained from diagonalizing the spin Hamiltonian, the calculation of $\langle \psi_s | S_z^2 | \psi_s \rangle$ is simple. Since we shall have to diagonalize the spin Hamiltonian to obtain E_s , this is a useful form for μ_{s_x} . We note that Eq. (D13) also gives Eq. (D9) if $\tilde{H} = H \hat{e}_z$ and Eq. (D10) is used to obtain the value of E_s . We also note that the equations in this section involve no approximations, and that in general no approximations may be made in the calculation of τ for the compounds discussed in this thesis.

2. Calculation of τ for $S=3/2$

We shall now briefly outline the calculation of τ for two specific cases with $S=3/2$. For this spin value, the expansion of the eigenvectors in terms of eigenstates of S_z can be obtained from the integration tables printed out by the program SHAZAM, discussed in Appendix B. If the eigenstate β of S_z with eigenvalue m_β is represented by $|m_\beta\rangle$ the expansion is

$$|\psi_s\rangle = \sum_{\beta} \alpha_{s\beta} |m_\beta\rangle \quad (D14)$$

where the coefficients of $\alpha_{s\beta}$ must be calculated for $\tilde{H} \parallel \hat{z}$. In particular,

$$|\psi_s\rangle = \alpha_{s1} \left| \frac{3}{2} \right\rangle + \alpha_{s2} \left| \frac{1}{2} \right\rangle + \alpha_{s3} \left| -\frac{1}{2} \right\rangle + \alpha_{s4} \left| -\frac{3}{2} \right\rangle \quad (D15)$$

and the evaluation of $\langle \psi_s | S_z^2 | \psi_s \rangle$ is simply

$$\langle \psi_s | S_z^2 | \psi_s \rangle = \frac{9}{4} [|\alpha_{s1}|^2 + |\alpha_{s4}|^2] + \frac{1}{4} [|\alpha_{s2}|^2 + |\alpha_{s3}|^2] \quad (D16)$$

a. Case 1

We choose the specific case $D=+7.58 \text{ cm}^{-1}$, $T=4.2^\circ\text{K}$, and $H=52.2 \text{ kOe}$,

which is appropriate to our measurements for the compound

$((C_2H_5)_2NCS_2)_2 Fe(III) Br$. Some useful values are

$$k(T=4.2^\circ K) = 2.919 \text{ cm}^{-1}$$

and

$$\mu_B(H=52.2 \text{ kOe}) = 2.4370 \text{ cm}^{-1}$$

With these values and the information obtained from SHAZAM, the calculated values of $\langle \mu_{\parallel} \rangle$ and $\langle \mu_{\perp} \rangle$ are

$$\langle \mu_{\parallel} \rangle = +0.7462 \mu_B$$

$$\langle \mu_{\perp} \rangle = +2.2804 \mu_B$$

where we have used Eqs. (D8), (D9) and (D13). We note that $\langle \mu_{\perp} \rangle > \langle \mu_{\parallel} \rangle$. This result is due to the fact that the magnetic moment is largely due to the states originating in the ground doublet, because the zero field splitting is large. However, the ground doublet has $g_{\perp} \approx 4$, $g_{\parallel} \approx 2$, indicating that $\langle \mu_{\perp} \rangle > \langle \mu_{\parallel} \rangle$, as found.

Using Eqs. (D7), we may calculate χ_{\parallel} and χ_{\perp} :

$$\chi_{\parallel} = \frac{N}{H} \langle \mu_{\parallel} \rangle \quad \chi_{\perp} = \frac{N}{H} \langle \mu_{\perp} \rangle$$

Then Eq. (D6) becomes

$$\tilde{\tau} = \frac{N\mu_B}{2} (\langle \mu_{\parallel} \rangle - \langle \mu_{\perp} \rangle) H \sin 2\theta \hat{e}_y$$

and substitution of the value $N=2.33 \times 10^{21}$ ions/cm³, which is obtained from x-ray crystallographic data for the bis Fe(III) dithiocarbamates, gives

$$\tilde{\tau} = -(8.65 \times 10^5) \sin 2\theta \hat{e}_y$$

where the units are dyne-cm/cm³. Note that this torque tends to rotate the crystallite toward $H \perp \hat{z}$.

b. Case 2

For $D=2.35 \text{ cm}^{-1}$, $T=4.2^\circ\text{K}$, and $H=52.2 \text{ kOe}$, a similar calculation yields

$$\langle \mu_{\parallel} \rangle = +2.8631 \mu_B$$

$$\langle \mu_{\perp} \rangle = +2.0384 \mu_B$$

We note that in this case, $\langle \mu_{\parallel} \rangle$ is more nearly equal to $\langle \mu_{\perp} \rangle$. Although consideration of the ground doublet alone ($g_{\parallel} \simeq 6$, $g_{\perp} \simeq 0$) would imply $\langle \mu_{\parallel} \rangle \gg \langle \mu_{\perp} \rangle$, the value of D chosen is small enough so that all of the states must be included. This calculation is appropriate to the compound $((i-C_3H_7)_2NCS_2)_2Fe(III)Cl$. In this case

$$\tau = +(4.67 \times 10^5) \sin 2\theta \hat{e}_y$$

with the same units. This torque tends to rotate the crystallite toward $H \parallel \hat{z}$.

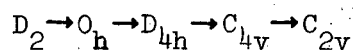
These calculations serve to illustrate two important points:

- (i) If $D > 0$, the torque tends to rotate the crystallite toward $H \perp \hat{z}$; if $D < 0$, the torque tends to rotate the crystallite toward $H \parallel \hat{z}$.
- (ii) If $|D|$ is such that $|D|/kT \leq 1$, the torque becomes small. However, the calculated torque in both cases is quite large, and is certainly sufficient to produce substantial orientation in a polycrystalline sample.

E. Stabilization of a 4A_2 State for Fe(III) in bis Fe(III) Dithiocarbamates

In this appendix, we shall give a brief plausibility argument for the stabilization of a d^5 ion 4A_2 state in C_{2v} symmetry, with the specific application of the comments to Fe(III) in the bis Fe(III) dithiocarbamates. The approach will be to examine the effects of successive reductions of symmetry from O_h to C_{2v} on the d^1 levels, and then to populate these levels with five electrons to obtain the d^5 state. We will use the notation and character tables given by Tinkham³, and the representation multiplication table given in G. F. Koster, J. O. Dimmock, R. G. Wheeler, and H. Statz, Properties of the Thirty-two Point Groups (M.I.T. Press, Cambridge, 1963).

We shall consider the specific reduction



where we have denoted the full rotation group for $\ell=2$ (appropriate to d^1) by D_2 . In terms of the bis Fe(III) dithiocarbamates, this reduction sequence corresponds to the changes in the iron environment shown in Fig. E1. We consider the iron to lie at the origin of the coordinate system shown in each case. The symmetry O_h corresponds to an octahedron of sulfur atoms surrounding the iron site. The reduction to D_{4h} is accomplished by replacing two sulfur atoms with halogen atoms, as shown. Two changes can be made in lowering the symmetry to C_{4v} : one of the halogen atoms is removed, and the iron site (the origin) is moved out of the plane of sulfur atoms to the approximate centroid of the square pyramid formed by the ligands. Finally, in the reduction to C_{2v} symmetry, the coordinate axes are rotated 45° as shown (in order to correspond to

the definitions of the operators of this group), the square formed by the sulfur atoms is distorted to a rectangle with the longer dimension in the x-direction, and additional ligands are added in the xz-plane as shown.

The effect of these changes on the d^1 orbitals is schematically indicated in Fig. E2. The splitting of states on a reduction of symmetry is found by decomposing the irreducible representations of the higher-symmetry group into those of the lower-symmetry group using the character tables given by Tinkham. Some care is required to determine the corresponding symmetry operators in the two groups, especially in the last reduction which is accompanied by a change of axes. (The general method is described by Tinkham.) However, the magnitude of the energy splittings and the order of the split states in energy must be obtained by arguments based upon the specific changes in the iron environment outlined above. We shall discuss these effects for each reduction in the following sections.

1. $D_2 \rightarrow O_h$

The effects of this reduction are well-known. The decomposition is

$$D_2 = E_g + T_{2g} \quad (E1)$$

where the O_h representations E_g and T_{2g} give respectively doubly- and triply-degenerate states with the basis functions

$$E_g: d_{x^2-y^2}, d_{3z^2-r^2}$$

$$T_{2g}: d_{xy}, d_{yz}, d_{xz}$$

Since the lobes of the E_g basis functions point toward the ligands, the energy of this state is higher than that of the T_{2g} state, where the lobes point between the ligands. The energy separation, commonly designated $10Dq$, should be of the order of 10^4 cm^{-1} for this system.

2. $O_h \rightarrow D_{4h}$

Here, the decomposition is

$$\begin{aligned} E_g(O_h) &= B_{1g}(D_{4h}) + A_{1g}(D_{4h}) \\ T_{2g}(O_h) &= B_{2g}(D_{4h}) + E_g(D_{4h}) \end{aligned} \quad (E2)$$

where the basis functions are indicated in Fig. E2. The order of these states in energy is obtained by assuming that the interaction of the iron and halide is weaker than that of the iron and sulfur. This assumption, which will be made in all of the remaining arguments, is consistent with the stability of the series of dithiocarbamate compounds with different halide ligands. With this assumption, the $A_{1g}(d_{z^2})$ state should decrease in energy and the $B_{1g}(d_{x^2-y^2})$ should increase in energy with respect to the octahedral E_g state, and the splitting of the octahedral T_{2g} state should be small, with the $E_g(d_{xz}, d_{yz})$ lying lowest.

3. $D_{4h} \rightarrow C_{4v}$

The irreducible representations of D_{4h} for d^1 have a one-to-one relationship with the corresponding representations of C_{4v} . However, substantial changes in the energies of the states should occur because of the changes in the environment shown in Fig. E1. The removal of one halide ligand should substantially reduce the energy of the $A_1(d_{z^2})$ state, and should slightly lower the $E(d_{yz}, d_{xz})$ state. (We have

dropped the subscript g since there is now no center of symmetry.)

However, the displacement of the iron site out of the sulfur plane should substantially increase the energy of the E states, while decreasing that of the $B_2(d_{xy})$ state. This situation is shown in Fig. E2 by the crossing of the two levels on the reduction from D_{4h} to C_{4v} . Similarly, the energy of the $B_1(d_{x^2-y^2})$ state should decrease.

4. $C_{4v} \rightarrow C_{2v}$

In this case, the only decomposition is

$$E(C_{4v}) = B_1(C_{2v}) + B_2(C_{2v})$$

The changes made in the environment should result in the small splitting shown, with the $B_2(d_{yz})$ state lying lowest. However, the change of axes has brought about a corresponding change in the basis functions and representations, as indicated. The shifts in energy of the remaining states should be small.

With this system, a quartet state may be stabilized by the large splitting between the ground $A_1'(d_{x^2-y^2})$ state and the cluster of three states $A_1(d_{z^2})$, $B_1(d_{xz})$, and $B_2(d_{xy})$. The large separation between this cluster and the highest $A_2(d_{xy})$ state suggests that an appropriate population of the d^1 levels, as shown in Fig. E2, would be

$$a_1'^2 b_2^1 b_1^1 a_1^1 : {}^4A_2$$

where the representation of the product state has been obtained by the relation

$$A_1 \times A_1 \times B_2 \times B_1 \times A_1 = A_2 \tag{E4}$$

obtained from Koster et al. A more complete analysis of this system

would require at least a calculation using the complete d^5 manifold of states, and the behavior of the tris and bis pyrrolidyl complexes suggests that a molecular orbital analysis would be more appropriate.

F. Exchange-coupled Paramagnetic Ions with $S=3/2$ in an Axial Ligand Field

In this appendix, we shall examine the behavior of a pair of paramagnetic ions with $S_1, S_2 = 3/2$, whose Hamiltonian is

$$\mathcal{H} = D[S_{1z}^2 + S_{2z}^2] + 2J[S_{1z}S_{2z}] - \frac{1}{3}D[S_1^2 + S_2^2] \quad (F1)$$

This Hamiltonian corresponds to two ions with spin S_1 and S_2 in the same axial field, and coupled by a Heisenberg exchange interaction. We shall study the variation of the eigenvalues and eigenvectors as a function of the dimensionless parameter J/D .

4. Limiting Cases

In the two limits, $J/D=0$ and $J/D=\infty$, the Hamiltonian in Eq. (F1) can be easily analyzed. For $J/D=0$, the appropriate representation is in terms of the operators $\{S_1, S_2, S_{1z}, S_{2z}\}$, and the eigenstates are simple products of eigenstates of S_{1z} ($|m_{s1}\rangle$) and S_{2z} ($|m_{s2}\rangle$). The eigenvalues are easily calculated from Eq. (F1) with $J=0$:

State	Eigenvalue	Degeneracy
$ \frac{3}{2}\rangle \frac{3}{2}\rangle$	2D	4
$ \frac{3}{2}\rangle \frac{1}{2}\rangle, \frac{1}{2}\rangle \frac{3}{2}\rangle$	0	8
$ \frac{1}{2}\rangle \frac{1}{2}\rangle$	-2D	4

(F2)

where all possible permutations of the states $|m_{s1}\rangle|m_{s2}\rangle$ are to be taken.

For $J/D=\infty$ ($D=0$), we choose a representation in terms of $\{S_1, S_2, S, S_z\}$, where

$$S = S_1 + S_2 \quad (F3)$$

The eigenstates of \mathcal{H} are now eigenstates of S^2 and S_z , $|S, m_s\rangle$. This

can be easily seen by noting

$$S^2 = S_1^2 + S_2^2 + 2S_1 \cdot S_2 \quad (F4)$$

and therefore

$$\mathcal{H} = 2JS_1 \cdot S_2 = J[S^2 - S_1^2 - S_2^2] \quad (F5)$$

The eigenvalues clearly only depend upon S, and they are easily obtained from Eq. (F5):

State	Eigenvalue	Degeneracy
$ 3, m_s\rangle$	$(9/2)J$	7
$ 2, m_s\rangle$	$-(3/2)J$	5
$ 1, m_s\rangle$	$-(11/2)J$	3
$ 0, 0\rangle$	$-(15/2)J$	1

(F6)

where we have used the fact that $|S_1 - S_2| \leq S \leq S_1 + S_2$.

2. Intermediate Case

We now consider the intermediate range $0 < J/D < \infty$. In this range, we must diagonalize the entire Hamiltonian of Eq. (F1). This task seems formidable at first, since, for two $S=3/2$ ions, \mathcal{H} is a 16×16 matrix. However, the form of the Hamiltonian introduces considerable simplification.

We shall choose as a basis set the product wave functions $|m_{s1}\rangle |m_{s2}\rangle$. In this representation, the axial ligand field terms in Eq. (F1) are easily evaluated. The exchange term may be written

$$2JS_1 \cdot S_2 = 2J(S_{1x}S_{2x} + S_{1y}S_{2y} + S_{1z}S_{2z}) \quad (F7)$$

and the substitution of the ladder operators for each ion,

$$S_+ = S_x + iS_y \quad (F8)$$

$$S_- = S_x - iS_y,$$

into Eq. (F7) yields

$$2JS_{1z} \cdot S_{2z} = J[S_{1+}S_{2-} + S_{1-}S_{2+} + 2S_{1z}S_{2z}] \quad (F9)$$

The term in $S_{1z}S_{2z}$ is diagonal, and the properties of the ladder operators show that the remaining terms couple the state $|m_{s1}\rangle|m_{s2}\rangle$ to $|m_{s1}+1\rangle|m_{s2}-1\rangle$ and $|m_{s1}-1\rangle|m_{s2}+1\rangle$. If the Hamiltonian matrix is arranged so that coupled states are adjacent, the result is a block-diagonal matrix with zeros everywhere except in seven blocks along the diagonal. These blocks are formed matrix elements of the coupled sets

$$\begin{aligned} & \left\{ \left| \frac{3}{2}, \frac{3}{2} \right\rangle \right\}, \left\{ \left| -\frac{3}{2}, -\frac{3}{2} \right\rangle \right\}, \\ & \left\{ \left| -\frac{3}{2}, -\frac{1}{2} \right\rangle, \left| -\frac{1}{2}, -\frac{3}{2} \right\rangle \right\}, \left\{ \left| \frac{3}{2}, \frac{1}{2} \right\rangle, \left| \frac{1}{2}, \frac{3}{2} \right\rangle \right\}, \\ & \left\{ \left| \frac{1}{2}, -\frac{3}{2} \right\rangle, \left| -\frac{1}{2}, -\frac{1}{2} \right\rangle, \left| -\frac{3}{2}, \frac{1}{2} \right\rangle \right\}, \left\{ \left| \frac{3}{2}, -\frac{1}{2} \right\rangle, \left| \frac{1}{2}, \frac{1}{2} \right\rangle, \left| -\frac{1}{2}, \frac{3}{2} \right\rangle \right\}, \\ & \left\{ \left| \frac{3}{2}, -\frac{3}{2} \right\rangle, \left| \frac{1}{2}, -\frac{1}{2} \right\rangle, \left| -\frac{1}{2}, \frac{1}{2} \right\rangle, \left| -\frac{3}{2}, \frac{3}{2} \right\rangle \right\}. \end{aligned}$$

Thus, there is one 4x4 block matrix and two 1x1, two 2x2, and two 3x3 matrices on the diagonal. A calculation of the matrix elements using the equation

$$S_{\pm}|m_s\rangle = [S(S+1) - m_s(m_s \pm 1)]^{1/2}|m_s \pm 1\rangle \quad (F10)$$

shows that the pairs of matrices of the same dimension have the same eigenvalues. In addition, an examination of the coupled sets of states listed above shows that each set corresponds to a single value of m_s , the eigenvalue of S_z , and that the paired matrices of the same dimension

have opposite values of m_s . We therefore observe

- (i) The quantity m_s is a good quantum number for all J/D
- (ii) For every state with $m_s \neq 0$, there will be another state with $m'_s = -m_s$ with the same energy.

The secular equation for each matrix can be solved in closed form by appropriate factorization. The resulting eigenvalues are

m_s	E	
± 3	$2D + (9/2)J$	
	$(9/2)J$	
± 2	$-(3/2)J$	
	$-(3/2)J$	(F11)
± 1	$-D - J/2 \pm [D^2 - 2DJ + 25J^2]^{1/2}$	
	$-(9/2)J \pm [4D^2 + 9J^2]^{1/2}$	
0	$-J/2 \pm [4D^2 - 16DJ + 25J^2]^{1/2}$	

It is easy to show that these eigenvalues tend to the proper values in the limits previously discussed.

It is clear from Eqs. (F11) that for values of $J/D > 0.1$, substantial splitting of the $J=0$ eigenvalues occurs. For example, in a magnetic resonance experiment such as that discussed in this thesis for

$\left((C_2H_5)_2NCS_2 \right)_2 Fe(III) Cl$ in the paramagnetic state, this splitting results in a large broadening of the zero-field magnetic resonance at

$\nu = 2D$.

G. Ferromagnetic Resonance Frequency for Ions in an Axial Ligand Field with $D < 0$

In this appendix, we shall use simple classical arguments to derive the relationship between the ferromagnetic resonance frequency for $H=0$ and $T=0$, for a system of ions in an axial ligand field, and the axial crystal field parameter $D < 0$. In the following discussion, we shall neglect demagnetization effects since the saturation magnetization of the Fe(III) dithiocarbamates, to which these results apply, is of the order of 65 gauss.

1. Ferromagnetic Resonance in the Uniform Mode

First, we shall discuss the motion of a system of ferromagnetically-coupled ions in an external field, \underline{H} . The equation of motion for the magnetization \underline{M} is

$$\frac{d\underline{M}}{dt} = g\mu_B \underline{M} \times \underline{H} \quad (G1)$$

The solution of this equation is discussed extensively by Kittel.⁵⁴ The solutions consist of plane waves of wavevector \underline{k} in which the ionic spins precess about the direction of the external field with frequency ν . For $T=0$, the deviation of the spin direction from the direction of the magnetic field \underline{H} is small, and the frequency of the precession in the uniform ($k=0$) mode is given by

$$\nu_0 = g\mu_B H \quad (G2)$$

A uniaxial anisotropy in the ionic environment may be represented by the energy density

$$\mathcal{H}_A = -\underline{M} \cdot \underline{H}_A \quad (G3)$$

where we have approximated the effects of anisotropy for small spin deviations by the effect of an "anisotropy field" \tilde{H}_A . For such a system, the spins precess with a frequency

$$\nu_0 = g\mu_B \tilde{H}_A \quad (G4)$$

at $T=0$ and in the absence of an applied magnetic field. Ferromagnetic resonance absorption will be observed for incident radiation of this frequency.

2. Anisotropy Field for Ions in an Axial Ligand Field with $D < 0$.

The axial part of the spin Hamiltonian of Eq. (2) for an ion in an axial field is

$$\mathcal{H} = DS_z^2 \quad (G5)$$

where we have ignored the constant term. If $D < 0$, the ionic spin at low temperatures will tend to align along the z-direction. This will give rise to an anisotropy energy density

$$\mathcal{H}'_A = -N|D|S_z^2 \quad (G6)$$

where N is the number of ions per unit volume. In order to obtain the effective anisotropy field \tilde{H}'_A such that

$$\mathcal{H}'_A = -M \cdot \tilde{H}'_A \quad (G7)$$

we expand the anisotropy energy density Eq. (G6) in terms of the polar angle θ between \tilde{S} and the +z-direction:

$$\mathcal{H}'_A = -N|D|S_z^2 \cong -N|D|S^2 \cos^2 \theta \quad (G8)$$

where we observe that, at $T=0$, $\theta \ll 1$ so Eq. (G8) becomes

$$\begin{aligned} \mathcal{H}'_A &\cong -N|D|S^2 \left(1 - \frac{\theta^2}{2}\right)^2 \\ &\cong -N|D|S^2(1 - \theta^2) \end{aligned} \quad (G9)$$

We note that an additional classical approximation has been made to obtain Eqs. (G8) and (G9). We have neglected the quantization of the projection of \underline{s} on \hat{e}_z in Eq. (G8), and therefore our result will be exact only for large spin S (where this approximation is valid).

We may obtain a more useful form of \mathcal{H}'_A :

$$\mathcal{H}'_A = -2N|D|S^2(1 - \frac{\theta^2}{2}) + N|D|S^2 \quad (G10)$$

where we have subtracted and added the constant $N|D|S^2$. A similar expansion of Eq. (G7) gives

$$\begin{aligned} \mathcal{H}'_A &= -\underline{M} \cdot \underline{H}'_A = -(-Ng\mu_B)S \cdot \underline{H}'_A \\ &= -Ng\mu_B SH'_A \cos \theta \\ &\cong -Ng\mu_B SH'_A (1 - \frac{\theta^2}{2}) \end{aligned} \quad (G11)$$

where we have assumed that $\underline{H}'_A = -H'_A \hat{e}_z$, and that S is nearly in the $+z$ -direction, as in Eq. (G9). A comparison of the angle-dependent parts of Eqs. (G10) and (G11) shows that

$$2N|D|S^2 = Ng\mu_B SH'_A$$

and that therefore

$$H'_A = \frac{2|D|S}{g\mu_B} \quad (G12)$$

Therefore, the effect of the axial ligand field for large S and $T=0$ may be approximated by that of the anisotropy field, Eq. (G12). As discussed in the text, this classical equation may be corrected to the appropriate quantum expression by multiplying S by the factor

$$\eta = (1 - 1/(2S)) \quad (G13)$$

Therefore,

$$H'_A = \frac{2|D|S\eta}{g\mu_B} = \frac{2|D|(S-\frac{1}{2})}{g\mu_B} \quad (G14)$$

and the corresponding ferromagnetic resonance at $T=0$ and $H=0$ is, from Eq. (G4)

$$\nu_0 = g\mu_B H'_A = 2|D|(S-\frac{1}{2}) \quad (G15)$$

3. Temperature Effects

In most ferromagnets, the anisotropy in the spin environment is due to the magnetic interactions of the paramagnetic ion with neighboring ions, and the spatial variation is due to the symmetry properties of the magnetic lattice. As the temperature increases, the disorder of the magnetic moments increases, and the ferromagnetic resonance will broaden due to local variations in the effective anisotropy field, H'_A . In addition, for such systems where the anisotropy field is due to exchange with neighboring spins, the average anisotropy field tends to zero as the temperature approaches the transition temperature T_c , since, at this temperature, the local spins are nearly completely disordered.

However, the anisotropy due to an axial ligand field does not decrease with temperature. As the temperature increases, the disorder in the spins will cause the semiclassical derivation of H'_A to break down, and in addition there will be a growth with temperature of "resonances" corresponding to "paramagnetic" states where the neighboring spins are not aligned, but are coupled by the exchange interaction. (As indicated in Appendix F, the paramagnetic resonance spectrum in zero field is broadened by the exchange interaction.) Thus, a smooth transition from a sharp resonance at $2|D|(S-\frac{1}{2})$ to the broad paramagnetic

spectrum should occur as T increases. This situation is observed in our measurements on the ferromagnet $((C_2H_5)_2NCS_2)_2Fe(III)Cl$.

4. Field Effects

At $T=0$, the application of an external magnetic field $H_{\sim ext}$ gives an effective field acting on the coupled spins

$$H_{\sim eff} = H_{\sim ext} + H'_A \quad (G16)$$

for ions with an axial ligand field. If θ_H is the angle between $H_{\sim ext}$ and H'_A , solution of Eq. (G1) in the uniform mode gives the ferromagnetic resonance frequency

$$\nu_0 = g\mu_B H_{\sim eff} \quad (G17)$$

where the magnitude $H_{\sim eff}$ is given by

$$H_{\sim eff} = [H'_A{}^2 + H_{\sim ext}^2 + 2H'_A H_{\sim ext} \cos \theta_H]^{1/2} \quad (G18)$$

For $H_{\sim eff} \parallel H'_A$, the frequency is

$$\begin{aligned} \nu_0 &= g\mu_B (H'_A + H_{\sim ext}) \\ &= 2|D|(S - \frac{1}{2}) + g\mu_B H_{\sim ext} \end{aligned} \quad (G19)$$

However, the lineshape for a polycrystalline sample is not easy to calculate. This is because the anisotropy field H'_A was calculated under the assumption that the deviation of the spin from the z-direction is small. If $H_{\sim ext} \ll H'_A$, this assumption will be valid, since the effective field $H_{\sim eff}$ will be nearly parallel to the z-direction for any orientation of $H_{\sim ext}$. However, for $((C_2H_5)_2NCS_2)_2Fe(III)Cl$, $|D| = 1.93 \text{ cm}^{-1}$ and $S=3/2$, so

$$H'_A = \frac{2|D|}{g\mu_B} = 41.2 \text{ kOe}$$

Therefore, in applied fields larger than a few kOe, the semi-classical derivation of H'_A breaks down, and a more rigorous calculation must be made. The observed ferromagnetic resonance for this compound is consistent with Eqs. (G17) and (G18) under the assumption that the magnetic torque produces a substantial alignment of the crystallites such that $H_{\text{ext}} \parallel \hat{z}$. This is very likely at the low temperature ($T=1.3^\circ\text{K}$) where the results shown in Fig. 17 were obtained.

ACKNOWLEDGEMENTS

I wish to thank Professor P. L. Richards for the suggestion of the subject of this thesis and for his continual guidance and encouragement. I also wish to dedicate this work to my wife Prilla, whose vigorous efforts and support made it possible.

It is also a pleasure to acknowledge the assistance of Dr. W. S. Caughey, Dr. G. Feher, Dr. M. P. Klein, Dr. A. M. Trozzolo and Dr. H. H. Wickman, who kindly supplied samples for this investigation. In addition, I have had a number of very informative discussions concerning the interesting properties of these compounds with these gentlemen, and with Dr. A. J. Bearden, Dr. W. E. Blumberg, Dr. G. Harris Loew, and Dr. K. Tsushima. Finally, I wish to acknowledge the assistance of Dr. A. M. Portis in analyzing the ferromagnetic resonance of $((C_2H_5)_2NCS_2)_2Fe(III)Cl$, and the helpful suggestions of C. L. Dodgson concerning appropriate notation.

This work was performed under the auspices of the United States Atomic Energy Commission.

REFERENCES

1. A. Abragam and M. H. L. Pryce, Proc. Roy. Soc. A205, 135 (1951).
2. Carl J. Ballhausen, Introduction to Ligand Field Theory (McGraw-Hill Book Co., Inc., N. Y., 1964).
3. Michael Tinkham, Group Theory and Quantum Mechanics (McGraw-Hill Book Co., Inc., N. Y., 1962).
4. William Low, Paramagnetic Resonance in Solids (Academic Press, N. Y., 1960).
5. M. Weissbluth, The Physics of Hemoglobin, B. L. Report No. 162, Biophysics Laboratory, Stanford University, 1966.
6. B. Bleaney and R. S. Trenam, Proc. Roy. Soc. A223, 1 (1954).
7. H. H. Wickman, M. P. Klein, and D. A. Shirley, J. Chem. Phys. 42, 2113 (1965).
8. For example, a detailed discussion of the electron paramagnetic resonance spectrum for $S = 5/2$ and various values of λ has been given by W. E. Blumberg, the EPR of High Spin Fe^{3+} in Rhombic Fields, in Magnetic Resonance in Biological Systems (Pergamon Press, Oxford, 1967) p. 119.
9. P. L. Richards, Fourier Transform Spectroscopy, in Spectroscopic Techniques for Far Infra-Red, Submillimetre and Millimetre Waves (North Holland Publishing Co., Amsterdam, 1967) p. 33.
10. R. R. Joyce and P. L. Richards, Phys. Rev. 179, 375 (1969).
11. Frank J. Low, J. Opt. Soc. Am. 51, 1300 (1961) and P. L. Richards, Far Infrared Detectors, in Proceedings of the NATO Conference on the Far Infrared Spectroscopy of Solids, Delft, The Netherlands, 1968 (to be published).

12. This effect is extensively discussed by H. C. Van de Hulst, Light Scattering by Small Particles (John Wiley and Sons, Inc., New York, 1957).
13. An example of the application of this technique to ferrimyoglobin is given by H. Morimoto, T. Iizuka, J. Otsuka, and M. Kotani, Biochim. Biophys. Acta 102, 624 (1965).
14. T. Emory and J. B. Neilands, J. Am. Chem. Soc. 83, 1626 (1961).
15. Allan Zalkin, J. D. Forrester, and David H. Templeton, J. Am. Chem. Soc. 88, 1810 (1966).
16. H. H. Wickman, M. P. Klein, and D. A. Shirley, Phys. Rev. 152, 345, (1966).
17. W. E. Blumberg (Bell Telephone Laboratories, Murray Hill, New Jersey), private communication, June 1970.
18. A. H. White, R. Roper, E. Kokot, H. Waterman, and R. L. Martin, Australian J. Chem. 17, 294 (1964).
19. A. H. Ewald, R. L. Martin, I. G. Ross, and A. H. White, Proc. Roy. Soc. A280, 235 (1964).
20. R. M. Golding and H. J. Whitfield, Trans. Faraday Soc. 62, 1713 (1966).
21. R. M. Golding, W. C. Tennant, C. R. Kanekar, R. L. Martin, and A. H. White, J. Chem. Phys. 45, 2688 (1966).
22. J. E. Falk, Porphyrins and Metalloporphyrins (Elsevier Publishing Company, Amsterdam, 1964).
23. R. Lemberg and J. W. Legge, Hematin Compounds and Bile Pigments (Interscience, New York, 1949) and J. E. Falk, R. Lemberg, and R. K. Morton, Haematin Enzymes (Pergamon Press, Oxford, 1961).

24. For recent examples of the extremely wide variety of experimental work on these substances, see Hemes and Hemoproteins, edited by Britton Chance, Ronald W. Estabrook, and Takashi Yonetani (Academic Press, New York, 1966).
25. Donald F. Koenig, *Acta. Cryst.* 18, 663 (1965).
26. P. L. Richards, W. S. Caughey, H. Eberspaecher, G. Feher, and M. Malley, *J. Chem. Phys.* 47, 1187 (1967).
27. N. Sadasivan, H. Eberspaecher, W. H. Fuchsman, and W. S. Caughey, *Biochemistry* 8, 534 (1969).
28. X-ray crystallographic data for α -chloro protoporphyrin IX Fe(III) (Ref. 26) indicate that the iron coordination for halogeno ligands is very close to square-pyramidal, which would imply a strictly axial ligand field.
29. W. Sheler, G. Schoffa, and F. Jung, *Biochem. Z.* 329, 232 (1957).
30. J. F. Gibson and D. J. E. Ingram, *Nature* 180, 29 (1957).
31. M. Kotani, *Supp. of the Prog. of Theoret. Phys.* 17, 4 (1961).
32. J. S. Griffith, *Biopolymers Symp.* 1, 35 (1964).
33. L. Stryer, J. C. Kendrew, and H. C. Watson, *J. Mol. Biol.* 8, 96 (1964).
34. Paul A. Loach and Melvin Calvin, *Biochemistry* 2, 361 (1963).
35. Akio Yamamoto, Linda K. Phillips, and Melvin Calvin, *Inorg. Chem.* 7, 847 (1968).
36. Takashi Yonetani and Toshio Asakura, *J. Biol. Chem.* 243, 3996 (1968).
37. W. S. Caughey, H. Eberspaecher, W. H. Fuchsman, S. McCoy and J. O. Alben, *Ann. of the N. Y. Acad. of Sci.* 153, 722 (1969).
38. D. J. E. Ingram, J. F. Gibson, and M. F. Perutz, *Nature* 178, 906 (1956).

39. J. E. Bennett, J. F. Gibson, and D. J. E. Ingram, *Nature* 177, 275 (1956).
40. R. J. P. Williams, *Discussions Faraday Soc.* 20, 291 (1955);
A. S. Brill and R. J. P. Williams, *Biochem. J.* 78, 253 (1961);
D. Keilin and E. F. Hartree, *Biochem. J.* 49, 88 (1951);
C. D. Coryell, F. Stitt, and L. Pauling, *J. Am. Chem. Soc.* 59, 633 (1937).
41. J. E. Bennett, D. J. E. Ingram, P. George, and J. Stanley Griffith, *Nature* 176, 394 (1955); J. F. Gibson, D. J. E. Ingram, and D. Schonland, *Disc. Far. Soc.* 26, 72 (1958); A. Ehrenberg, *Arkiv für Kemi* 19, 119 (1962); D. J. E. Ingram, in Paramagnetic Resonance, Vol. II, edited by W. Low (Academic Press, New York, 1963) p. 809.
42. P. Eisenberger and P. S. Pershan, *J. Chem. Phys.* 45, 2832 (1966).
43. A. Tasaki, "Susceptibility Measurements of Heme Proteins," in Conference on the Physical Properties of Iron Proteins, B. L. Report No. 208, Biophysics Laboratory, Stanford University, 1968, p. 64.
44. G. Lang and W. Marshall, *Proc. Phys. Soc. (London)* 87, 3 (1966).
45. Recent calculations have fit both the temperature-dependence of the magnetic moment and our data for the polycrystalline absorption due to the Zeeman splitting of the ground state for met myoglobin with a value of D in the range $D = 11 \pm 1 \text{ cm}^{-1}$ (G. Harris Loew, Department of Genetics, Stanford Medical School, Stanford, California, private communication, June 1969).
46. B. F. Hoskins, R. L. Martin, and A. H. White, *Nature* 211, 627 (1966).
47. H. H. Wickman, A. M. Trozzolo, H. J. Williams, G. W. Hull, and F. R. Merritt, *Phys. Rev.* 155, 563 (1967).

48. H. H. Wickman and F. R. Merritt, Chem. Phys. Letters, 1, 117 (1967).
49. H. H. Wickman and A. M. Trozzolo, Symposium Faraday Soc. 1, 21 (1967).
50. Y. Tanabe and S. Sugano, J. Phys. Soc. Japan 9, 766 (1954).
51. G. C. Brackett, P. L. Richards, and H. H. Wickman, Chem. Phys. Lett. 5, 1970 (in press).
52. A. M. Portis (Department of Physics, University of California, Berkeley, California), private communication, June 1969.
53. R. J. Joenk and R. M. Bozorth, Proceedings of the International Conference on Magnetism, Nottingham, 1964, p. 493.
54. For example, see the discussion given by Charles Kittel in Introduction to Solid State Physics, third edition (John Wiley and Sons, Inc., New York, 1966), p. 523.
55. Alan J. Bearden and W. R. Dunham, Structure and Bonding 8, (1970) (in press).

Table I. Experimental values of the zero field splittings Δ_1 and Δ_2 and derived values of the spin Hamiltonian parameters for several heme compounds obtained from the far-infrared spectra at $H=0$ for $T=4.2$ and 50°K .

Compound	Ligand	Δ_1 (cm^{-1})	D (cm^{-1})	λ
Protoporphyrin IX Dimethyl Ester Fe(III)	Fluoro	$\Delta_1=10.0\pm.20$	$5.0\pm.10$	~ 0
	Chloro ^a	$\Delta_1=13.9\pm.28$ $\Delta_1=19.5\pm.30$	$6.95\pm.14$	~ 0
	Azido	$\Delta_2=36.0\pm.75$	$9.10\pm.15$	$.085\pm.025$
Deuteroporphyrin IX Dimethyl Ester Fe(III)	Fluoro ^a	$\Delta_1=11.1\pm.22$	$5.55\pm.11$	~ 0
	Chloro ^a	$\Delta_1=17.9\pm.36$	$8.95\pm.18$	~ 0
	Bromo ^a	$\Delta_1=23.6\pm.46$	$11.8\pm.23$	~ 0
	Iodo	$\Delta_1=32.8\pm.30$ $\Delta_1=14.8\pm.10$	$16.4\pm.15$	~ 0
	Azido	$\Delta_2=29.2\pm.15$	$7.32\pm.05$	$.036\pm.015$

^aData from Ref. 27.

Table II. Experimental values of the zero field splitting Δ_1 and derived values of the spin Hamiltonian parameters for several Mn(III) deuteroporphyrins obtained from the far infrared spectra at $T = 4.2^\circ\text{K}$.

Compound	Ligand	Δ_1 (cm^{-1})	D (cm^{-1})	λ
Deuteropor- phyrin IX Dimethyl Ester Mn(III)	Chloro	$7.6 \pm .05$	$-2.53 \pm .02$	$\leq .005$
	Bromo	≤ 3.5	$-1.10 \pm .10$	~ 0
	Azido	$9.25 \pm .15$	$-3.08 \pm .10$	$\leq .04$

Table III. Observed zero field splittings and derived values of D for ferrihemoglobin and ferrimyoglobin obtained from the far-infrared spectra at 4.2°K. Several indirect values of D and the far-infrared results for fluoro protoheme are included for comparison.

Compound	Ligand	Δ_1 (cm^{-1})	D (cm^{-1})	Indirect value D (cm^{-1})
Ferrimyoglobin	Aquo	> 16	9.5 ± 1.5	$\sim 12^a$ $4.38 \pm .6^b$
	Fluoro	$11.88 \pm .16$	$5.94 \pm .08$	$\sim 7^c$
Ferrihemoglobin	Fluoro	$12.60 \pm .24$	$6.30 \pm .12$	$\sim 7^d$
Protoporphyrin IX Dimethyl Ester Fe(III)	Fluoro	$10.0 \pm .20$	$5.0 \pm .10$	

^aRef. 13

^bRef. 42

^cRef. 43

^dRef. 44

Table IV. Zero-field splittings Δ and derived values of the spin Hamiltonian parameters for bis (N,N dialkyl dithiocarbamate) Fe(III) halides $[(R_2NCS_2)_2 Fe(III) X]$, obtained from the far-infrared spectra. The difference in the zero field splitting for compounds with the same dithiocarbamate ligand and different halogeno ligands, $\Delta_{Br} - \Delta_{Cl}$, and the quadrupole splitting obtained from Mössbauer data^a are also included.

Ligands		Δ (cm^{-1})	$\Delta_{Br} - \Delta_{Cl}$ (cm^{-1})	D (cm^{-1})	λ	ΔE_Q (cm/sec)
R = CH ₃	X=Br	14.60 ± .20	18.80	+7.30 ± .10		.290
	X=Cl	4.20 ± .04		-2.10 ± .02		.266
R = C ₂ H ₅	X=Br	15.10 ± .20	18.95	+7.50 ± .10	.067 ± .005	.288
	X=Cl	3.85 ± .02		-1.93 ± .01		.268
R = (i-C ₃ H ₇)	X=Cl	4.70 ± .06		-2.35 ± .03	.036 ± .003 ^b	.268
NR ₂ =Pyrro- lidyl	X=Br	16.33 ± .20	11.13	+8.17 ± .10		.277
	X=Cl	5.20 ± .09		+2.60 ± .05		.268

^aRef.49

^bRef.48

Table V. Frequencies of absorption maxima for the magnetic field-independent absorptions observed in the far-infrared spectra of several compounds at 4.2°K.

Compound	Absorption Maxima (cm^{-1})
Fluoro ferrimyoglobin	8.9
Bromo deuteroporphyrin IX dimethyl ester Mn(III)	25.2, 34.0, 39.3, 46.0
Phenoxy deuteroporphyrin IX dimethyl ester Mn(III)	13.3, 31.0
Bromo bis (N,N diethyl dithiocarbamate) Fe(III)	27.3, 31.5, 34.5, 42.9, 44.7, 46.5, 52.8
Chloro bis (di-isopropyl dithiocarbamate) Fe(III)	26.5
Chloro bis (N,N diethyl dithiocarbamate) Fe(III)	33.0, 38.8, 43.6
Bromo bis (pyrrolidyl dithiocarbamate) Fe(III)	27.0, 29.8

FIGURE CAPTIONS

- Fig. 1. Zero field eigenvalues in units of D as a function of $\lambda = E/D$ for the spin Hamiltonian Eq. (2) with $S = 3/2, 2,$ and $5/2$. The m_s values of the states for $\lambda = 0$ are indicated at the left, and doubly-degenerate eigenvalues are identified at the right.
- Fig. 2. Eigenvalues in units of D as a function of $H' = g\mu_B H/D$ for the spin Hamiltonian Eq. (2) with $\lambda = 0$ and $S = 3/2, 2,$ and $5/2$. The dotted curves are for $H \parallel z$, the solid curves for $H \perp z$. The m_s and m_H values of the states for large H' and $D > 0$ are indicated at the right.
- Fig. 3. The polycrystalline absorption coefficient $\bar{\alpha}$ calculated from Eq. (5) for $S = 3/2, D < 0, D/kT = 0.8, \lambda = 0.036,$ and various values of H' . The contribution of each transition to the total lineshape is shown in the upper curve; the transition index n is identified in the inset diagram. The lower composite plot indicates the variation of the total lineshape with H' . The scale of $\bar{\alpha}$ for $H' = 0$ has been reduced for clarity.
- Fig. 4. Raw data and ratios as obtained from the Fourier spectrometer for ~ 200 mg of polycrystalline iodo deuteroporphyrin IX dimethyl ester Fe(III).
- Fig. 5. Absolute configuration of the ligands surrounding the Fe(III) ion in Ferrichrome A, after Zalkin, Forrester, and Templeton, Ref. 15.
- Fig. 6. Theoretical and experimental absorption coefficients for polycrystalline ferrichrome A at $H = 52.2$ KOe and $T = 4.2^\circ\text{K}$. The points are the average of three experimental lineshapes, and

the bars indicate plus or minus one standard deviation. The experimental points have been corrected for small linear variations of the background, due to instrumental effects, obtained from the value of the absorption coefficient at frequencies below and above the plotted range. The solid curve is the theoretical bare absorption coefficient for $g=2.0$, $D = -0.27 \text{ cm}^{-1}$ and $|\lambda| = 0.25$; the dotted curve was calculated for $D = +0.27 \text{ cm}^{-1}$ and $\lambda = 0.333$. The frequencies of the absorption edges and maxima, defined in the text, are indicated for the solid curve.

Fig. 7. Probable molecular structure for $\text{Fe(III)} (\text{S}_2\text{CNR}_2)_3$, after Ewald, Martin, Ross, and White, Ref. 19. R is an alkyl group.

Fig. 8. Data for polycrystalline tris (pyrrolidyl dithiocarbamate) Fe(III) at $T=4.2^\circ\text{K}$, obtained from the far-infrared spectra. The points are the frequencies of the observed absorption maxima, and the bars show the approximate width of the absorptions. Smooth curves have been drawn through the points.

Fig. 9. Approximate structure of the porphyrin skeleton and local coordination of the iron atom in heme compounds.

Fig. 10. Data for a sample of ~ 150 mg of polycrystalline fluoro protoporphyrin IX dimethyl ester Fe(III) at $T = 4.2^\circ\text{K}$. The points indicate the position of the experimental maxima, and the bars the approximate width of the observed absorptions. The curves are the transition frequencies predicted by the spin Hamiltonian in Eq. (2) for $D = +5.0 \text{ cm}^{-1}$, $\lambda = 0$, and $\text{H} \perp \hat{z}$; the dotted portions indicate weaker absorption due to

the effects of the Boltzmann term P_n ($T=4.2^\circ\text{K}$). The approximate spectral bandpass of the sample is indicated by the range of frequencies plotted.

Fig. 11. Data for a sample of ~ 100 mg of polycrystalline azido deuteroporphyrin IX dimethyl ester Mn(III) at $T = 4.2^\circ\text{K}$. The format is the same as that used in previous figures. The curves are the predicted transition frequencies calculated from Eq. (2) for $D = -3.08 \text{ cm}^{-1}$, $\lambda = 0$, and $\underline{H} \perp \hat{z}$.

Fig. 12. Data obtained from the far-infrared spectra of paste samples containing ~ 1 gm of the fluoro derivatives of ferrihemoglobin (HbF) and ferrimyoglobin (MbF) at 4.2°K . The points are the frequencies of the measured absorption maxima, and the bars indicate the approximate width of the observed absorptions. The curves are the frequencies of strong transitions calculated from Eq. (2) for $\lambda = 0$, $\underline{H} \perp \hat{z}$, and $D = +6.30 \text{ cm}^{-1}$ (HbF), and $D = +5.94 \text{ cm}^{-1}$ (MbF); the dotted portions indicate regions of weak absorption. The range of frequencies plotted indicates the approximate spectral bandpass of the samples.

Fig. 13. Data from the far-infrared spectra of ~ 1 gm of polycrystalline met-myoglobin at 4.2°K . The points are the average values of the frequencies of the measured absorption maxima for eight experimental runs. The curves are the calculated transition frequencies using Eq. (2) with $\lambda = 0$, $\underline{H} \perp \hat{z}$, and the values of D indicated at the right.

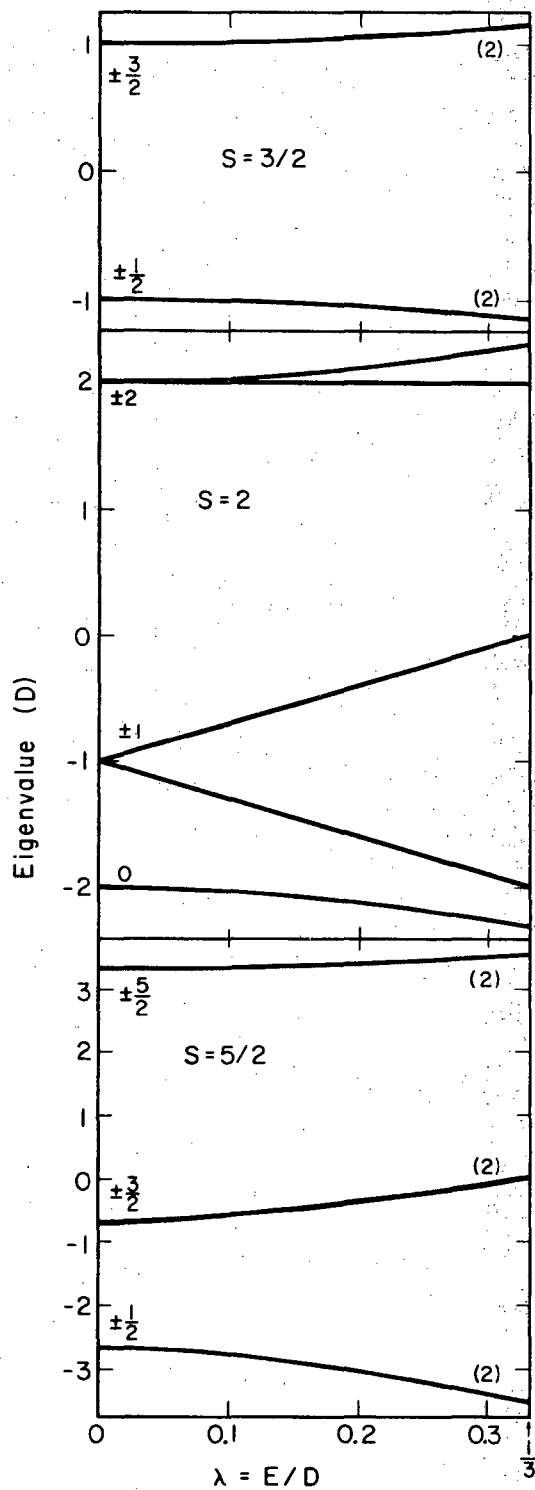
Fig. 14. Molecular structure of $(R_2NCS_2)_2 \text{Fe(III) X}$, after Hoskins, Martin, and White, Ref. 46. R is an alkyl group, and X is a halogeno ligand.

- Fig. 15. Data obtained from the far-infrared spectra of ~ 100 mg of polycrystalline bis (di-isopropyl dithiocarbamate) Fe(III) chloride. The points are the frequencies of the observed absorption maxima and the bars indicate the approximate width. The curves plot the principal maxima of the polycrystalline absorption coefficient, calculated using the program described in Section II-C for $D = -2.35 \text{ cm}^{-1}$, $\lambda = 0.036$, and $T = 4.2^\circ\text{K}$. The dotted portions indicate regions of weak absorption.
- Fig. 16. Data for the ordered sample of bis (N,N diethyl dithiocarbamate) Fe(III) bromide, described in the text at 4.2°K . The points are the frequencies of the observed maxima and the bars indicate the approximate width. The curves are the transition frequencies calculated from Eq. (2) for $\theta_H \sim 3\pi/8$, $D = +7.50 \text{ cm}^{-1}$, and $\lambda = 0.067$.
- Fig. 17. Data obtained from the far-infrared spectra of a polycrystalline sample of bis (N,N diethyl dithiocarbamate) Fe(III) chloride in the ordered state at $T = 1.3^\circ\text{K}$. The points are the frequencies of the single sharp absorption maxima observed, and the bars indicate the experimental width. The line is $\nu = 2\mu_B H + 3.85 \text{ cm}^{-1}$.
- Fig. 18. Far-infrared transmission spectrum of ~ 50 mg of polycrystalline $((\text{C}_2\text{H}_5)_2\text{NCS}_2)_2 \text{Fe(III) Br}$ at $T=4.2^\circ\text{K}$ and $H=0$. The absorption due to the zero-field splitting is indicated at $\Delta=15.1 \text{ cm}^{-1}$, and the transmission with no sample in place is given by the dotted curve.
- Fig. B1. Flow chart for the subroutine ABSRBNC, the main control subroutine of SHAZAM.

Fig. C1. The function $\bar{f}(\Delta)$, as defined in Appendix C, for several values of $\lambda \equiv |\lambda|$.

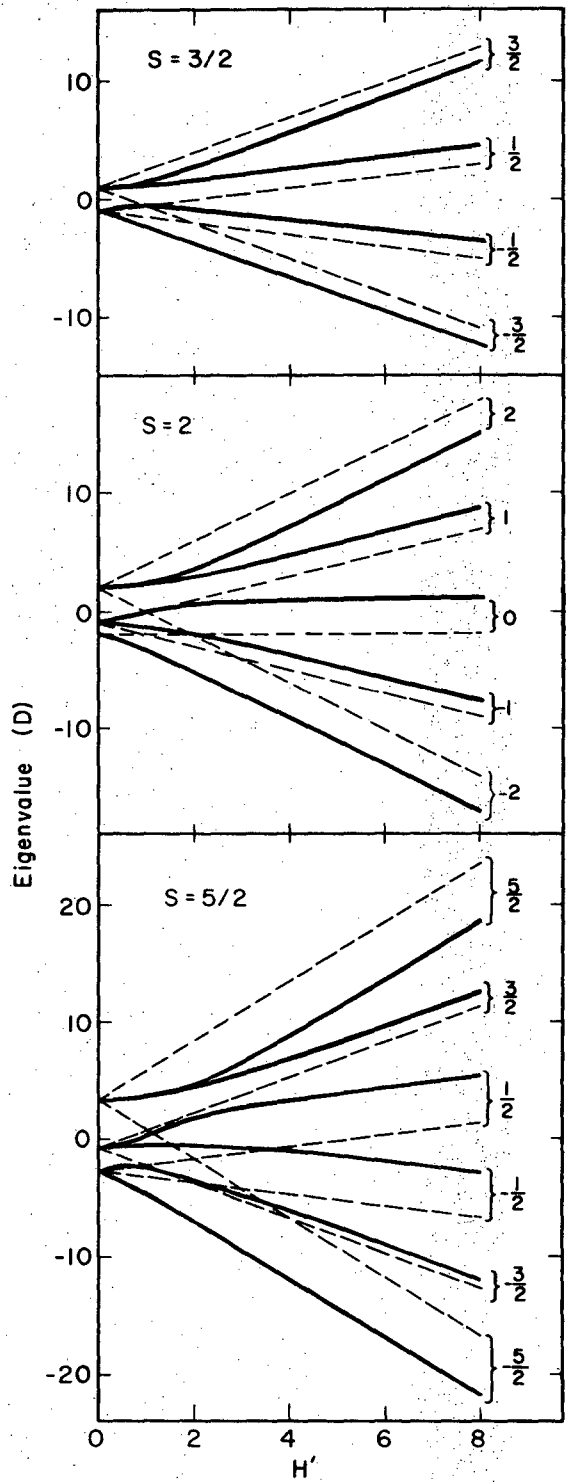
Fig. E1. Changes in the local environment of Fe(III) in bis Fe(III) dithiocarbamates for the symmetry-reduction series discussed in Appendix E. The Fe(III) ion lies at the origin of the coordinate system in each case.

Fig. E2. Schematic diagram of the variation of the d^1 representations, basis functions, and energy levels for the symmetry-reduction series discussed in Appendix E.



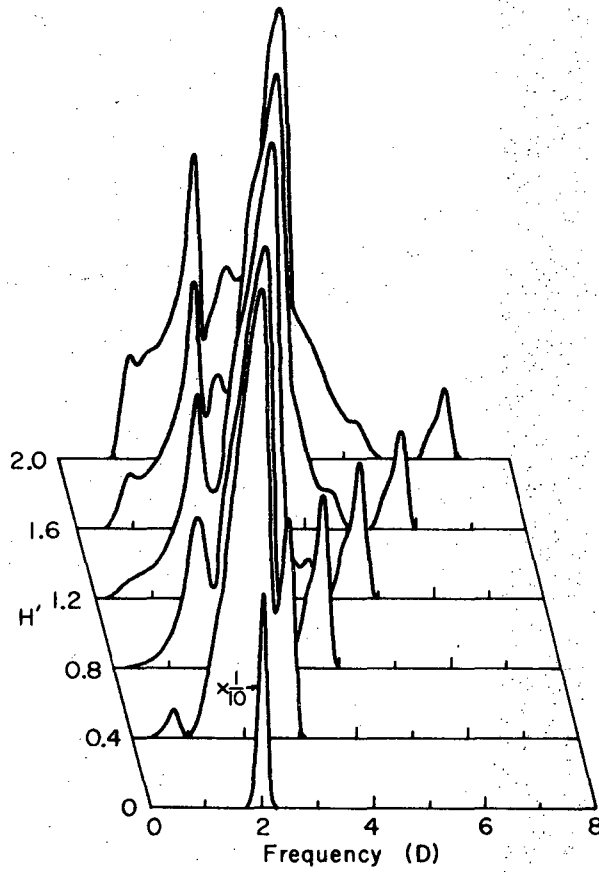
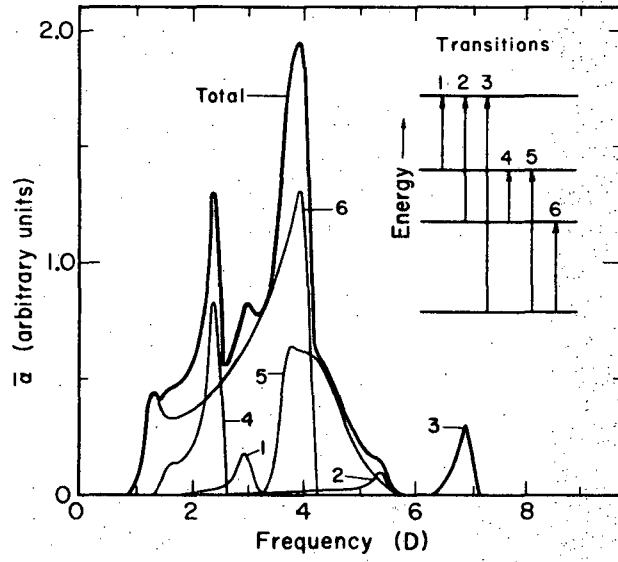
XBL705-2955

Fig. 1



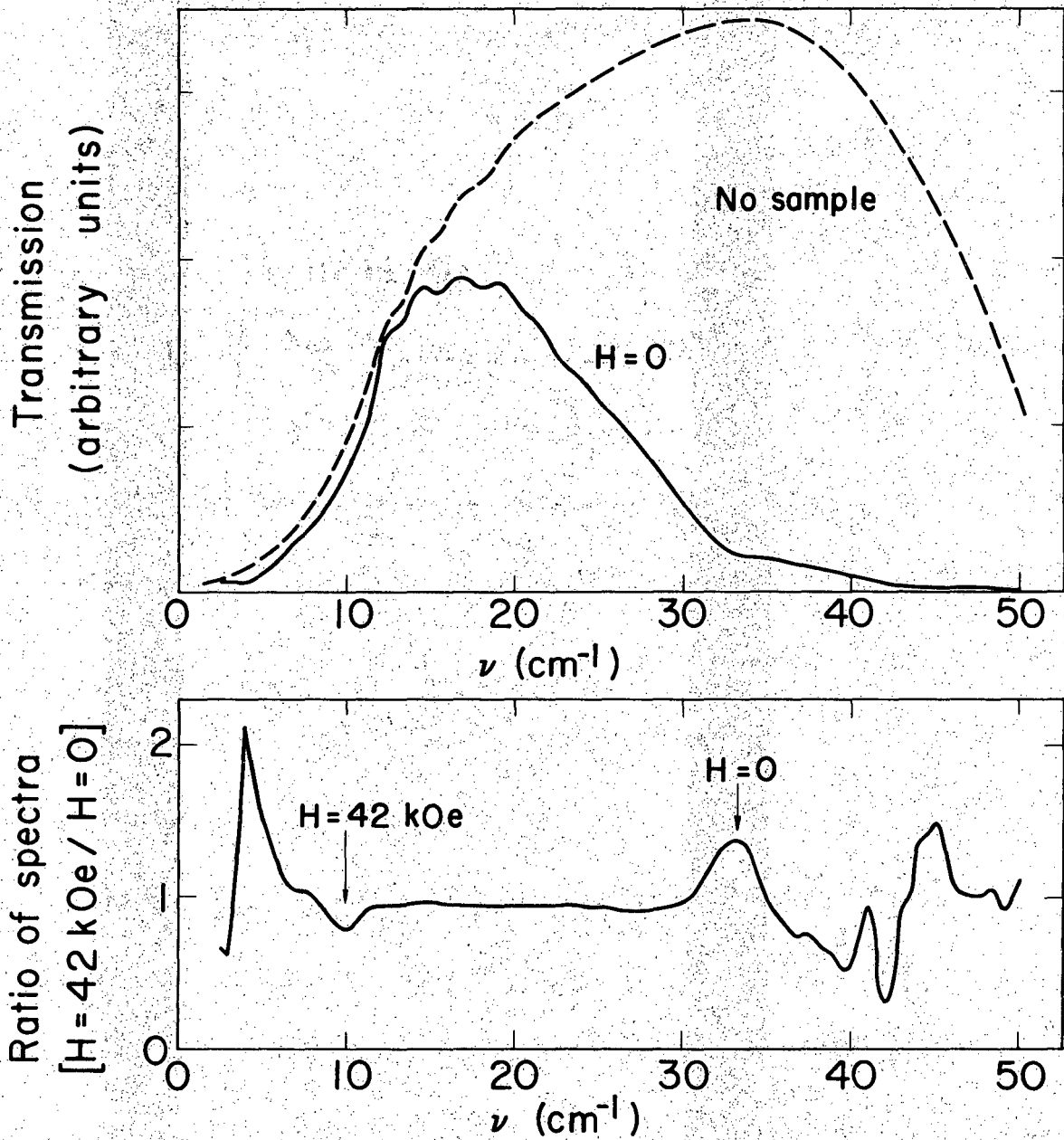
XBL 705-2956

Fig. 2



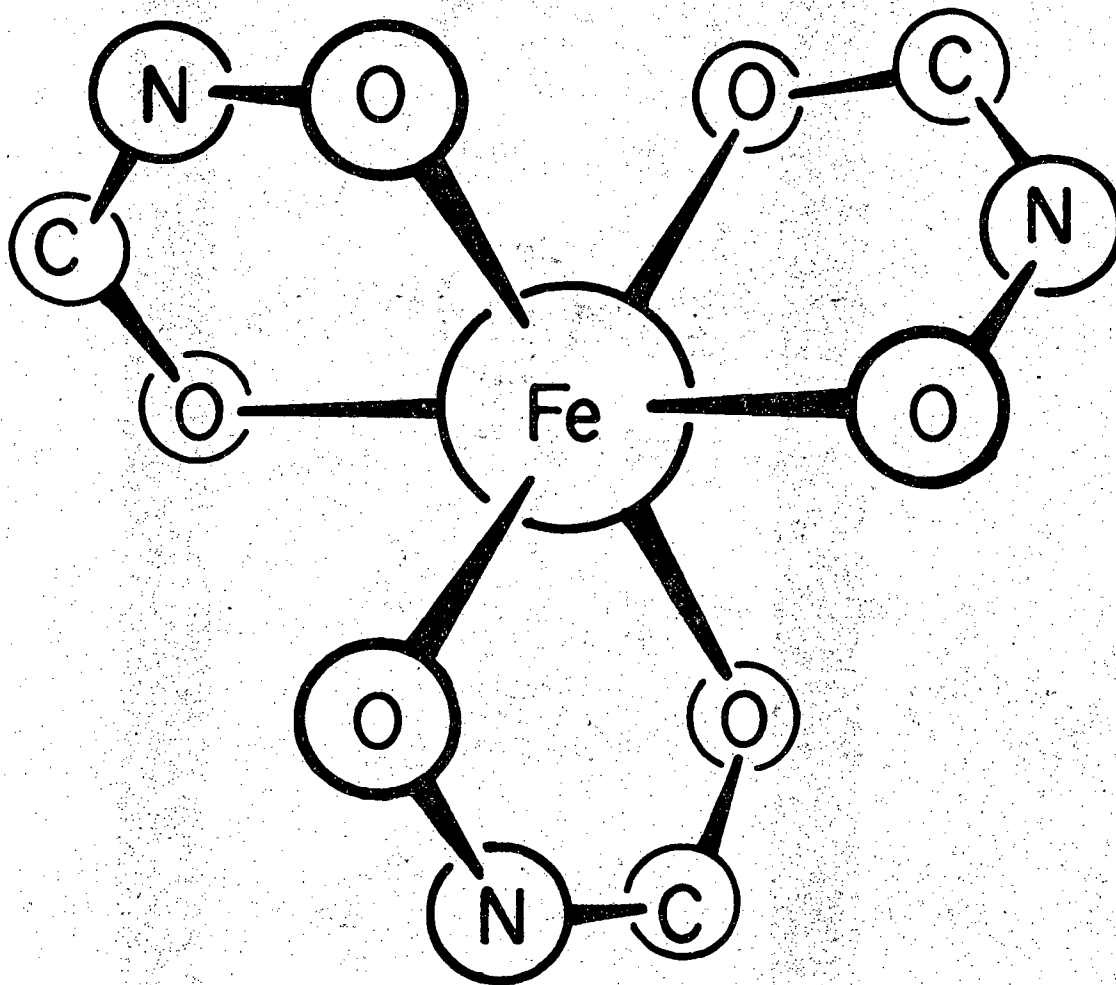
XBL705-2957

Fig. 3



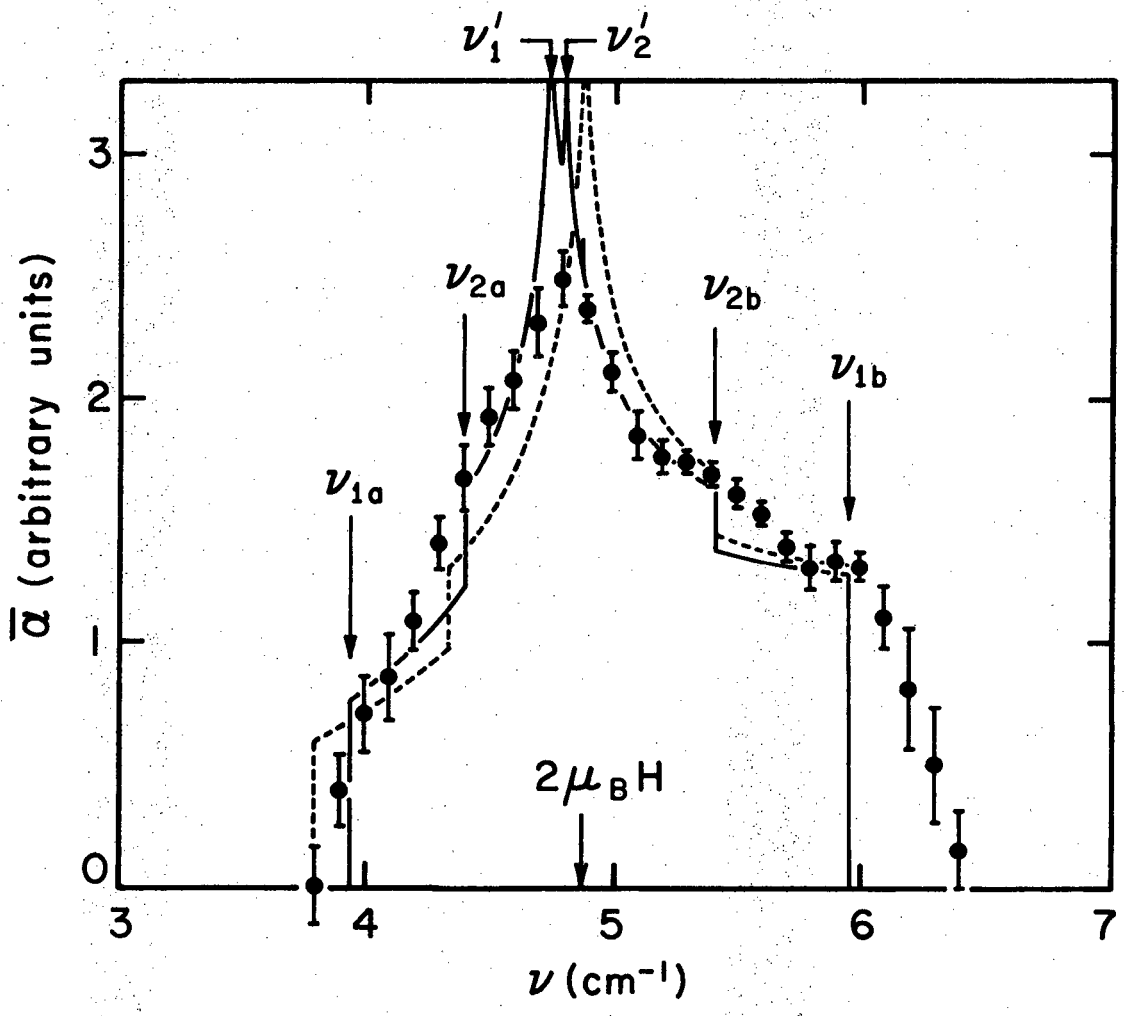
XBL6810-7093

Fig. 4



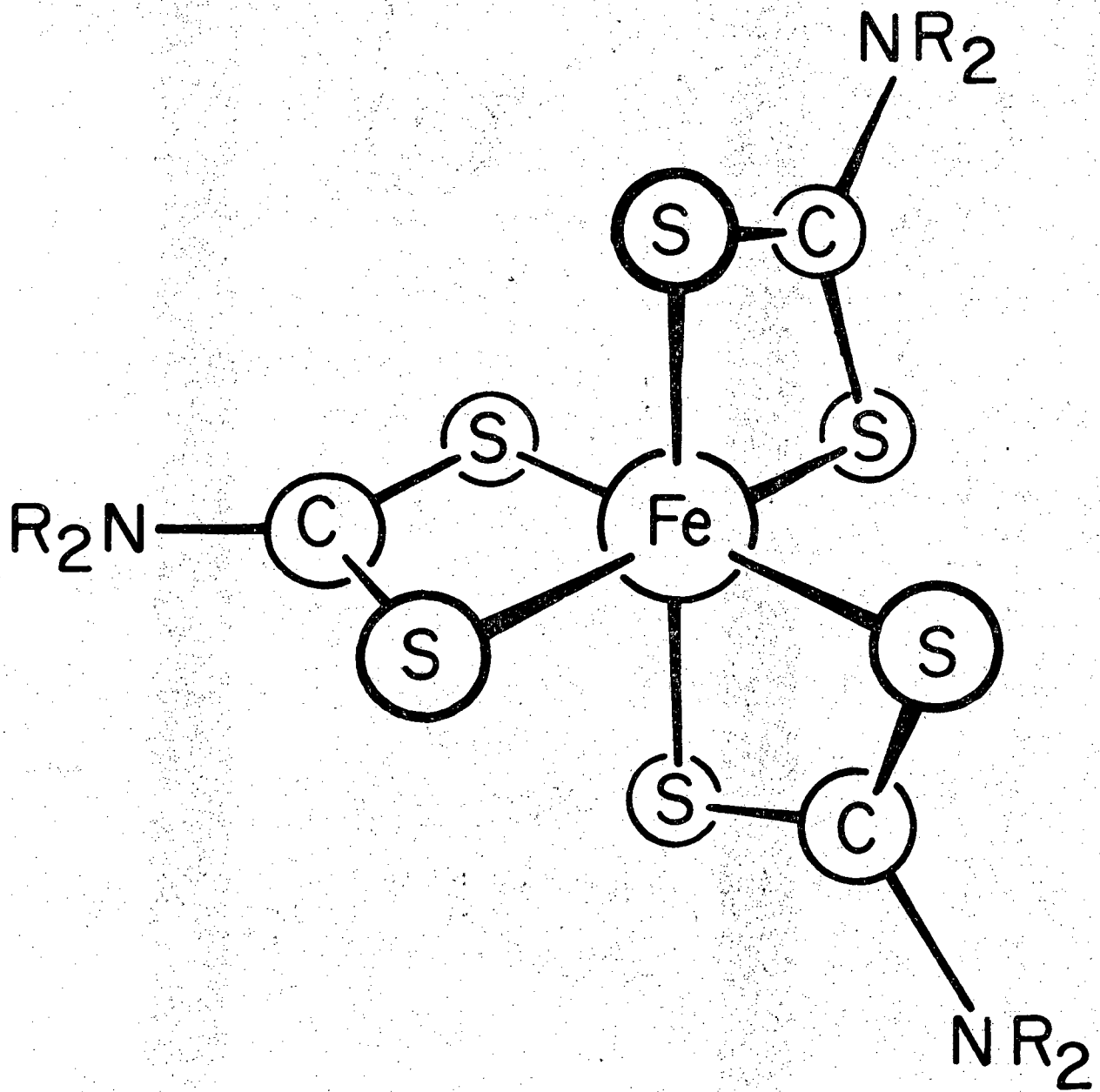
XBL705 - 2961

Fig. 5



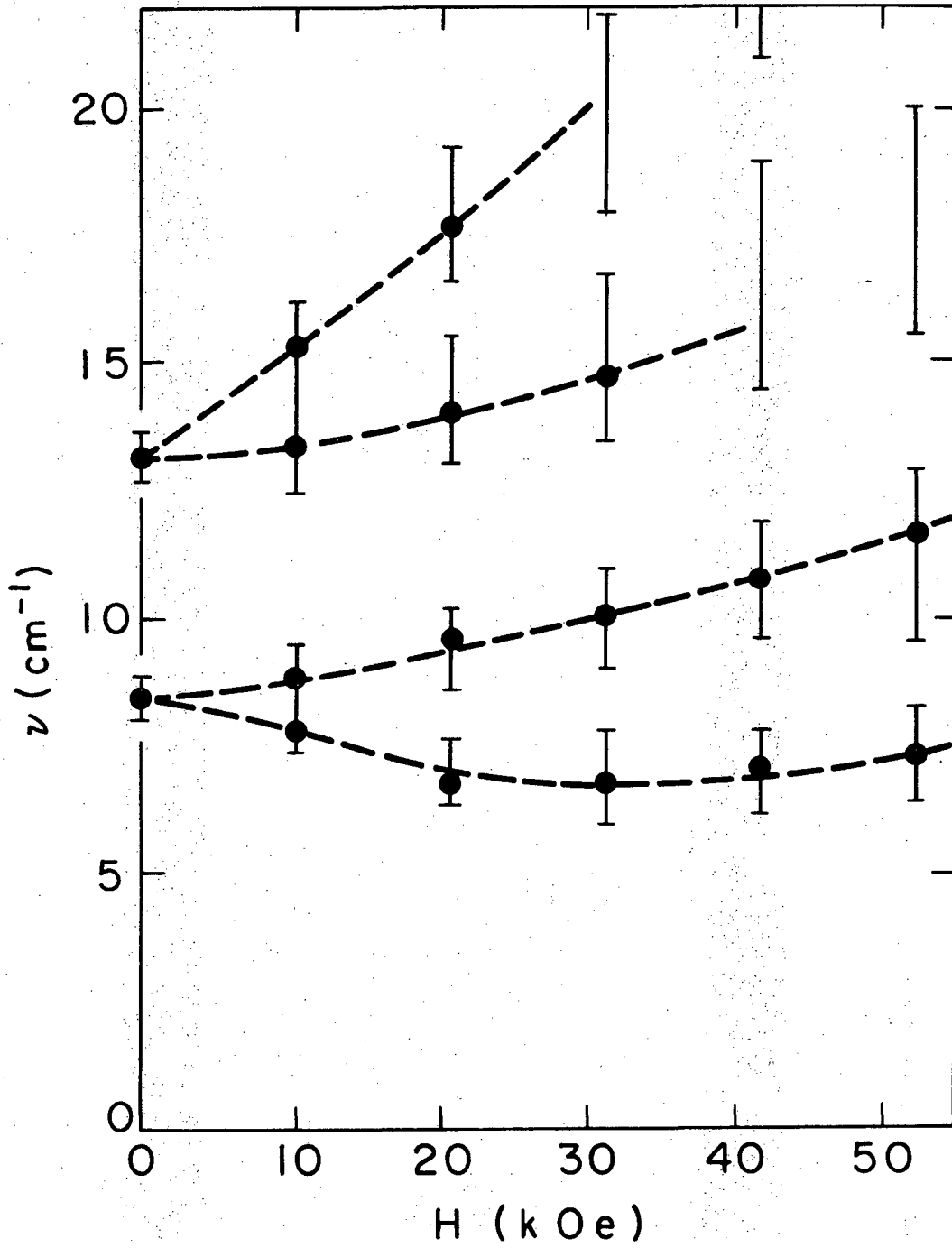
XBL706-3183

Fig. 6



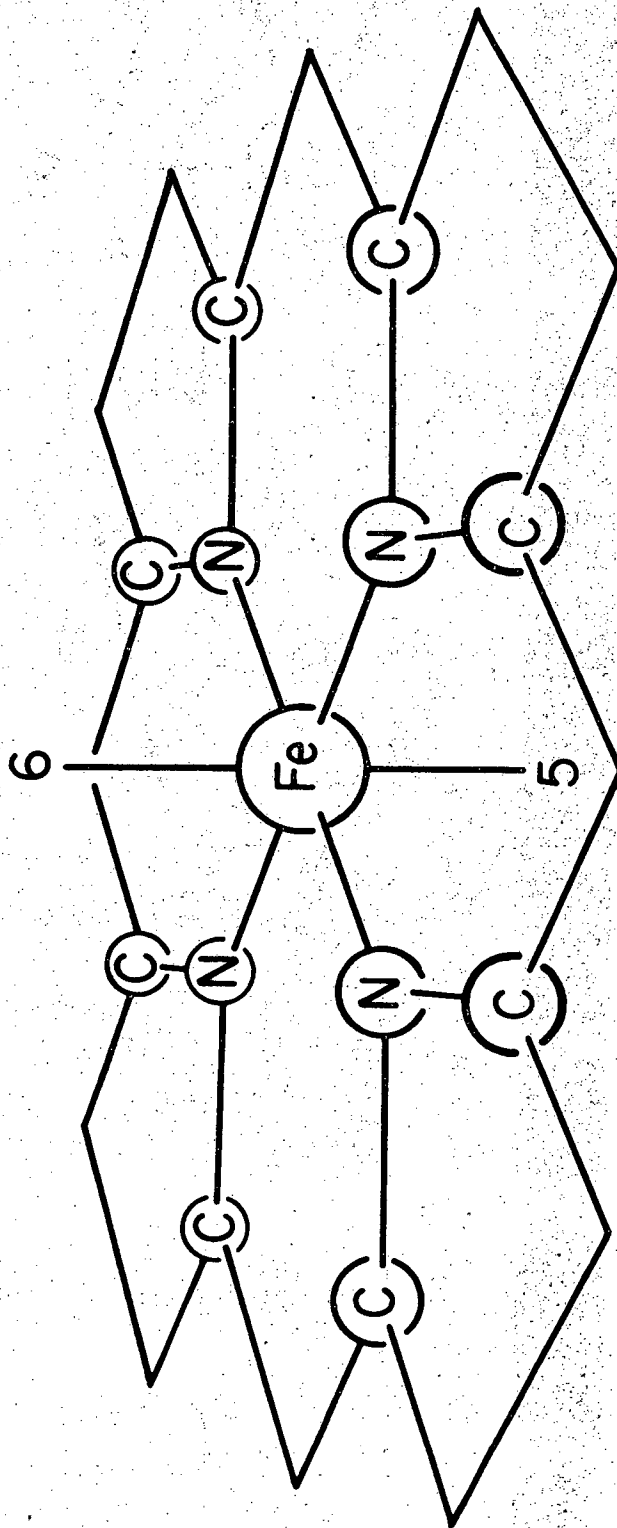
XBL 705 - 2958

Fig. 7



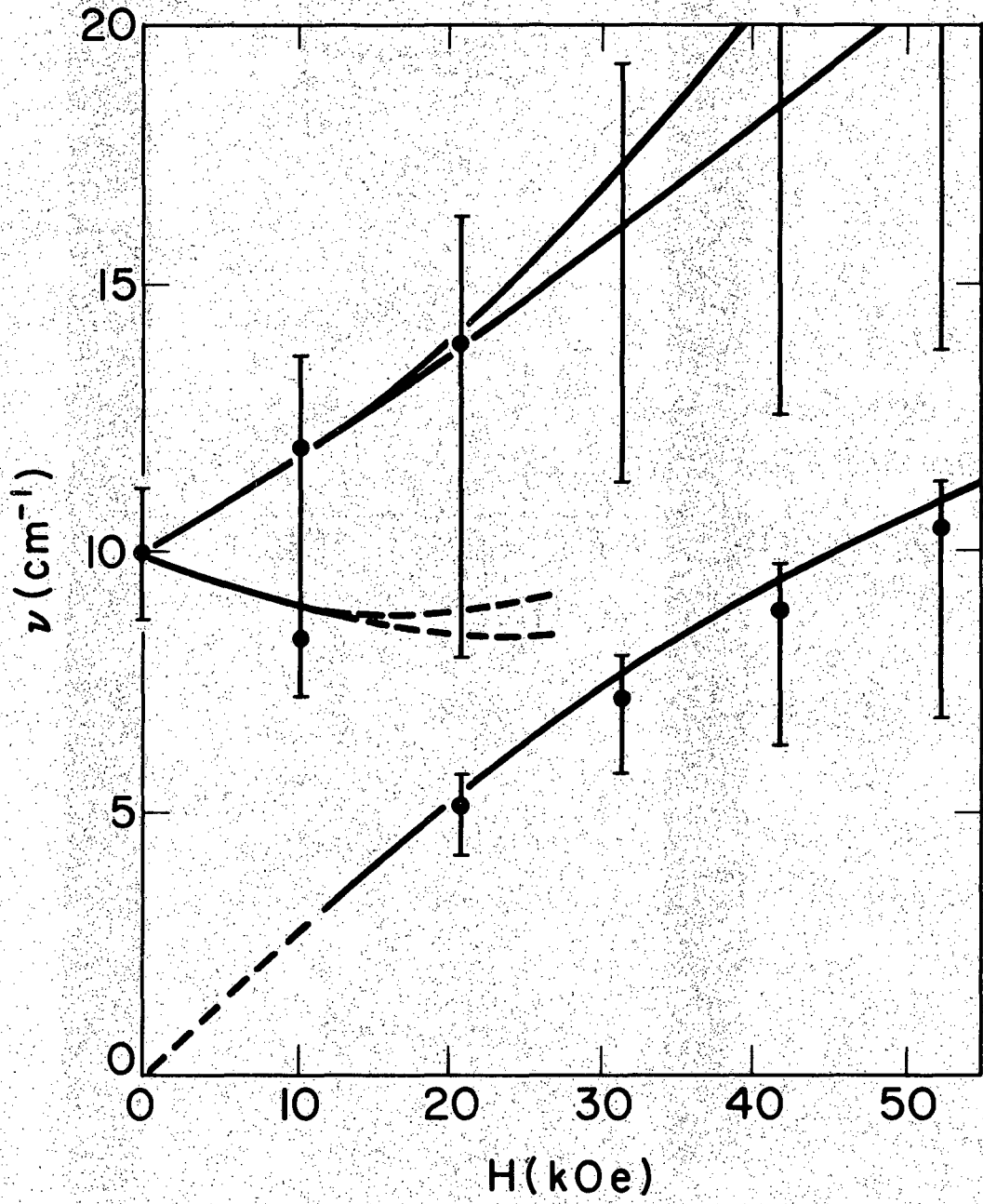
XBL 706-3234

Fig. 8



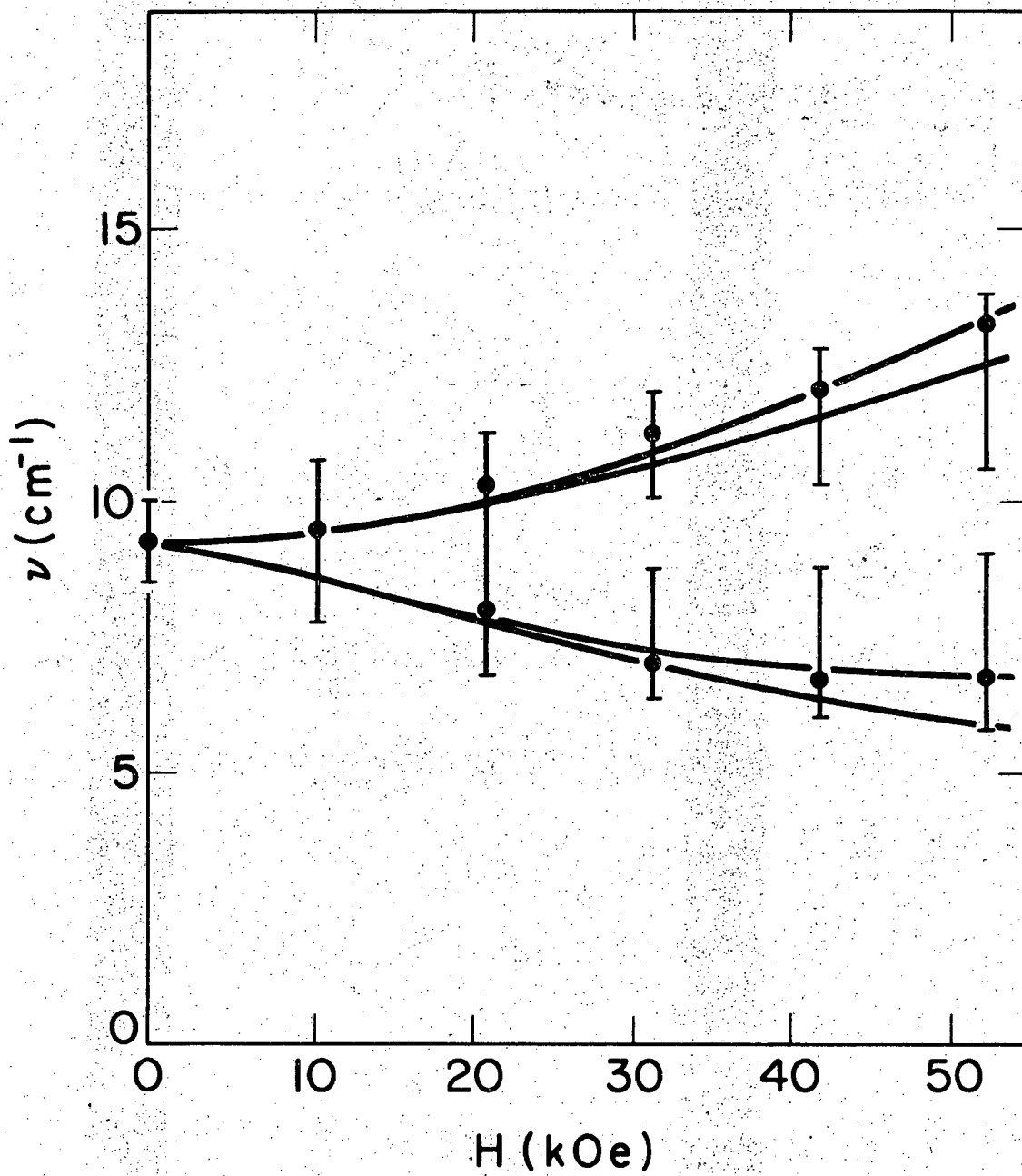
XBL705 - 2960

Fig. 9



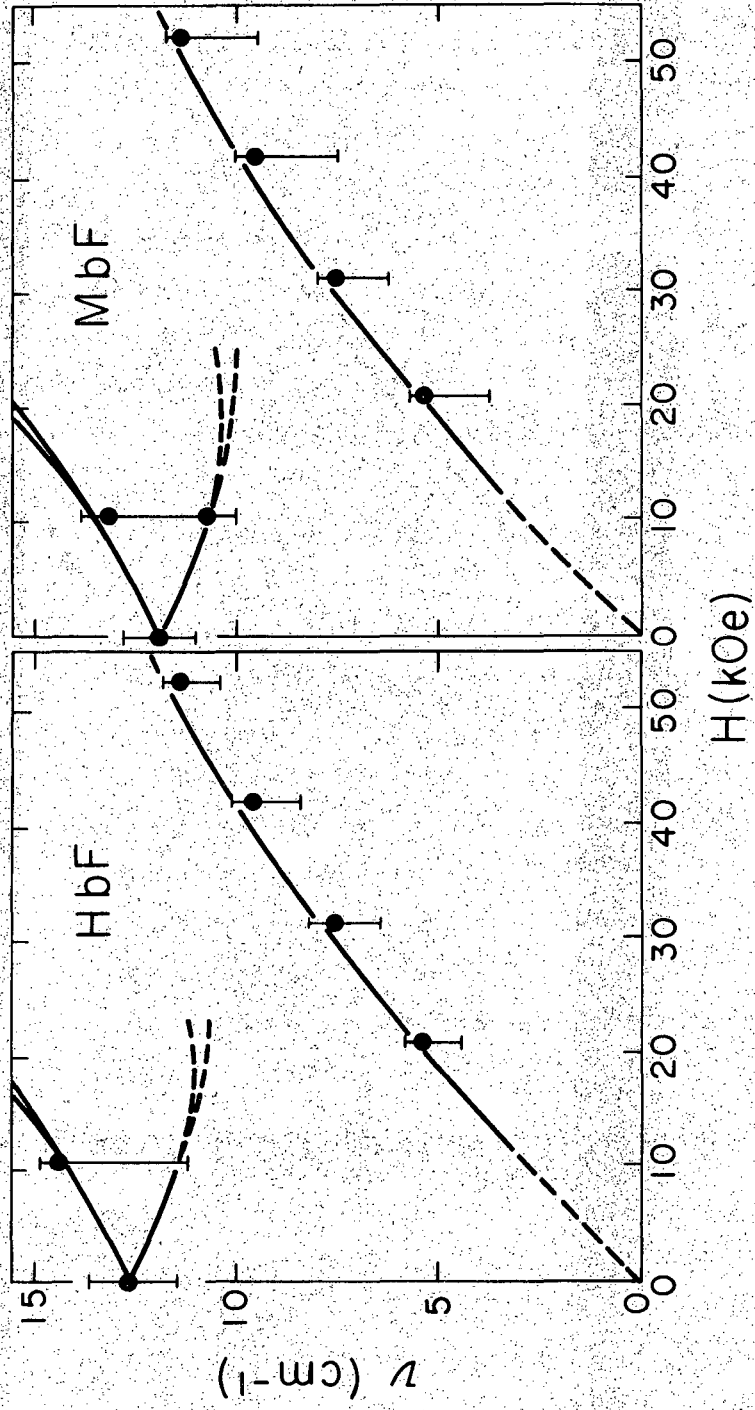
XBL706-3181

Fig. 10



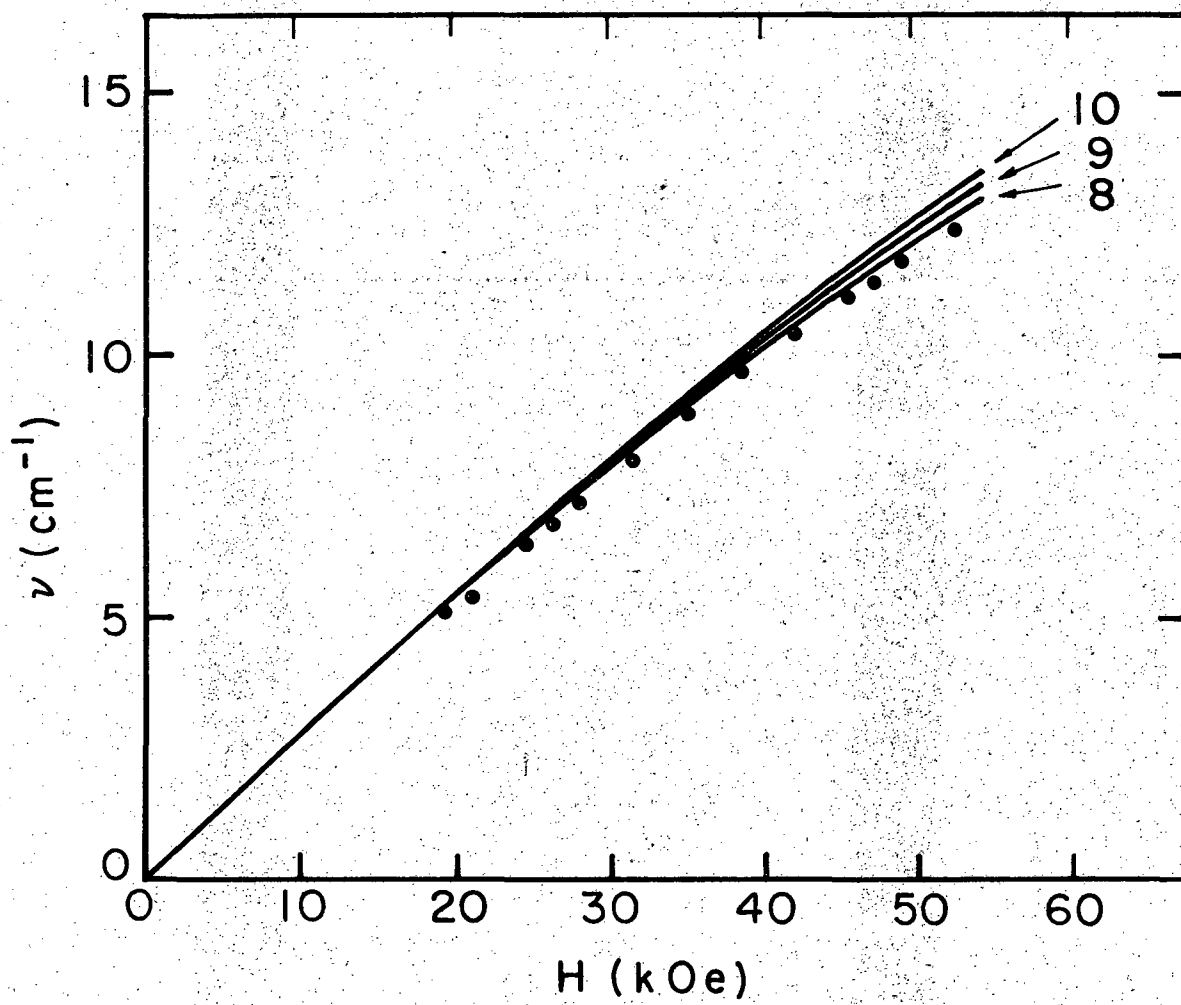
XBL706-3182

Fig. 11



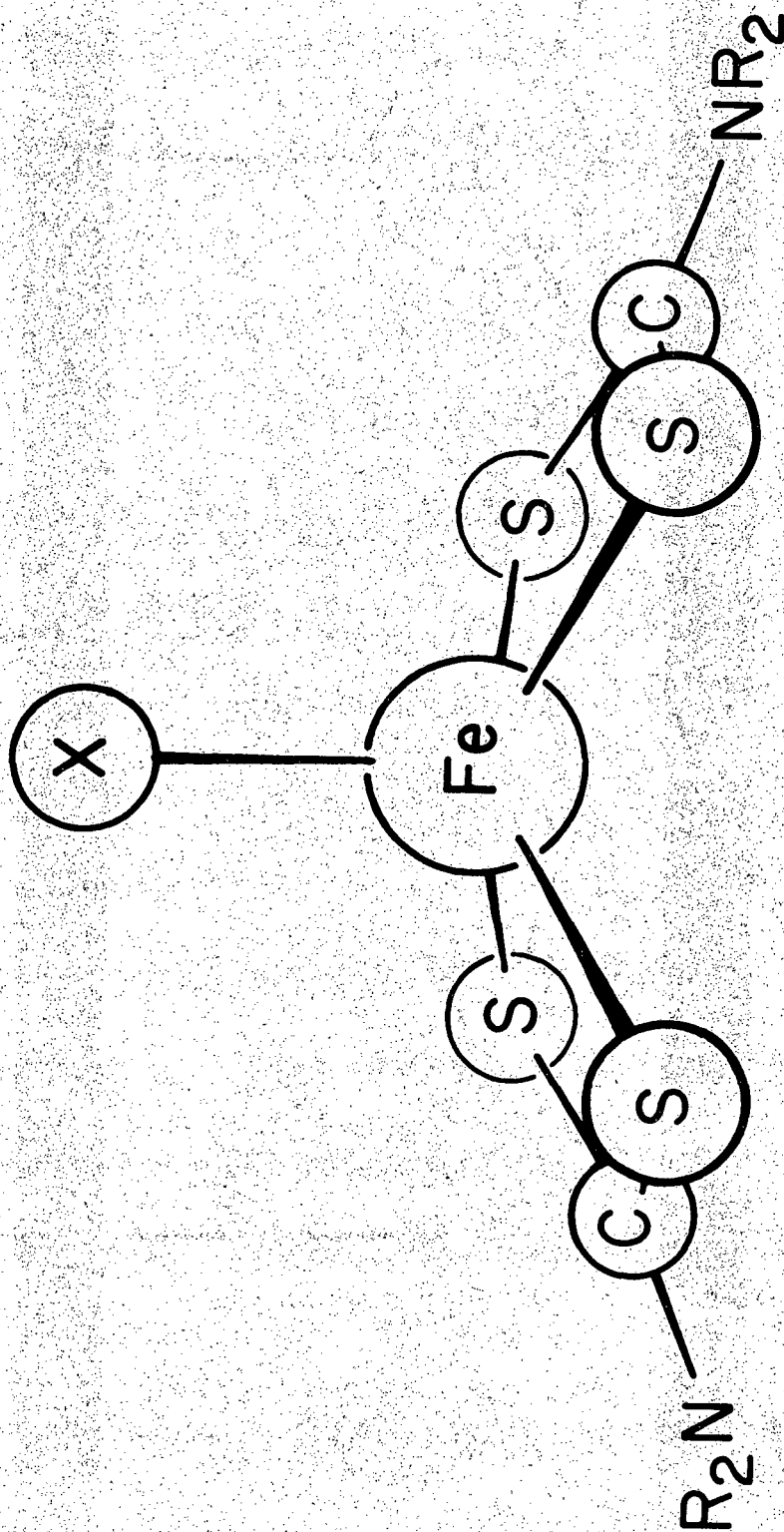
XBL 706 -3236

Fig. 12



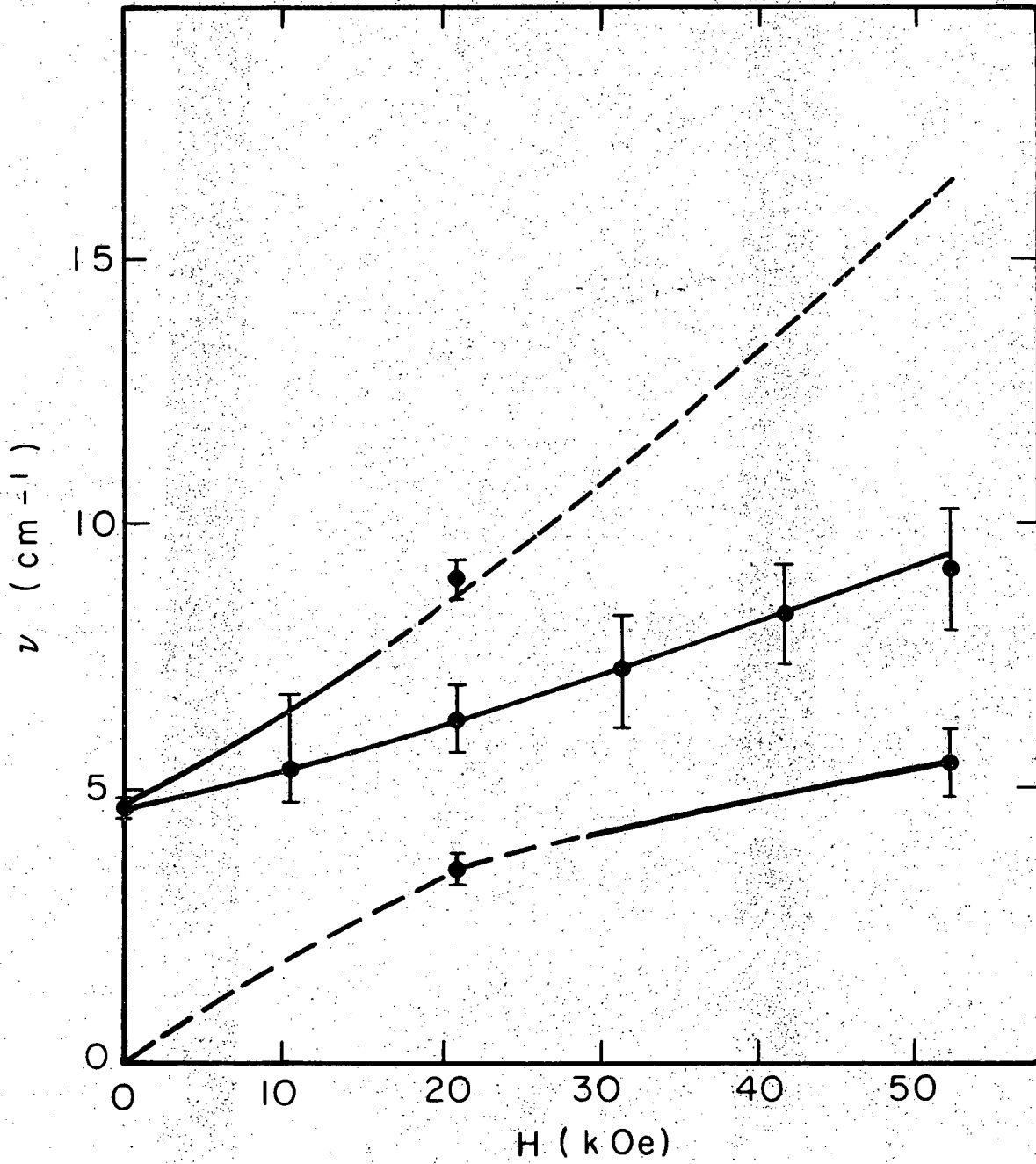
XBL706-3235

Fig. 13



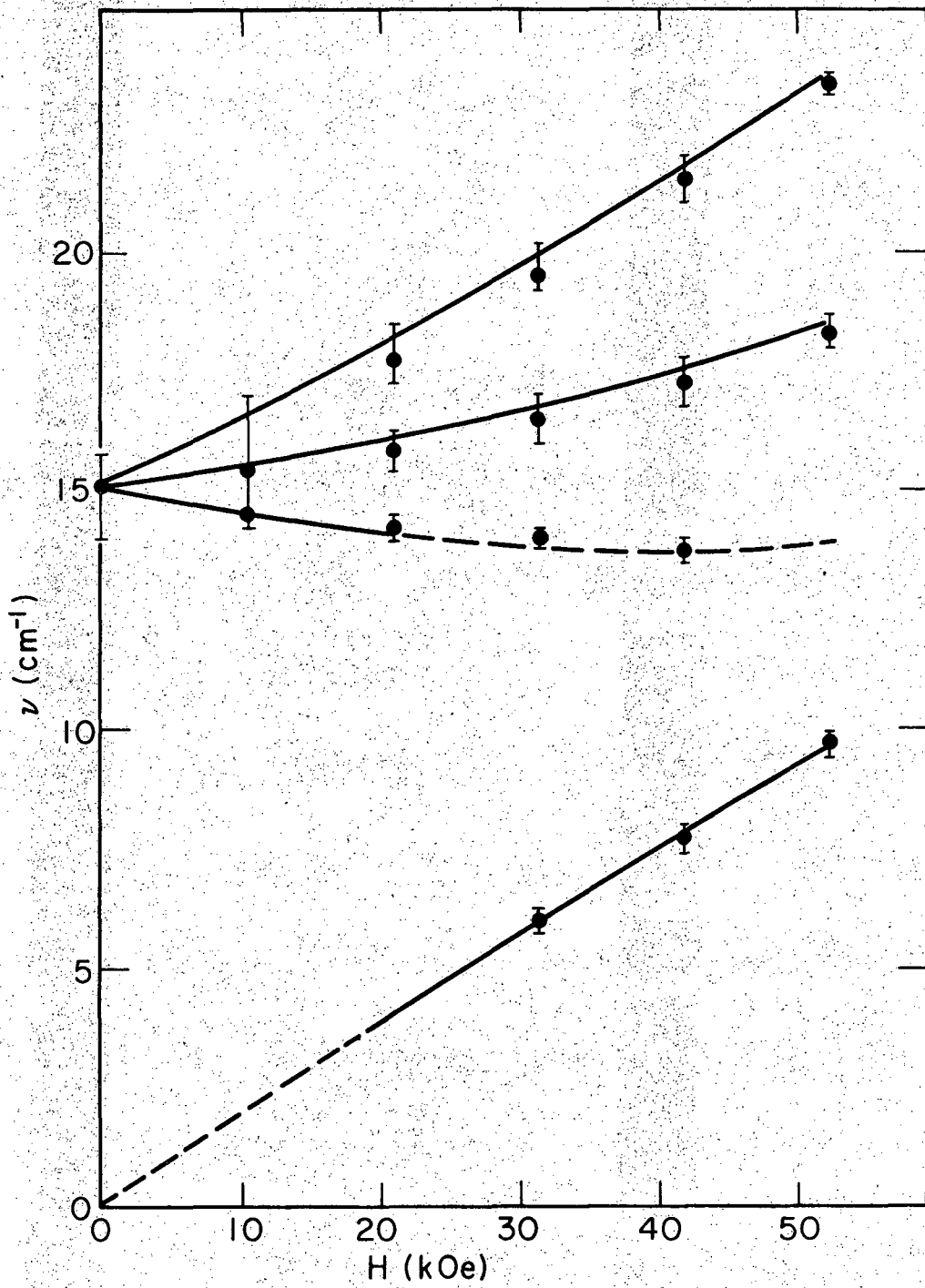
XBL705-2959

Fig. 14



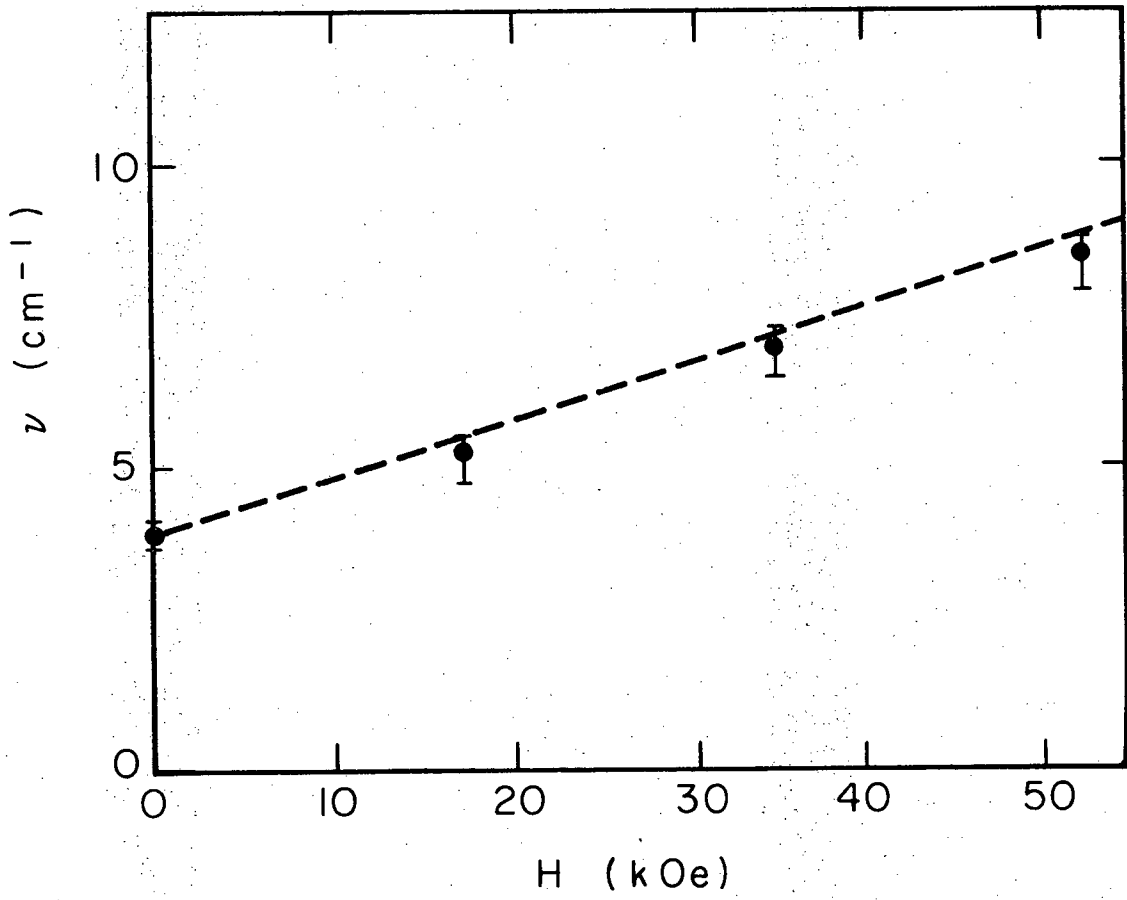
XBL6912-6385-A

Fig. 15



XBL702-2309-A

Fig. 16



XBL6912-6386-A

Fig. 17

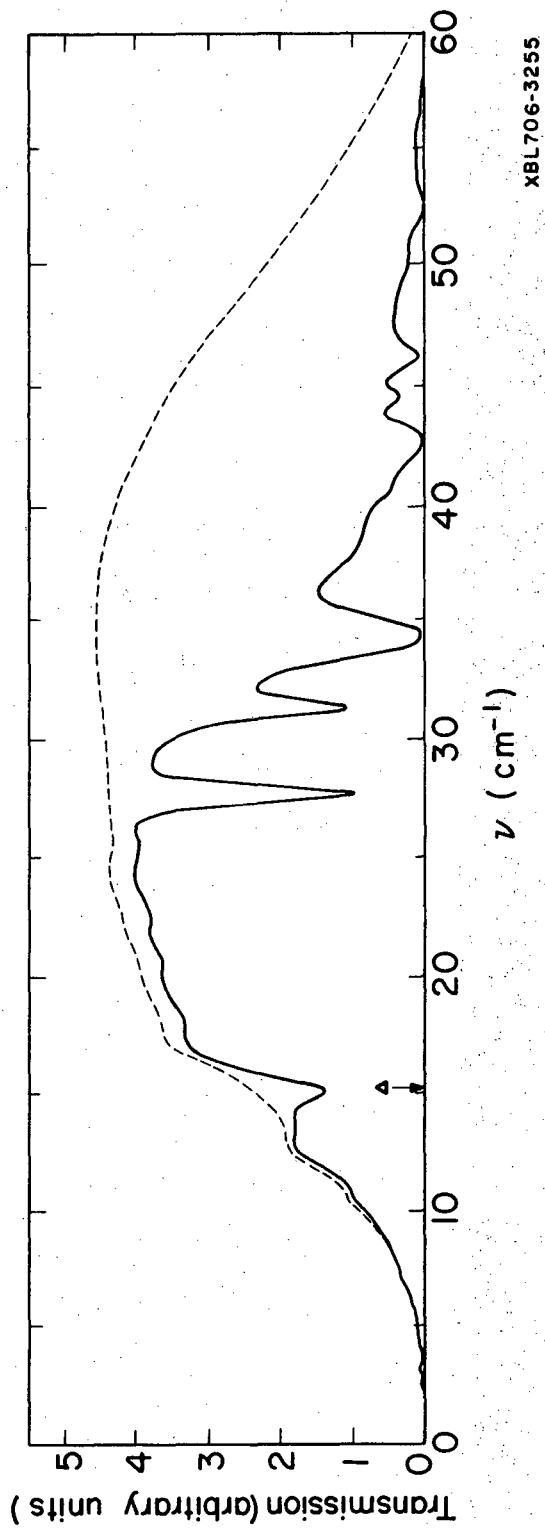
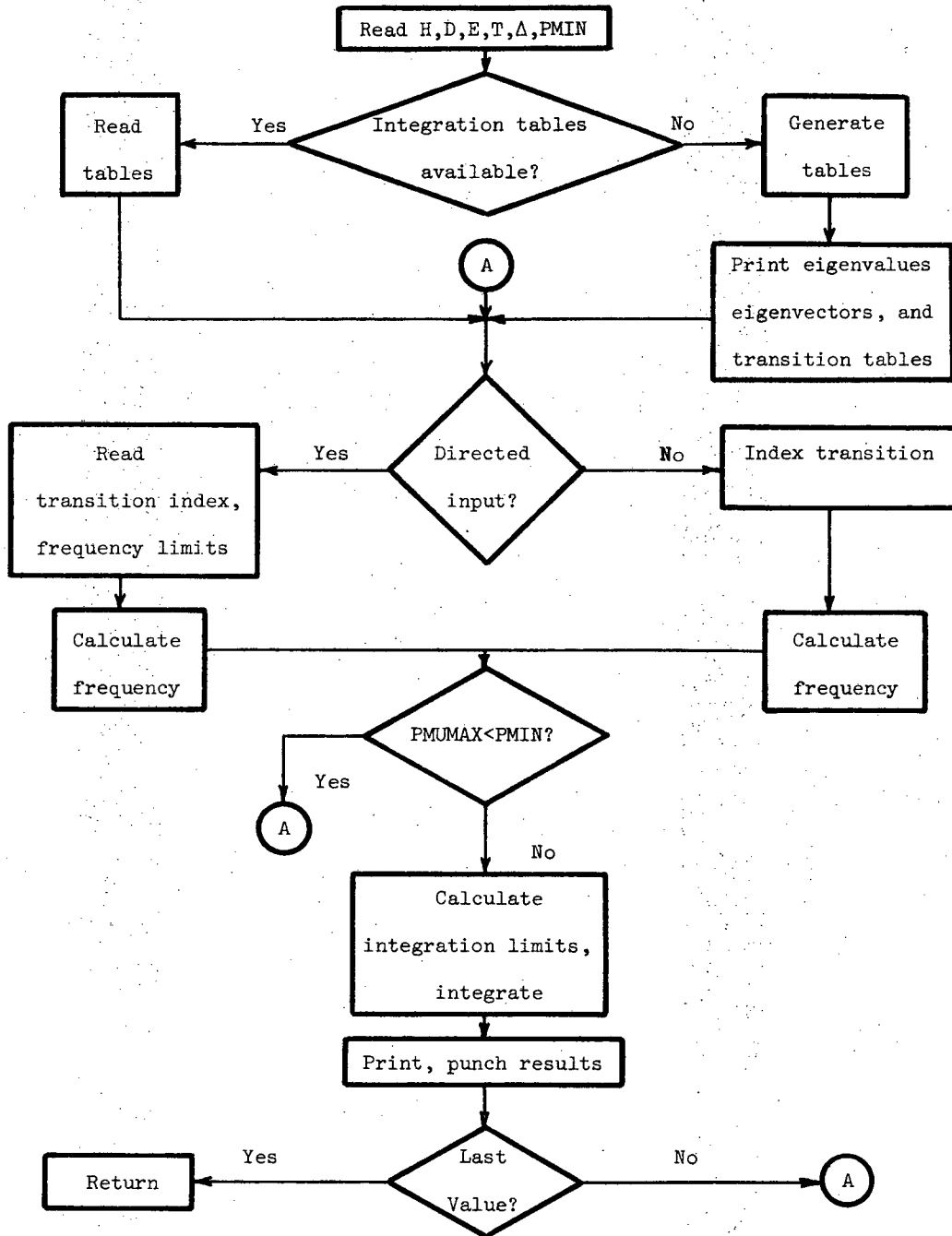
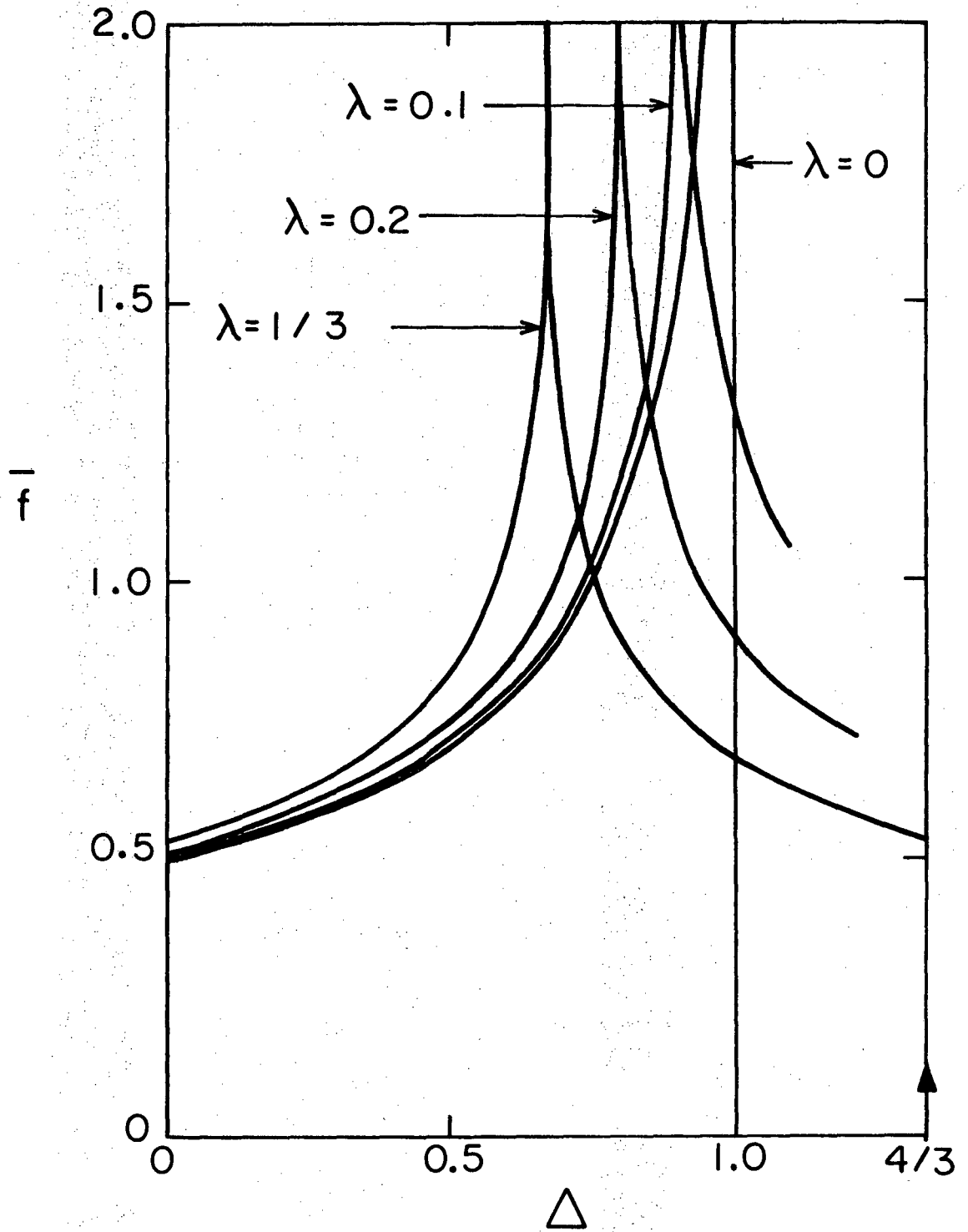


Fig. 18



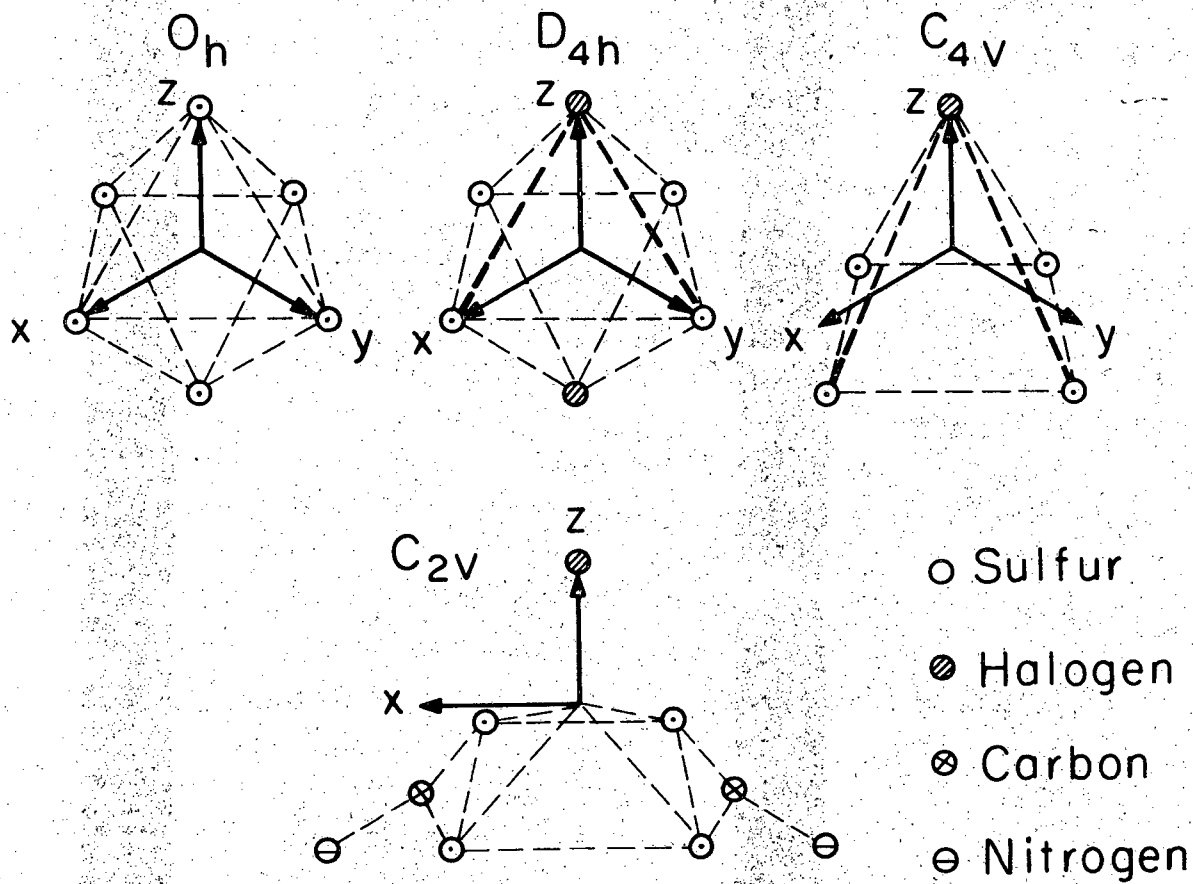
XBL 706-1302

Fig. B1



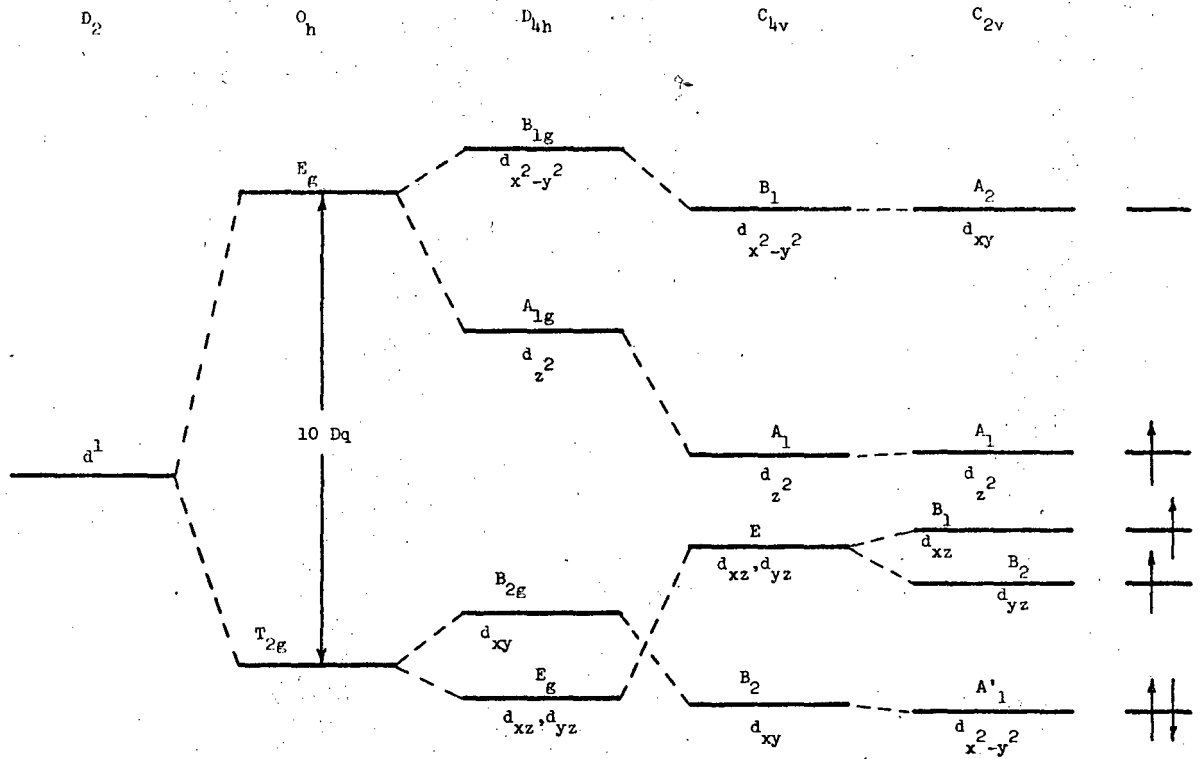
XBL 706 - 3254

Fig. C1



XBL 706 - 3253

Fig. E1



XBL 707-1575

Fig. E2

LEGAL NOTICE

This report was prepared as an account of Government sponsored work. Neither the United States, nor the Commission, nor any person acting on behalf of the Commission:

- A. Makes any warranty or representation, expressed or implied, with respect to the accuracy, completeness, or usefulness of the information contained in this report, or that the use of any information, apparatus, method, or process disclosed in this report may not infringe privately owned rights; or*
- B. Assumes any liabilities with respect to the use of, or for damages resulting from the use of any information, apparatus, method, or process disclosed in this report.*

As used in the above, "person acting on behalf of the Commission" includes any employee or contractor of the Commission, or employee of such contractor, to the extent that such employee or contractor of the Commission, or employee of such contractor prepares, disseminates, or provides access to, any information pursuant to his employment or contract with the Commission, or his employment with such contractor.

TECHNICAL INFORMATION DIVISION
LAWRENCE RADIATION LABORATORY
UNIVERSITY OF CALIFORNIA
BERKELEY, CALIFORNIA 94720